Engineering Journal

Third Quarter 2021 | Volume 58, No. 3

Smarter.
Stronger.
Steel.

Engineering Journal

American Institute of Steel Construction

Dedicated to the development and improvement of steel construction, through the interchange of ideas, experiences, and data.

The articles contained herein are not intended to represent official attitudes, recommendations or policies of the Institute. The Institute is not responsible for any statements made or opinions expressed by contributors to this Journal.

The opinions of the authors herein do not represent an official position of the Institute, and in every case the officially adopted publications of the Institute will control and supersede any suggestions or modifications contained in any articles herein.

The information presented herein is based on recognized engineering principles and is for general information only. While it is believed to be accurate, this information should not be applied to any specific application without competent professional examination and verification by a licensed professional engineer. Anyone making use of this information assumes all liability arising from such use.

Manuscripts are welcomed, but publication cannot be guaranteed. All manuscripts should be submitted in duplicate. Authors do not receive a remuneration. Guidelines for authors are printed on the inside back cover.

Engineering Journal (ISSN 0013-8029) is published quarterly. Subscriptions: Members: one subscription, $40 per year, included in dues; Additional Member Subscriptions: $40 per year. Non-Members U.S.: $160 per year. Foreign (Canada and Mexico): Members $80 per year. Non-Members $160 per year. Published by the American Institute of Steel Construction at 130 E Randolph Street, Suite 2000, Chicago, IL 60601.

Subscriptions: subscriptions@aisc.org, 312.670.2400

Archives: Search at **aisc.org/ej**. Article downloads are free for current members and are avaialable for a nominal fee for non-members.

Analysis of the Shear Lag Factor for Slotted Rectangular HSS Members

BO DOWSWELL

ABSTRACT

Rectangular HSS tension members are often connected by slotting two opposite walls and welding the slotted walls to a gusset plate. Due to a nonuniform stress distribution in these connections, the tensile rupture strength of the member is dependent on a shear lag factor. The accuracy of the 2016 AISC *Specification* provisions for the tensile rupture strength of slotted HSS tension members was evaluated using existing data from five previous research projects. The results revealed that the current equations are excessively conservative. The accuracy can be improved by replacing the existing equation for the connection eccentricity with the equation proposed in this paper.

Keywords: shear lag factor, HSS, gusset plate, tensile rupture, nonuniform stress distribution.

INTRODUCTION

Rectangular hollow structural sections (HSS) are often used as vertical bracing members in steel structures. A common connection detail for these members is shown in Figure 1, where two opposite walls are slotted to allow the brace to be inserted over the gusset plate. The brace is then connected to the gusset plate with four fillet welds.

A nonuniform stress distribution exists at the connection, which can reduce the tensile rupture strength of the member. This effect is addressed in the 2016 AISC *Specification for Structural Steel Buildings* (AISC, 2016), hereafter referred to as the AISC *Specification*, with a shear lag factor, U. For conditions where some cross-sectional elements are unconnected, the AISC *Specification* equation (Equation 3) was empirically derived using experimental results on open structural shapes (Chesson and Munse, 1963). However, the reliability of this equation has not been documented for slotted rectangular HSS connections. The objective of this paper is to analyze the existing data from previous research projects to determine the accuracy of the AISC *Specification* provisions for these connections.

TENSILE RUPTURE STRENGTH

AISC *Specification* Section D2 defines the nominal tensile rupture strength as

$$P_n = F_u A_e \qquad (Spec.\ \text{Eq. D2-2})$$

where $\phi = 0.75$ (LRFD), $\Omega = 1.67$ (ASD), F_u is the specified minimum tensile strength of the HSS, and A_e is the effective net area, which is defined in AISC *Specification* Section D3 as

$$A_e = A_n U \qquad (Spec.\ \text{Eq. D3-1})$$

where A_n is the net area, calculated by subtracting the slot area from the gross area according to Equation 1:

$$A_n = A_g - 2tw_s \tag{1}$$

where t is the HSS wall thickness and w_s is the slot width, as shown in Figure 2.

The gross area, calculated with Equation 2, is based on a corner radius equal to twice the wall thickness. Equation 2 was used to calculate the areas listed in AISC *Steel Consstruction Manual* (AISC, 2017) Tables 1-11 and 1-12.

$$A_g = 2t(H+B) + t^2(3\pi - 16) \tag{2}$$

where B is the width of the HSS member perpendicular to the gusset plate and H is the width of the HSS member parallel to the gusset plate. Case 6 in AISC *Specification* Table D3.1 corresponds to slotted rectangular HSS members, where the shear lag factor, U, is defined with Equation 3.

$$U = 1 - \frac{\bar{x}}{l} \tag{3}$$

where l is the connection length. For the 2016 AISC *Specification*, l must be greater than H.

The connection eccentricity, $\bar{x}$, calculated with Equation 4, is the distance from the center of the gusset plate to the centroid of the C-shaped portion of the HSS on each side of the gusset plate. Equation 4 is conservative because the derivation was based on the outside HSS dimensions, while neglecting the gusset plate thickness.

Bo Dowswell, PE, PhD, ARC International, LLC, Birmingham, Ala. Email: bo@arcstructural.com

Paper No. 2020-03

$$\bar{x} = \frac{B^2 + 2BH}{4(B+H)} \tag{4}$$

The accuracy can be improved by defining $\bar{x}$ as the distance from the edge of the gusset plate to the centroid of the C-shaped portion of the HSS on each side of the gusset plate. In this case, $\bar{x}$ is calculated with Equation 5, which is less conservative than Equation 4 because both the HSS wall thickness and the gusset plate thickness were considered in the derivation.

$$\bar{x} = b - \frac{2b^2 + Ht - 2t^2}{2H + 4b - 4t} \tag{5}$$

where b is the distance from the HSS outer surface to the gusset edge as shown in Figure 2.

$$b = \frac{B - t_g}{2} \tag{6}$$

DATA ANALYSIS

Existing Data

Slotted rectangular HSS connections have been studied using both finite element models (Girard et al., 1995; Zhao et al., 2009) and experimental specimens. As noted by Martinez-Saucedo and Packer (2007), many of the available experimental specimens failed by either block shear rupture (Zhao et al., 1999; Zhao and Hancock, 1995) or weld rupture (Wilkinson et al., 2002), not circumferential rupture, which is indicative of a tension rupture failure. Due to inconsistent results from the finite element models, the data for this study includes only the experimental specimens that failed by circumferential rupture at the connection.

A total of 47 specimens from five research projects were analyzed. All specimens were connected by four longitudinal fillet welds as shown in Figure 1. For the 10 specimens tested by Yeomans (1993), additional transverse welds connected the HSS walls to the edge of the gusset plates. The geometric and material variables for the test specimens are listed in columns 2 through 8 of Table 1, and the experimental rupture load, P_e, is listed in column 9. The specimens tested by Zhao et al. (2008), Korol et al. (1994), and Yeomans (1993) were loaded statically, and the specimens tested by Han et al. (2007) and Yang and Mahin (2005) were loaded cyclically to simulate seismic loading.

Using the measured dimensions and tensile strengths (where available), the tension rupture strength, P_c, was calculated for each specimen. For the 10 specimens tested by Yeomans (1993), the transverse welds were considered in the calculations by setting the net area equal to the gross area. The strengths, with $\bar{x}$ calculated with Equations 4 and 5 are listed in columns 5 and 6 of Table 2, respectively.

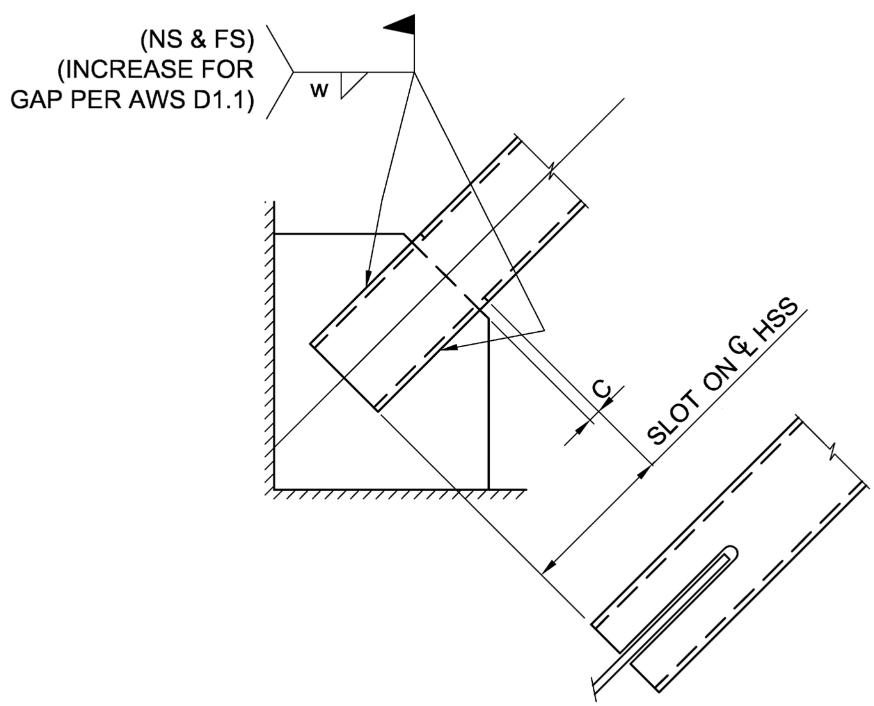

Fig. 1. Slotted rectangular HSS brace connection.

The measured tensile strength, σ_u, was not reported for the specimens tested by Korol et al. (1994); therefore, the calculated strength was based on the specified minimum tensile strength, F_u. The experimental-to-calculated load ratios, P_e/P_c, are listed in columns 7 and 8.

Reliability Analysis

The reduction factor required to obtain a specific reliability level is (Galambos and Ravinda, 1978):

$$\phi = C\rho_R e^{-\beta\alpha_R V_R} \tag{7}$$

where

C = correction factor

V_R = coefficient of variation

α_R = separation factor

β = reliability index

ρ_R = bias coefficient

Based on AISC *Specification* Section B3.1 Commentary, the target reliability index used in this paper is 4.0. Galambos and Ravinda (1973) proposed a separation factor, α_R, of 0.55. For a live-to-dead load ratio, L/D, of 3.0, Grondin et al. (2007) developed Equation 8 for calculating the correction factor.

$$C = 1.4056 - 0.1584\beta + 0.008\beta^2 \tag{8}$$

The bias coefficient is

$$\rho_R = \rho_M \rho_G \rho_P \tag{9}$$

where

ρ_G = bias coefficient for the geometric properties

ρ_M = bias coefficient for the material properties

ρ_P = bias coefficient for the test-to-predicted strength ratios. Mean value of the professional factor calculated with the measured geometric and material properties

The coefficient of variation is

$$V_R = \sqrt{V_M^2 + V_G^2 + V_P^2} \tag{10}$$

where

V_G = coefficient of variation for the geometric properties

V_M = coefficient of variation for the material properties

V_P = coefficient of variation for the test-to-predicted strength ratios

The relevant geometric parameters for slotted HSS connections are the wall thickness and weld length. Wall thickness measurements for the 30 ASTM A500 Grade C specimens tested by Zhao et al. (2008) resulted in a mean measured-to-nominal thickness ratio of 0.924. Using a design wall thickness equal to 0.93 times the nominal wall thickness according to AISC *Specification* Section B4.2, the mean measured-to-design thickness ratio is 0.994, with a coefficient of variation of 0.00710.

To the author's knowledge, the required statistical information on weld length is not available. For the block shear limit state of slotted HSS connections, Oosterhof and Driver (2011) used ρ_G = 1.00 and V_G = 0.050. These values were originally used by Hardash and Bjorhovde (1984) for bolted gusset plates, and they were "assumed to be appropriate in the absence of better statistical data" for slotted HSS connections. Because the same parameters are relevant for the tensile rupture limit state, V_G = 0.050 was used for the analysis in this paper. The slightly more conservative value of ρ_G = 0.994, which was based on the wall thickness measurements by Zhao et al. (2008), was used in the analysis.

Statistical values for the tensile strength of as-formed rectangular HSS shapes, summarized by Schmidt and Bartlett (2002), are ρ_M = 1.18 and V_M = 0.063. A more recent data set compiled by Liu et al. (2007) resulted in ρ_M = 1.27 and V_M = 0.04 based on 309 specimens from rectangular ASTM A500 Grade B shapes.

For five of the projects discussed in this paper (Zhao et al., 2008; Han et al., 2007; Yang and Mahin, 2005; Zhao et al., 1999; Zhao and Hancock, 1995), 20 data points are available with coupons extracted from the flat portions of the HSS walls. These tests—on ASTM A500 Grade B, ASTM A500 Grade C, and similar international grades—resulted in ρ_M = 1.12 and V_M = 0.0405, with only a small variation between grades.

Three tension specimens were extracted from the HSS corners and tested by Zhao et al. (2008). Due to the cold-bending of the corners, the tensile strength at the corners was 23% higher than the tensile strength at the flat portions of the walls.

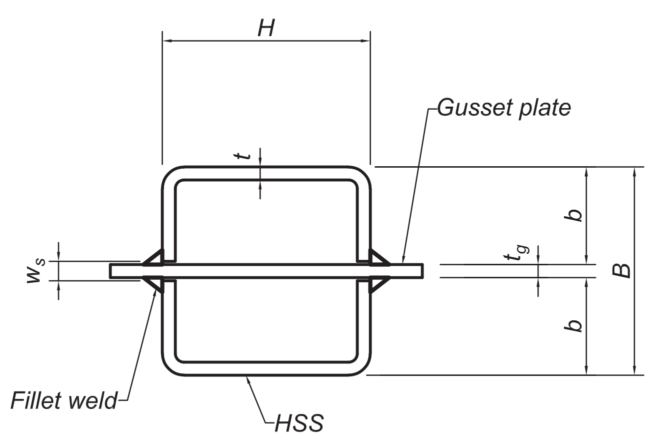

Fig. 2. HSS section at slot.

Results

Conservative values for the geometric and material properties are $\rho_G = 0.994$, $V_G = 0.050$, $\rho_M = 1.12$, and $V_M = 0.063$. These values were used to analyze two data sets: (1) the 36 specimens tested by Zhao et al. (2008) and Yeomans (1993) and (2) all 47 specimens listed in Table 1.

The rupture strengths calculated with Equation 4 varied from 0.865 to 0.968 times the values calculated with Equation 5, with an average of 0.935. Because Equation 4 is more conservative than Equation 5, only Equation 5 was used in the analysis.

For the 36 specimens tested by Zhao et al. (2008) and Yeomans (1993), the average test-to-predicted strength ratio, ρ_P, is 1.26 with a coefficient of variation, V_P, of 0.0872. Substituting these values into Equations 9 and 10 results in $\rho_R = 1.40$ and $V_R = 0.119$. Using Equations 7 and 8, $\phi = 0.970$ at $\beta = 4.0$ and $\beta = 5.57$ at $\phi = 0.75$.

Because the measured tensile strength, σ_u, was not reported for the specimens tested by Korol et al. (1994), the experimental-to-calculated load ratio, P_e/P_c, for these specimens was divided by ρ_M prior to the calculation of ρ_P. For all 47 specimens, $\rho_P = 1.22$, $V_P = 0.104$, $\rho_R = 1.36$, and $V_R = 0.132$. Using Equations 7 and 8, $\phi = 0.916$ at $\beta = 4.0$ and $\beta = 5.15$ at $\phi = 0.75$.

The analysis showed that the reliability index, with $\bar{x}$ calculated using Equation 5, is greater than the target reliability index of 4.0. Therefore, $\phi = 0.75$ is conservative. At least a portion of this conservatism can be attributed to the increase in tensile strength at the corners that is caused by cold-working.

Discussion

For the 2016 AISC *Specification*, l must be greater than H. This requirement evolved from the 1986 AISC *Specification* (AISC, 1986) limit that was initially applicable only to plates with longitudinal welds along both edges. In the 2016

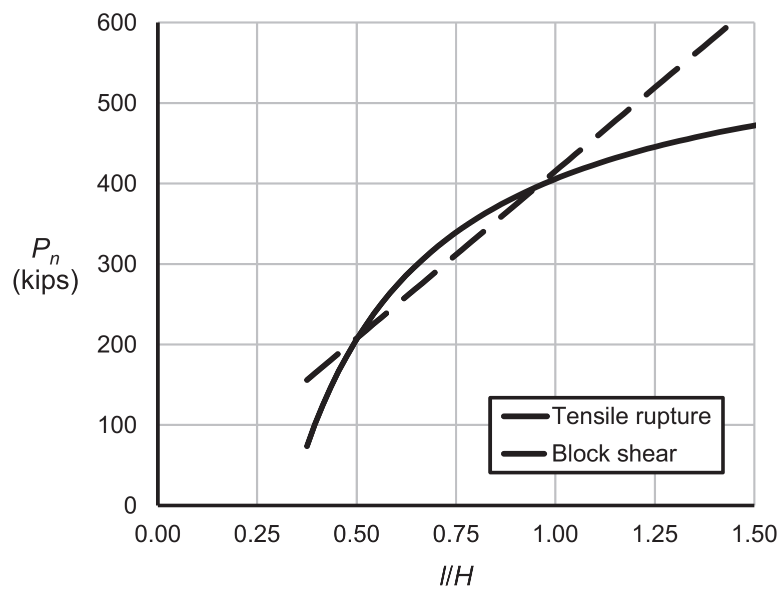

Fig. 3. Nominal strength of a slotted HSS8×8×⅜ connection vs. length-to-height ratio.

Specification provisions, this limit is not required for plates with longitudinal welds.

Column 10 in Table 1 shows only one specimen with an l/H ratio less than 1.0. For Zhao et al. (2008) specimen RS3G05P16, l/H = 0.924 and the experimental-to-calculated strength ratio, P_e/P_c = 1.24 with $\bar{x}$ calculated using Equation 5. However, only the specimens that failed by circumferential rupture at the net section were included in Table 1.

Figure 3 shows the variation in nominal strength with the l/H ratio for a slotted HSS8×8×⅜ connection of ASTM A500 Grade C material. In this case, the strength is controlled by the block shear limit state for $0.504 < l/H < 0.951$, and the tensile rupture limit state controls the strength for other l/H ratios. The curves for rectangular HSS with $H/B >$ 1.0 are similar to the curve for square HSS in Figure 3. For example, for an HSS12×4×⅜, the strength is controlled by the block shear limit state for $0.125 < l/H < 0.845$. For some conditions with $H/B < 1$, the tensile rupture strength is always lower than the block shear strength, potentially leading to uneconomical designs when both $H/B < 0.50$ and $l/H < 1.0$.

The 72 slotted HSS specimens that were tested by Zhao et al. (1999) and Zhao and Hancock (1995) failed by block shear. For these specimens, the l/H ratios were between 0.533 and 1.10, and most of the specimens had $l/H < 1.0$. Oosterhof and Driver (2011) showed that the 2016 AISC *Specification* equations for block shear are appropriate but slightly conservative for calculating the strength of these specimens.

Column 11 in Table 1 shows that the specimens had aspect ratios in the range $0.40 \le B/H \le 2.5$. Figure 4 shows the variation in the test-to-predicted strength ratio, P_e/P_c, with the B/H ratio. Although the conservatism of the proposed design equations is generally higher for the four specimens with $B/H \approx 2.5$ compared to the total data set, a significant trend cannot be established using the existing data.

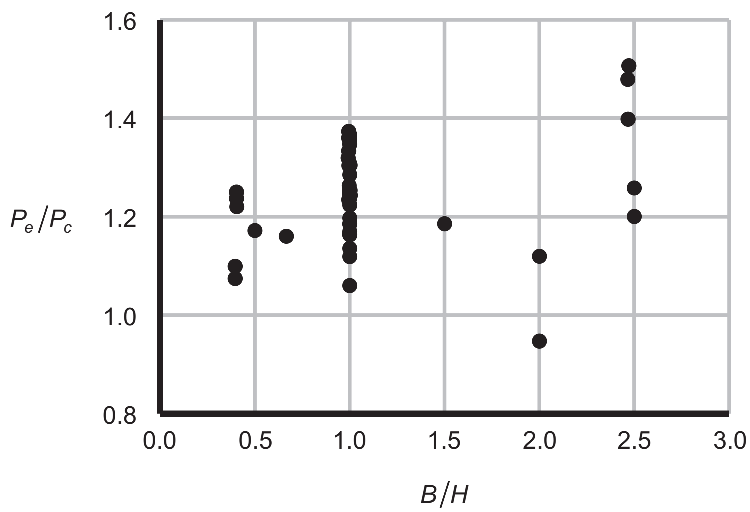

Fig. 4. Test-to-predicted strength ratio vs. width-to-height ratio.

Table 1. Specimen Details											
Specimen	B in.	H in.	t in.	l in.	t_g in.	F_u ksi	σ_u ksi	P_e kips	l/H	B/H	Notes
Zhao et al. (2008)											
RL5G05P16	5.01	2.03	0.176	7.69	0.619	62	65.0	152	3.79	2.47	
RS5G05P16	2.02	5.01	0.176	7.68	0.620	62	65.0	152	1.53	0.404	
SM5G05P16	3.53	3.53	0.174	7.67	0.619	62	70.3	153	2.17	1.00	
SM5G05P16R	3.52	3.53	0.174	7.75	0.620	62	70.3	151	2.20	1.00	
RL4G05P16	5.01	2.03	0.176	6.12	0.620	62	65.0	152	3.01	2.47	
RS4G05P16	2.03	5.01	0.177	6.13	0.621	62	65.0	147	1.22	0.405	
SM4G05P16	3.52	3.53	0.173	6.15	0.621	62	70.3	152	1.74	1.00	
SM4G05P16R	3.53	3.52	0.174	6.19	0.621	62	70.3	152	1.76	1.00	
RL3G05P16	5.00	2.02	0.176	4.55	0.618	62	65.0	138	2.25	2.47	
RS3G05P16	2.02	5.01	0.178	4.63	0.626	62	65.0	144	0.924	0.404	
SM3G05P16	3.53	3.53	0.174	4.54	0.614	62	70.3	146	1.29	1.00	
SM3G05P16R	3.52	3.52	0.174	4.56	0.619	62	70.3	147	1.29	1.00	
SM3G05P12	3.52	3.52	0.174	4.70	0.498	62	70.3	152	1.33	1.00	
SM3G05P12R	3.52	3.52	0.174	4.64	0.500	62	70.3	150	1.32	1.00	
SM5G05P12	3.53	3.52	0.174	7.93	0.501	62	70.3	156	2.25	1.00	
SM5G05P12R	3.54	3.53	0.174	7.93	0.499	62	70.3	155	2.25	1.00	
SM3G05P20	3.50	3.50	0.174	4.50	0.754	62	70.3	140	1.29	1.00	
SM3G05P20R	3.52	3.55	0.175	4.48	0.752	62	70.3	143	1.26	0.992	
SM5G05P20	3.53	3.53	0.174	7.50	0.755	62	70.3	150	2.13	1.00	
SM5G05P20R	3.52	3.53	0.174	7.48	0.754	62	70.3	152	2.12	1.00	
SM3G25P16	3.52	3.53	0.174	4.62	0.620	62	70.3	149	1.31	1.00	
SM3G25P16R	3.52	3.54	0.174	4.60	0.619	62	70.3	150	1.30	0.994	
SM3G50P16	3.51	3.53	0.174	4.59	0.618	62	70.3	150	1.30	0.995	
SM3G50P16R	3.51	3.53	0.174	4.56	0.617	62	70.3	146	1.29	0.995	
SM5G50P16	3.52	3.53	0.174	7.72	0.619	62	70.3	151	2.19	1.00	
SM5G50P16R	3.51	3.53	0.173	7.69	0.618	62	70.3	151	2.18	1.00	
Yeomans (1993)											
S-SEP-2	1.97	1.97	0.134	3.15	0.602	—	66.7	62	1.60	1.00	1
S-SEP-3	1.97	1.97	0.244	2.95	0.787	—	69.9	114	1.50	1.00	1
S-SEP-4	3.54	3.54	0.146	5.91	0.787	—	63.7	107	1.67	1.00	1
S-SEP-5	3.54	3.54	0.205	5.91	0.965	—	72.8	187	1.67	1.00	1
S-SEP-6	3.54	3.54	0.241	5.71	1.16	—	74.0	213	1.61	1.00	1
R-SEP-3	2.36	1.57	0.262	2.95	0.787	—	67.3	107	1.88	1.50	1
R-SEP-5	1.57	2.36	0.160	3.15	0.602	—	76.9	86	1.33	0.667	1
R-SEP-8	4.72	2.36	0.215	5.71	1.16	—	77.5	160	2.42	2.00	1
R-SEP-9	4.72	2.36	0.253	5.71	1.58	—	70.8	205	2.42	2.00	1
R-SEP-10	2.36	4.72	0.140	5.91	0.602	—	65.8	126	1.25	0.500	1

Table continues on the next page

Table 1. Specimen Details (continued)											
Specimen	***B*** **in.**	***H*** **in.**	***t*** **in.**	***l*** **in.**	t_g **in.**	F_u **ksi**	σ_u **ksi**	P_e **kips**	l/H	B/H	**Notes**
Korol et al. (1994)											
1A	4.92	1.97	0.252	6.30	0.630	65	—	168	3.20	2.50	2
1B	4.92	1.97	0.244	6.18	0.630	65	—	171	3.14	2.50	2
2A	3.46	3.46	0.242	6.18	0.630	65	—	164	1.78	1.00	2
2B	3.46	3.46	0.252	6.38	0.630	65	—	175	1.84	1.00	2
3A	1.97	4.96	0.242	6.14	0.630	65	—	174	1.24	0.397	2
3B	1.97	4.96	0.246	6.34	0.630	65	—	173	1.28	0.397	2
5A	3.50	3.50	0.236	3.86	0.630	65	—	149	1.10	1.00	2
Han et al. (2007)											
S90-8	3.94	3.94	0.354	9.88	0.669	58	66.1	293	2.51	1.00	3
S69-11	4.92	4.92	0.236	9.02	1.22	58	67.0	250	1.83	1.00	3
Yang and Mahin (2005)											
2	6.00	6.00	0.375	15.0	0.875	58	65.0	486	2.50	1.00	3
3	6.00	6.00	0.375	15.0	0.875	58	65.0	537	2.50	1.00	3

Note 1: Additional transverse welds connected the HSS walls to the edge of the gusset plates.
Note 2: The measured tensile strength, σ_u, was not reported.
Note 3: Cyclic loading was used to simulate seismic loading.

Table 2. Calculated Strengths							
		U		P_c, kips		P_e/P_c	
Specimen	A_n, in.^{2}	**Equation 4**	**Equation 5**	**Equation 4**	**Equation 5**	**Equation 4**	**Equation 5**
Zhao et al. (2008)							
RL5G05P16	2.03	0.790	0.821	104	109	1.45	1.40
RS5G05P16	2.01	0.887	0.928	116	121	1.31	1.25
SM5G05P16	2.02	0.827	0.862	118	122	1.30	1.25
SM5G05P16R	2.01	0.830	0.863	118	122	1.29	1.24
RL4G05P16	2.04	0.736	0.775	97.8	103	1.56	1.48
RS4G05P16	2.04	0.858	0.910	114	120	1.29	1.22
SM4G05P16	2.01	0.785	0.828	111	117	1.37	1.30
SM4G05P16R	1.99	0.786	0.829	110	116	1.37	1.30
RL3G05P16	2.03	0.646	0.698	85.1	91.9	1.63	1.51
RS3G05P16	2.04	0.813	0.881	108	117	1.34	1.24
SM3G05P16	2.02	0.708	0.766	100	109	1.46	1.35
SM3G05P16R	2.02	0.710	0.768	101	109	1.46	1.35
SM3G05P12	2.06	0.719	0.766	104	111	1.46	1.37
SM3G05P12R	2.07	0.715	0.763	104	111	1.45	1.36
SM5G05P12	2.06	0.833	0.861	121	125	1.30	1.25
SM5G05P12R	2.06	0.833	0.861	121	125	1.29	1.24
SM3G05P20	1.95	0.709	0.776	97.4	107	1.43	1.31

Table continues on the next page

Table 2. Calculated Strengths (continued)							
		U		P_c, kips		P_e/P_c	
Specimen	A_n, in.^{2}	Equation 4	Equation 5	Equation 4	Equation 5	Equation 4	Equation 5
Zhao et al. (2008) (continued)							
SM3G05P20R	1.99	0.705	0.773	98.6	108	1.45	1.32
SM5G05P20	1.97	0.824	0.864	114	120	1.31	1.25
SM5G05P20R	1.97	0.824	0.865	114	120	1.33	1.26
SM3G25P16	2.01	0.714	0.771	101	109	1.48	1.37
SM3G25P16R	2.02	0.713	0.770	101	109	1.48	1.37
SM3G50P16	2.03	0.713	0.770	102	110	1.47	1.36
SM3G50P16R	2.03	0.711	0.768	101	110	1.44	1.33
SM5G50P16	2.01	0.829	0.863	117	122	1.29	1.24
SM5G50P16R	2.01	0.828	0.862	117	122	1.28	1.23
Yeomans (1993)							
S-SEP-2	0.936	0.766	0.843	48	53	1.29	1.17
S-SEP-3	1.53	0.750	0.867	80	93	1.41	1.22
S-SEP-4	1.93	0.775	0.827	95	101	1.13	1.06
S-SEP-5	2.63	0.775	0.840	148	161	1.26	1.17
S-SEP-6	3.04	0.767	0.849	172	191	1.24	1.12
R-SEP-3	1.61	0.720	0.831	78	90	1.37	1.19
R-SEP-5	1.09	0.800	0.888	67	74	1.29	1.16
R-SEP-8	2.74	0.724	0.795	154	169	1.04	0.947
R-SEP-9	3.16	0.724	0.819	162	183	1.27	1.12
R-SEP-10	1.85	0.833	0.881	102	107	1.24	1.17
Korol et al. (1994)							
1A	2.72	0.749	0.791	133	140	1.27	1.20
1B	2.65	0.744	0.787	128	136	1.33	1.26
2A	2.65	0.790	0.837	136	144	1.20	1.14
2B	2.74	0.796	0.842	142	150	1.23	1.16
3A	2.65	0.863	0.919	149	159	1.17	1.10
3B	2.68	0.867	0.922	152	161	1.14	1.07
5A	2.63	0.659	0.734	113	126	1.32	1.19
Han et al. (2007)							
S90-8	4.22	0.851	0.885	238	247	1.23	1.19
S69-11	3.67	0.795	0.849	196	209	1.28	1.20
Yang and Mahin (2005)							
2	7.33	0.850	0.878	405	418	1.20	1.16
3	7.33	0.850	0.878	405	418	1.33	1.28

CONCLUSIONS

Rectangular HSS tension members are often connected by slotting two opposite walls and welding the slotted walls to a gusset plate. Due to nonuniform stress distributions in these connections, the tensile rupture strength of the member is dependent on a shear lag factor. The accuracy of the AISC *Specification* provisions for the tensile rupture strength of slotted HSS tension members was evaluated using existing data from previous research projects. A total of 47 specimens from five projects were analyzed.

The results revealed that the current equations are excessively conservative. The accuracy can be improved by replacing the 2016 AISC *Specification* equation (Equation 4) for the connection eccentricity, $\bar{x}$, with the proposed Equation 5, which is less conservative than Equation 4 because both the HSS wall thickness and the gusset plate thickness were considered in the derivation. The rupture strengths calculated with Equation 4 averaged 0.935 times the values calculated with Equation 5. Although the conservatism is reduced with the proposed Equation 5, the reliability analysis showed that the reduction factor, $\phi = 0.75$, in AISC *Specification* Section D2 is overly conservative when used with the proposed equation.

For practical connection geometries, the block shear limit state controls the strength of slotted HSS connections with low l/H ratios and the tensile rupture limit state controls the strength for high l/H ratios. If both limit states are checked, the connection rupture strength can be accurately predicted for the full range of available specimen geometries ($0.504 < l/H < 3.79$) without the 2016 AISC *Specification* requirement that l must be greater than H.

REFERENCES

AISC (1986), *Load and Resistance Factor Design Specification for Structural Steel Buildings*, American Institute of Steel Construction, Chicago, Ill.

AISC (2016), *Specification for Structural Steel Buildings*, ANSI/AISC 360-16, American Institute of Steel Construction, Chicago, Ill.

AISC (2017), *Steel Construction Manual*, 15th Ed., American Institute of Steel Construction, Chicago, Ill.

Chesson, E., Jr., and Munse, W.H. (1963), "Riveted and Bolted Joints: Truss Type Tensile Connections," *Journal of the Structural Division*, ASCE, Vol. 89, No. 1, January, pp. 67–106.

Galambos, T.V. and Ravinda, M.K. (1973), *Tentative Load and Resistance Factor Design Criteria for Steel Buildings*, Research Report No. 18, Department of Civil and Environmental Engineering, Washington University, September.

Galambos, T.V. and Ravinda, M.K. (1978), "Properties of Steel for Use in LRFD," *Journal of the Structural Division*, ASCE, Vol. 104, No. ST9, September, pp. 1,459–1,468.

Girard, C., Picard, A., and Fafard, M. (1995), "Finite Element Modelling of the Shear Lag Effects in an HSS Welded to a Gusset Plate," *Canadian Journal of Civil Engineering*, Vol. 22, pp. 651–659.

Grondin, G., Jin, M., and Josi, G. (2007), *Slip Critical Bolted Connections—A Reliability Analysis for Design at the Ultimate Limit State*, Structural Engineering Report No. 274, Department of Civil Engineering, University of Alberta, October.

Han, S.W., Kim, W.T., and Foutch, D.A. (2007), "Tensile Strength Equation for HSS Bracing Members Having Slotted End Connections," *Earthquake Engineering and Structural Dynamics*, Vol. 36, pp. 995–1,008.

Hardash, S.G. and Bjorhovde, R. (1984), *Gusset Plate Design Utilizing Block-Shear Concepts*, Department of Civil Engineering and Engineering Mechanics, University of Arizona, Tuscon, Ariz.

Korol, R.M., Mirza, F.A., and Mirza, M.Y. (1994), "Investigation of Shear-Lag in Slotted HSS Tension Members," *Tubular Structures VI*, Balkema, Rotterdam, pp. 473–479.

Liu, J., Sabelli, R., Brockenbrough, R.L., and Fraser, T.P. (2007), "Expected Yield Stress and Tensile Strength Ratios for Determination of Expected Member Capacity in the 2005 AISC *Seismic Provisions*," *Engineering Journal*, AISC, Vol. 44, No. 1, pp. 15–26.

Martinez-Saucedo, G. and Packer, J.A. (2007), "Discussion of Shear Lag in Rectangular Hollow Structural Section Tension Members: Comparison of Design Equations to Test Data," *Practice Periodical on Structural Design and Construction*, ASCE, Vol. 12, No. 2, pp. 135–136.

Oosterhof, S.A. and Driver, R.G. (2011), "Performance of the Unified Block Shear Equation for Common Types of Welded Steel Connections," *Engineering Journal*, AISC, Vol. 48, No. 2, pp. 77–92.

Schmidt, B.J. and Bartlett, F.M. (2002), "Review of Resistance Factor for Steel: Data Collection," *Canadian Journal of Civil Engineering*, Vol. 29, pp. 98–108.

Wilkinson, T., Petrovski, T., Bechara, E., and Rubal, M. (2002), "Experimental Investigation of Slot Lengths in RHS Bracing Members," *Proceedings of the 3rd International Conference on Advances in Steel Structures*, Elsevier, New York, N.Y., pp. 205–212.

Yang, F. and Mahin, S. (2005), "Limiting Net Section Fracture in Slotted Tube Braces," *Steel Tips*, Structural Steel Education Council, April.

Yeomans, N.F. (1993), *Slotted End Plate Connections*, TS and MD Technical Development Report No. P004.S.08-1, British Steel, March.

Zhao, R.G., Huang, R.F., Khoo, H.A., and Cheng, J.J.R. (2008), "Experimental Study on Rectangular and Square Hollow Structural Section (HSS) Tension Connections," *Canadian Journal of Civil Engineering*, Vol. 35, pp. 1,318–1,330.

Zhao, R.G., Huang, R.F., Khoo, H.A., and Cheng, J.J.R. (2009), "Parametric Finite Element Study on Slotted Rectangular and Square HSS Tension Connections," *Journal of Constructional Steel Research*, Vol. 65, pp. 611–621.

Zhao, X.L., Al-Mahaidi, R., and Kiew, K.P. (1999), "Longitudinal Fillet Welds in Thin-Walled C450 RHS Members," *Journal of Structural Engineering*, ASCE, Vol. 25, No. 8, August, pp. 821–828.

Zhao, X.L. and Hancock, G.J. (1995), "Longitudinal Fillet Welds in Thin Cold-Formed RHS Members," *Journal of Structural Engineering*, ASCE, Vol. 121, No. 11, November, pp. 1,683–1,690.

Tearout Strength of Concentrically Loaded Bolted Connections

NICOLO FRANCESCHETTI and MARK D. DENAVIT

ABSTRACT

The limit state of tearout can complicate the design of steel bolted connections since, in contrast to the limit states of bearing and bolt shear rupture, tearout strength can vary from bolt to bolt within a connection. Under the current AISC *Specification*, tearout strength is proportional to the clear distance, in the direction of force, between the edge of the hole and the edge of the adjacent hole or edge of the material. However, recent studies on concentrically loaded bolt groups have suggested that the use of clear distance may not accurately represent tearout strength and have proposed alternative lengths for use in strength equations. A reevaluation of the limit state of tearout in concentrically loaded bolt groups is presented in this work, including a thorough evaluation of the proposed alternative tearout lengths using a large database of previously published experimental work and new experiments with various edge distances and hole types. Equations with the alternative tearout lengths were found to be more accurate than those with clear distance, especially for small edge distances. Design recommendations including the alternative tearout lengths were developed. The results of this work increase understanding of the limit state of tearout and offer improved methods of evaluating this limit state in design.

Keywords: bolted connections, tearout, bearing, experiment, design.

INTRODUCTION

The current AISC *Specification for Structural Steel Buildings* (AISC, 2016), hereafter referred to as the AISC *Specification*, includes a user note, added in the 2010 edition (AISC, 2010), stating that the strength of a bearing-type bolt group in shear should be taken as the sum of the effective strengths of the individual bolts. The effective strength of a bolt is equal to the minimum strength computed for the limit states of bolt shear rupture, bearing, and tearout. By this method, it is possible, for example, to have the strength of a bolt group controlled by a combination of tearout for the bolts near an edge and bolt shear rupture for the remaining bolts. The possibility of this interaction of limit states is in contrast to a common practice where bolt shear rupture is treated as independent from bearing and tearout (Salmon et al., 2009). Evaluating the potential interaction of bolt shear rupture, bearing, and tearout complicates the design of bolt groups, primarily because the strength of an individual bolt for the limit state of tearout can vary from bolt to bolt within a group. Given the increased complexity and recently proposed alternative strength equations (Clements and Teh, 2013; Kamtekar, 2012), a reevaluation of the limit state of tearout is warranted to determine if changes can be made that lead to more accurate and efficient connection designs.

For bolts sufficiently far from edges of material and adjacent bolts, the strength of the connected material near the bolt is controlled by bearing. The limit state of bearing is characterized by plastic deformations of the connected material near the bolt hole and a long yield plateau in the load-deformation relationship. However, the connected material eventually ruptures with continued loading. In experimental testing, the peak load has been noted to occur upon reaching yield, prior to rupture or somewhere in between. However, once the yield plateau is reached, the variation in load is small.

Bearing strength has been observed to depend on the diameter of the bolt, the thickness of the connected material, and the tensile strength of the connected material. The edge distance (i.e., the distance from the center of hole to edge of connected material), when large, does not impact bearing strength. Near edges of material or adjacent bolts, the strength of the connected material near the bolt is less than the full bearing strength because one of several other limit states will control.

The primary limit state for connected material with smaller edge distance is tearout. Tearout is characterized by the rupture of the connected material on either side of the bolt. A similar failure mode is splitting, which involves a tensile rupture initiating at the end of the connected material. Some experiments have also shown modes of failure for bolted connections that include out-of-plane curling of unconfined plates. These three limit states are depicted in Figure 1.

Nicolo Franceschetti, Engineer, Palmer Engineering, Nashville, Tenn. (formerly Graduate Research Assistant, The University of Tennessee, Knoxville, Knoxville, Tenn.) Email: nfranceschetti@palmernet.com

Mark D. Denavit, Assistant Professor, The University of Tennessee, Knoxville, Knoxville, Tenn. Email: mdenavit@utk.edu (corresponding)

Paper No. 2020-07

AISC *Specification* Section J3.10 (2016) governs bearing and tearout strength at bolt holes. The nominal bearing strength of a bolt in a standard, oversize, or short-slotted hole, R_n, is given by Equations 1 and 2 (2016 AISC *Specification* Equations J3-6a and J3-6b).

$$R_n = 2.4dtF_u \tag{1}$$

$$R_n = 3.0dtF_u \tag{2}$$

where F_u is the specified minimum tensile strength of the connected material, d is the nominal bolt diameter, and t is the thickness of the connected material.

Equation 1 is used when deformation at the bolt hole at service load is a design consideration, whereas Equation 2 is used when deformation at the bolt hole at service load is not a design consideration. Significant bolt hole ovalization is expected to occur prior to reaching the full bearing strength of the connected material, which may limit the effectiveness of the connection. Frank and Yura (1981) identified ¼-in. deformation as a practical limit to define a bearing strength, which also prevents excessive ovalization.

The tearout strength of a bolt in a standard, oversize, or short-slotted hole is given by Equations 3 and 4 (2016 AISC *Specification* Equations J3-6c and J3-6d), where the distinction between Equations 3 and 4 is the same as that between Equations 1 and 2.

$$R_n = 1.2l_ctF_u \tag{3}$$

$$R_n = 1.5l_ctF_u \tag{4}$$

where l_c is the clear distance, in the direction of force, between the edge of the hole and the edge of the adjacent hole or edge of the material.

Provisions in the AISC *Specification* related to the limit state of tearout have changed over the various editions. In early editions—for example, the 1936 AISC *Specification* (AISC, 1936)—tearout was prevented by a limitation on edge distance. However, the limitation did not apply if there were three or more bolts in a line. In more recent editions—for example, the 1993 AISC *Specification* (AISC, 1993)—tearout was considered as a reduction to the bearing strength based on edge distance. An exception was also in place for these provisions. The reduction did not apply when there were two or more bolts in a line, a minimum edge distance of 1.5d was provided, a minimum spacing of 3d was provided, and deformation at the bolt hole was a design consideration. These exceptions were justified on the premise of load redistribution to the interior bolts or that sufficient interior bolts in a connection would diminish the effects of reduced strength at the edge bolts.

The form of the current provisions was introduced to the AISC *Specification* in the 1999 edition (AISC, 1999). An important change in these provisions was the use of the clear distance, l_c, for determining tearout strength instead of the edge distance. Also, no exceptions to the tearout check were provided.

This paper presents an investigation of tearout strength in concentrically loaded bolted connections. Recently proposed alternative strength equations (Clements and Teh, 2013; Kamtekar, 2012) are examined through comparisons to results from previously published experimental work and new experiments conducted by the authors. The comparisons provide a thorough evaluation of both the current and alternative strength equations. Based on the results, improvements to current design equations are recommended.

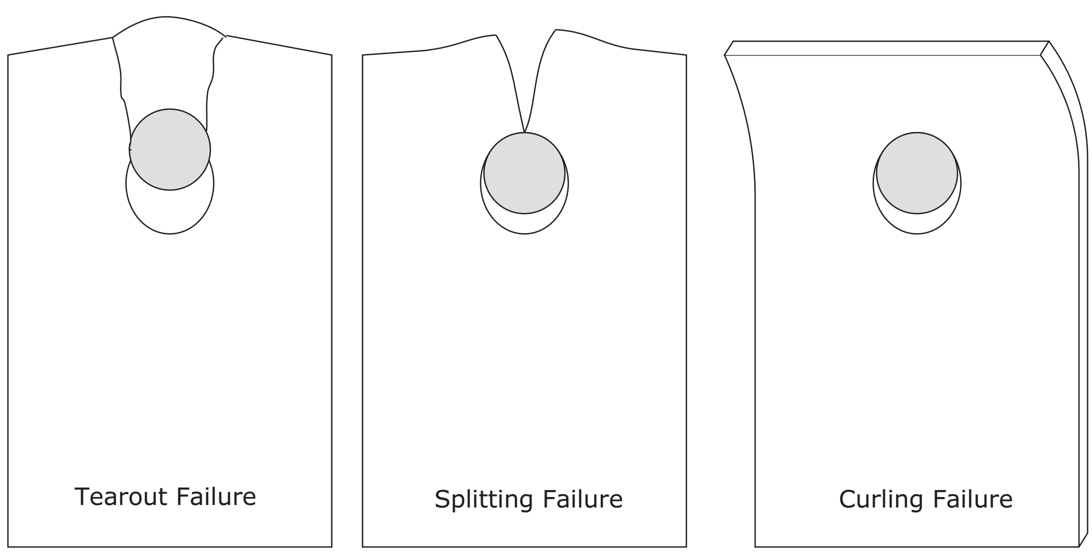

Fig. 1. Common failure modes of concentrically loaded bolted connections.

ALTERNATIVE TEAROUT LENGTHS

Under the current AISC *Specification* (AISC, 2016), strength for the limit state of tearout is based on the clear distance, in the direction of force, between the edge of the bolt hole and the edge of the adjacent hole or edge of the material. This distance is denoted as l_c. For the case illustrated in Figure 2, the clear distance is computed as a function of the edge distance, L_e, and the diameter of the hole, d_h:

$$l_c = L_e - \frac{d_h}{2} \tag{5}$$

Examination of experimental results has shown that the length of failure planes from specimens that exhibited tearout are somewhat longer than the clear distance. Researchers have proposed various alternative lengths that, when used in lieu of l_c, provide a more accurate assessment of strength. The first alternative tearout length that is investigated in this work, denoted as l_{v1}, was proposed by Kamtekar (2012) and is equal to the clear distance, in the direction of force, between the edge of the bolt hole and the edge of the adjacent hole or edge of the material along lines tangent to the bolt. For the case illustrated in Figure 2, l_{v1} is computed as:

$$l_{v1} = L_e - \frac{\sqrt{d_h^{\,2} - d^2}}{2} \tag{6}$$

The second alternative tearout length that is investigated in this work, denoted as l_{v2}, was proposed by Clements and Teh (2013) and is equal to the average of the clear distance, l_c, and the edge distance, L_e. For the case illustrated in Figure 2, l_{v2} is computed as:

$$l_{v2} = L_e - \frac{d_h}{4} \tag{7}$$

Elliot et al. (2019) evaluated the use of l_{v1} and l_{v2} in strength equations for a small set of experiments that failed in tearout. They found them both to provide similarly improved predictions of tearout strength in comparison to current equations. They also evaluated alternative net areas for block shear rupture that are similar in concept to the alternative tearout lengths.

Other tearout lengths have been proposed (e.g., Duerr, 2006). However, differences among the lengths are slight. Also, some are more complicated than l_{v1} and l_{v2} to compute for general bolted connections. Therefore, this work focuses on evaluating l_c, l_{v1}, and l_{v2}.

EVALUATION OF PUBLISHED EXPERIMENTS

Hundreds of physical experimental tests on concentrically loaded bolted connections susceptible to tearout have been performed in past research. These data have been collected and organized into a database for the purpose of evaluating alternative tearout lengths.

Experimental Database

The experimental database developed for this work includes 899 specimens collected from 20 published works, including this paper. Two types of connections are included: lap splices, in which the bolts are in single shear, and butt splices, in which the bolts are in double shear. A summary of the sources for the experimental data is presented in Table 1.

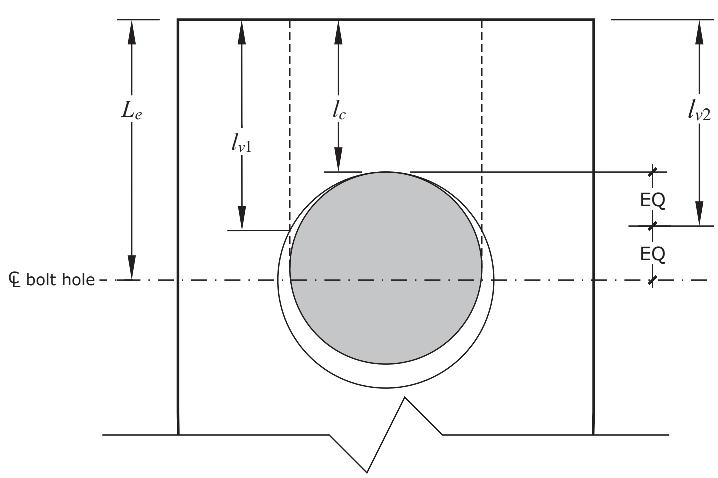

Fig. 2. Tearout length comparison.

Table 1. Summary of Experimental Data Sources			
Reference	Connection Type	Number of Specimens Included in Database	Number of Specimens with Bearing, Tearout, or Splitting Failures
Gillett (1978)	Lap splice	54	33
Frank and Yura (1981)	Butt splice	16	6
Sarkar (1992)	Lap splice	19	2
Karsu (1995)	Lap splice	64	38
Kim and Yura (1999)	Lap splice	41	41
Lewis and Zwerneman (1996)	Butt splice	92	87
Udagawa and Yamada (1998)	Butt splice	219	47
Puthli and Fleischer (2001)	Butt splice	25	9
Rex and Easterling (2003)	Butt splice	31	20
Udagawa and Yamada (2004)	Butt splice	42	5
Freitas (2005)	Butt splice	29	26
Brown et al. (2007)	Butt splice	94	63
Cai and Driver (2008)	Butt splice	44	23
Može and Beg (2010)	Butt splice	38	16
Može and Beg (2011)	Butt splice	24	14
Draganić et al. (2014)	Lap splice	9	0
Može and Beg (2014)	Butt splice	19	8
Teh and Uz (2016)	Lap splice	10	10
Wang et al. (2017)	Butt splice	24	18
This paper	Butt splice	5	5
Total		**899**	**471**

To be included in the database, either the ultimate load, $R_{exp,u}$, or load at ¼-in. deformation, $R_{exp,d}$, must have been recorded. For specimens where $R_{exp,d}$ was not specifically reported, but a plot of the load-deformation response of the connection was provided, the load at ¼-in. deformation was interpolated from the plot. If the specimen reached its peak load prior to attaining ¼-in. deformation, $R_{exp,d}$ was set equal to the ultimate load. Accordingly, $R_{exp,d}$ should be interpreted as a failure load at which peak strength is attained or the connection experiences ¼-in. deformation, whichever occurs first.

Additionally, material testing must have been conducted to determine the tensile strength, F_u, of the connected material in which failure occurred. Only specimens with standard holes were included in the database. A few specimens with slotted holes were identified and were evaluated separately. Connections with composite materials, with cold-formed steel, or subjected to high-temperature testing were not included.

Fields in the database consist of geometric properties (e.g., bolt diameter, plate thicknesses, and edge distances), material properties (e.g., tensile strength and bolt grade), and failure information (e.g., failure mode, $R_{exp,d}$, $R_{exp,u}$, and deformation at $R_{exp,u}$), as well as other relevant information such as bolt installation method.

Only connections categorized as failing in bearing, tearout, or splitting were utilized in this work. The limit state of splitting is distinct from the limit state of tearout. Equations have been proposed to predict splitting strength (Duerr, 2006) and some standards treat tearout and splitting separately (e.g., ASME, 2017). However, splitting is not recognized within the AISC *Specification* (AISC, 2016). Therefore, equations for the limit state of tearout are implicitly covering splitting as well. This approach is justified because experimental results have shown the two limit states to have similar strengths and splitting failures are typically included in the evaluation of the tearout equations, as is done in this work.

Of the 899 specimens in the database, 471 failed in bearing, tearout, or splitting as documented in Table 1. The remaining specimens experienced other failure modes including bolt shear rupture, tensile yielding, tensile rupture, and curling.

Table 2. Test-to-Predicted Ratio Statistics for Various Evaluations of the Load at ¼-in. Deformation for Single-Bolt Specimens (data from 223 specimens, data from 192 specimens meeting minimum edge distance requirements in parentheses)

	C_t	l_x	C_b	Mean TTP	COV TTP
Current equations	1.2	l_c	2.4	1.223 (1.180)	0.186 (0.172)
Current coefficients	1.2	l_{v1}	2.4	0.952 (0.953)	0.137 (0.144)
Current coefficients	1.2	l_{v2}	2.4	0.992 (0.988)	0.140 (0.147)
Optimized coefficients	1.63	l_c	2.29	0.957 (0.934)	0.153 (0.144)
Optimized coefficients	1.17	l_{v1}	2.36	0.975 (0.976)	0.137 (0.144)
Optimized coefficients	1.23	l_{v2}	2.36	0.975 (0.972)	0.137 (0.144)

Strength of Single-Bolt Specimens

Specimens with a single bolt in the direction of force allow for a direct evaluation of individual limit states. These specimens are evaluated separately from specimens with multiple bolts in the direction of force which may experience multiple limit states (e.g., bearing and tearout). Of the 471 specimens in the database with bearing, tearout, or splitting failures, 313 contained a single bolt in the direction of force. Of these single-bolt specimens, $R_{exp,d}$ was available for 223, $R_{exp,u}$ was available for 301, and both loads were available for 211 of the specimens. The analysis included 265 specimens with one bolt perpendicular to the line of force and 48 with two bolts perpendicular to the line of force. These specimens include many that do not meet the minimum edge distances of AISC *Specification* Table J3.4 (AISC, 2016). Additionally, not all specimens met the AISC *Specification* requirement for bolt installation (i.e., installed to a snug-tight condition or pretensioned).

Experimentally obtained strengths are compared to strengths computed from various instances of a generic bearing and tearout strength equation given by Equation 8.

$$R_n = C_t l_x t F_u \leq C_b d t F_u \tag{8}$$

where C_t is the coefficient applied to the tearout strength, C_b is the coefficient applied to the bearing strength, and l_x is the length used for determining tearout strength (i.e., either l_c, l_{v1}, or l_{v2}).

The test-to-predicted ratio (TTP) for each specimen is computed as the ratio of the experimentally obtained strength to the strength from Equation 8 for various selections of C_t, l_x, and C_b. The mean and coefficient of variation (COV) of the test-to-predicted ratio across the specimens is presented in Table 2 for comparisons to the load at ¼-in. deformation and Table 3 for comparisons to the ultimate load. Two values of the mean and COV are presented. The value outside the parentheses includes data from specimens that did not meet the minimum edge distances of AISC *Specification* Table J3.4 (AISC, 2016). The value inside the parentheses excludes specimens that did not meet the minimum edge distances. Note that Table J3.4 has a footnote that permits lesser edge distances, this footnote was not considered in this work.

The data is also presented in Figure 3, where the experimentally obtained strength is normalized against the value of dtF_u and plotted against normalized edge distance. Where the specimen included multiple bolts perpendicular to the direction of load, the experimental strengths were divided by the number of bolts in the connection, n, for plotting purposes.

Optimized coefficients are among the instances of Equation 8 that are compared in Table 2, Table 3, and Figure 3. Six sets of optimized coefficients were computed, one for each of the three tearout lengths (i.e., l_c, l_{v1}, and l_{v2}) at the ultimate and ¼-in. deformation levels. The coefficients were obtained using a numerical optimization to minimize the sum of the square of the difference between the test-to-predicted ratio and unity over all specimens. Single-bolt and multiple-bolt specimens were included in the optimization.

The mean test-to-predicted ratio for the current equations is 1.223 for single-bolt specimens and 1.180 for single-bolt specimens meeting minimum edge distance requirements (Table 2), indicating that current provisions for bearing and tearout are conservative in predicting the load at ¼-in. deformation. This is also seen in Figure 3(b), where most experimental data are above the line representative of current design equations. This is especially true for specimens with smaller edge distances. Either of the two alternative tearout lengths (i.e., l_{v1} or l_{v2}) provides a more accurate and precise assessment of strength when using the current coefficients as seen in both a mean value of the test-to-predicted ratio that is closer to unity and a COV of the test-to-predicted ratio that is lower than for the current equations. However, the use of l_{v1} with current coefficients somewhat overestimates the strength. Results with the optimized coefficients indicate that current coefficients are generally appropriate for use with l_{v1} or l_{v2}.

Similar trends are seen when comparing to the ultimate load (Table 3). A key difference is that the current

Table 3. Test-to-Predicted Ratio Statistics for Various Evaluations of Ultimate Load for Single-Bolt Specimens (data from 301 specimens, data from 234 specimens meeting minimum edge distance requirements in parentheses)					
	C_t	l_x	C_b	Mean TTP	COV TTP
Current equation	1.5	l_c	3	1.065 (1.003)	0.192 (0.140)
Current coefficients	1.5	l_{v1}	3	0.804 (0.812)	0.139 (0.151)
Current coefficients	1.5	l_{v2}	3	0.841 (0.842)	0.133 (0.144)
Optimized coefficients	1.65	l_c	2.95	0.972 (0.921)	0.189 (0.145)
Optimized coefficients	1.16	l_{v1}	3.21	1.009 (1.010)	0.117 (0.128)
Optimized coefficients	1.22	l_{v2}	3.23	1.010 (1.005)	0.120 (0.129)
Rounded coefficients	1.2	l_{v1}	3	0.981 (0.984)	0.119 (0.130)
Rounded coefficients	1.2	l_{v2}	3	1.030 (1.025)	0.120 (0.129)

coefficients with the alternative tearout lengths result in a significant overestimation of strength. Rather, a coefficient of 1.2, the same as is used in the equations for load at the ¼-in. deformation limit state, can provide an accurate prediction of strength with less variation than the current equation.

These results suggest that the difference between the load at ¼-in. deformation and the ultimate load is far smaller than implied by current provisions. Figure 4 shows the ratio $R_{exp,u}/R_{exp,d}$ for single-bolt specimens plotted against the normalized clear distance. The ratio of ultimate load to load at ¼-in. deformation is 1.25 according to the current AISC *Specification* (AISC, 2016) (i.e., the ratio between Equation 4 and Equation 3 equals 1.25). However, the experimental ratios are lower, especially for cases with smaller edge distances. The average ratio of the 211 specimens plotted is 1.05 and only 6 of the specimens have a ratio greater than 1.25.

Strength of Multiple-Bolt Specimens

Of the 471 specimens in the database with bearing, tearout, or splitting failures, 158 have more than one bolt in the direction of force. Of these multiple-bolt specimens, $R_{exp,d}$ was available for 100, $R_{exp,u}$ was available for 136, and both loads were available for 78 of the specimens.

Tables 4 and 5 provide summary statistics for the test-to-predicted ratios computed using the various instances of Equation 8 for multiple-bolt specimens. The values of the COV are approximately the same as those for the single-bolt cases, indicating a good fit of the data. At the ultimate load, when including all specimens, and with rounded coefficients, the mean test-to-predicted ratio is 0.927 for l_{v1} and 0.954 for l_{v2}. These values are lower than that for the single-bolt case and lower than is generally acceptable. A possible reason for this is deformation compatibility between bolts. Achieving the full bearing strength of $3.0dtF_u$ requires significant deformation. It is possible, for example, that by the time the full bearing strength of the interior bolts is achieved, the end bolts have passed their peak strength and contribute only a lower post-peak strength. Nonetheless, when specimens not meeting minimum edge distance and spacing requirements are excluded, the mean test-to-predicted ratios are slightly above unity.

Previous editions of the AISC *Specification* included exceptions to tearout provisions when enough bolts were in a line and certain geometric conditions were met. It was theorized that if the interior bolts fail in bearing, the tearout strength of the end bolt would be less critical. To investigate the effect of neglecting tearout, a test-to-predicted ratio equal to the load at ¼-in. deformation divided by the bearing strength (i.e., the result of Equation 1 times the number of bolts in the connection) is plotted against the normalized clear distance in Figure 5. Only specimens meeting the minimum edge distance and minimum spacing requirements of the current AISC *Specification* (AISC, 2016) are plotted. Specimens that meet the criteria for the tearout exception in the 1993 edition of the AISC *Specification* (AISC, 1993) (i.e., two or more bolts in a line, edge distance greater than 1.5d, and spacing greater than 3d) are differentiated with circular markers. The figure shows significant variation; however, many of the specimens have low test-to-predicted ratios, including several that meet the criteria in the 1993 AISC *Specification*.

To summarize, increased accuracy in predicting tearout strength was achieved using either l_{v1} or l_{v2} with a coefficient on the tearout strength of 1.2. This was shown to be true for both the ultimate load and the load at ¼-in. deformation. Based on these initial results, the remaining analyses are conducted with the following equations for tearout strength:

$$R_n = 1.2 l_{v1} t F_u \tag{9}$$

$$R_n = 1.2 l_{v2} t F_u \tag{10}$$

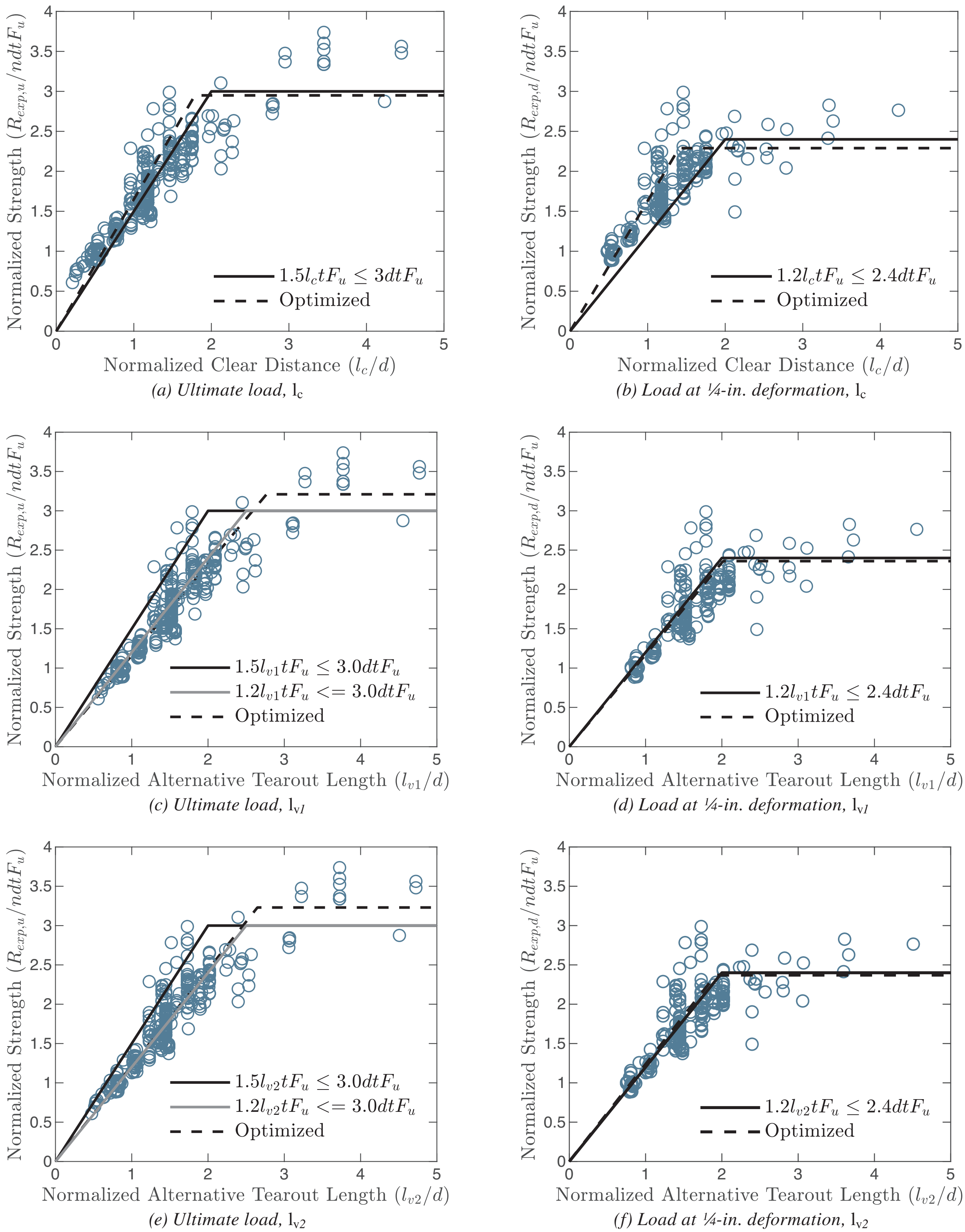

Fig. 3. Normalized strength comparisons between tearout lengths.

Table 4. Test-to-Predicted Ratio Statistics for Various Evaluations of the Load at ¼-in. Deformation for Multiple-Bolt Specimens (data from 100 specimens, data from 62 specimens meeting minimum edge distance and spacing requirements in parentheses)					
	C_t	l_x	C_b	Mean TTP	COV TTP
Current equations	1.2	l_c	2.4	1.137 (1.106)	0.155 (0.159)
Current coefficients	1.2	l_{v1}	2.4	0.973 (1.013)	0.127 (0.126)
Current coefficients	1.2	l_{v2}	2.4	0.992 (1.024)	0.122 (0.127)
Optimized coefficients	1.63	l_c	2.29	1.032 (1.048)	0.122 (0.129)
Optimized coefficients	1.17	l_{v1}	2.36	0.992 (1.033)	0.126 (0.126)
Optimized coefficients	1.23	l_{v2}	2.37	0.995 (1.032)	0.125 (0.127)

Table 5. Test-to-Predicted Ratio Statistics for Various Evaluations of Ultimate Load for Multiple-Bolt Specimens (data from 136 specimens, data from 48 specimens meeting minimum edge distance and spacing requirements in parentheses)					
	C_t	l_x	C_b	Mean TTP	COV TTP
Current equations	1.5	l_c	3	1.011 (1.047)	0.140 (0.172)
Current coefficients	1.5	l_{v1}	3	0.812 (0.951)	0.188 (0.178)
Current coefficients	1.5	l_{v2}	3	0.829 (0.961)	0.182 (0.178)
Optimized coefficients	1.65	l_c	2.95	0.958 (1.029)	0.148 (0.179)
Optimized coefficients	1.16	l_{v1}	3.21	0.937 (1.003)	0.138 (0.164)
Optimized coefficients	1.22	l_{v2}	3.23	0.928 (1.000)	0.140 (0.166)
Rounded coefficients	1.2	l_{v1}	3	0.927 (1.015)	0.145 (0.168)
Rounded coefficients	1.2	l_{v2}	3	0.954 (1.038)	0.144 (0.168)

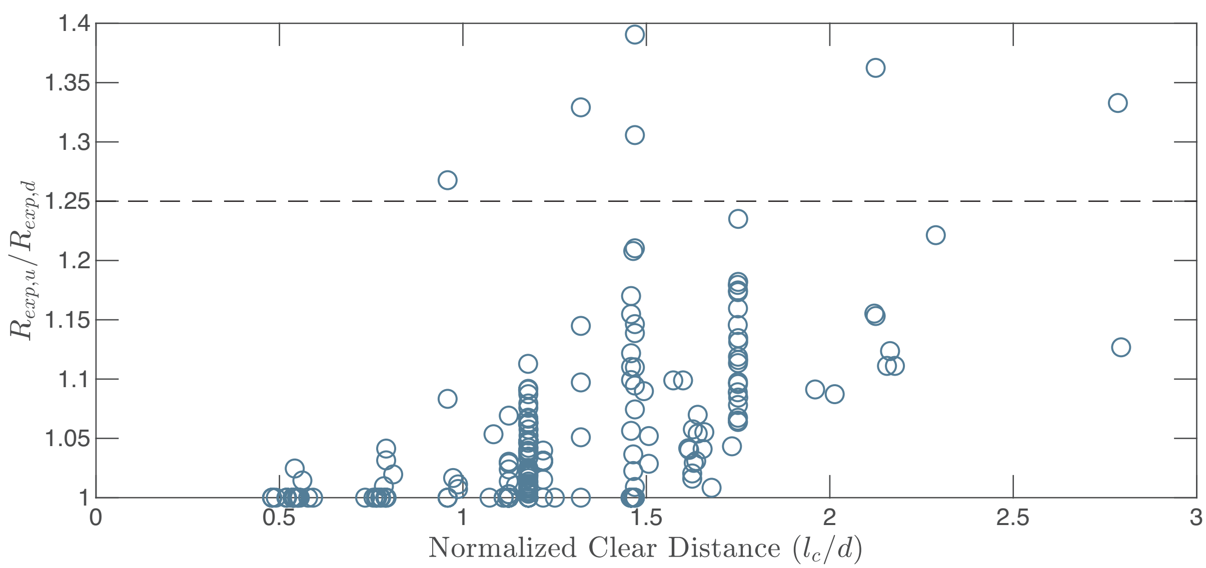

Fig. 4. Ratio of ultimate load to load at ¼-in. deformation versus normalized clear distance.

Table 6. Mean Values of Test-to-Predicted Ratios Based on Level of Tightening			
Load Level	**Pretensioned**	**Snug-Tightened**	**Loose Connection**
Ultimate	1.049	1.023	1.067
¼-in. deformation	1.246	1.197	1.157

Effects of Bolt Tightening

The AISC *Specification* (AISC, 2016) requires that bolts be installed to a snug-tight condition or pretensioned. Many of the experiments in the database utilize untightened bolts or had a gap between the plates. These loose connections do not satisfy the requirements of the AISC *Specification*, but help minimize the contribution of friction to the strength of the connection and better evaluate the strength of the connected material alone.

Frank and Yura (1981) tested connections with different levels of tightening, although loose connections were not considered. They found that specimens with pretensioned bolts had 10% higher strength at ¼-in. deformation when compared to snug-tightened bolts but that the ultimate strength was unaffected by the level of tightening.

Table 6 presents a comparison of experimental strength to strength equations from the current AISC *Specification* (AISC, 2016) for all 471 specimens in the database that failed in bearing, tearout, or splitting. No clearly identifiable trend is seen in the mean test-to-predicted ratios at ultimate load. However, as observed by Frank and Yura (1981), the mean test-to-predicted ratios for the load at ¼-in. deformation tend to increase as the level of tightening increases.

Mixed Failures

Several multiple-bolt specimens tested by Cai and Driver (2008) exhibited mixed failures of bearing or tearout of the end bolts and shear rupture of the interior bolts. This mode of failure is a validation of the premise underlying the use of effective strengths of individual bolts when computing the strength of a bolt group. These specimens were not included in the preceding discussion because they exhibited mixed failures. However, they are examined here to validate the use of the alternative tearout lengths for connections where a mixed failure may occur.

The connected material in which the failures occurred was the web of a wide flange with a measured thickness of 0.36 in. and a measured tensile strength of 74.11 ksi. The connections each had six ¾-in.-diameter bolts (two lines of three) in standard holes. The shear strength of the bolts was measured to be 50.13 kips. Most of these specimens reached their ultimate strength prior to reaching ¼-in. deformation, so only ultimate load was considered. Table 7 summarizes the specimens along with test-to-predicted ratios calculated using different computed strengths.

The test-to-predicted ratios presented in Table 7 were calculated with tearout strength given by the current equation

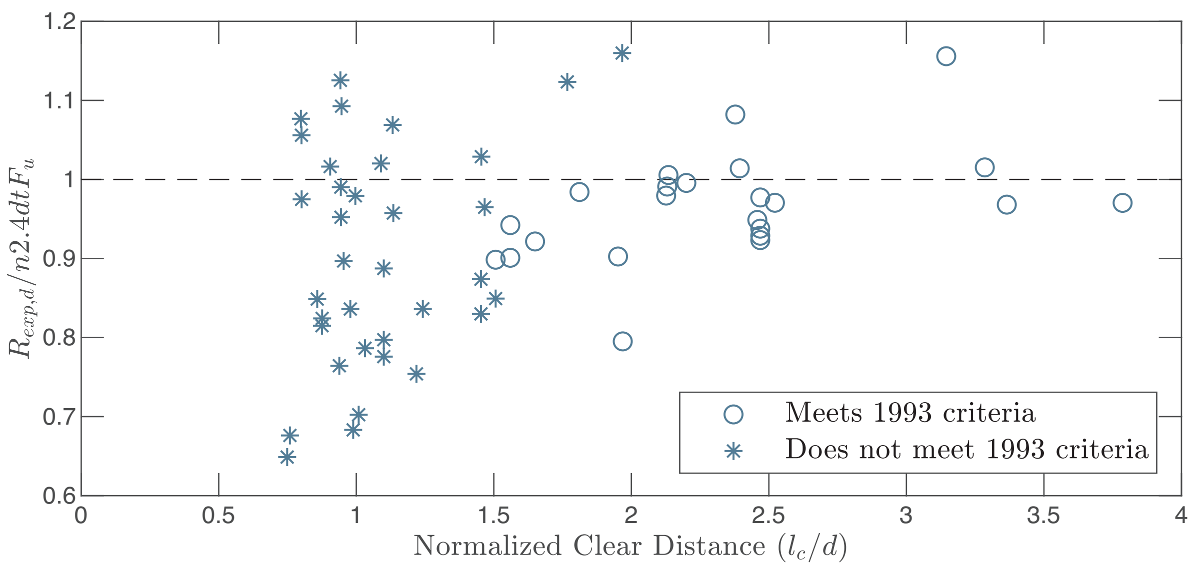

Fig. 5. Test-to-predicted ratio excluding tearout versus normalized clear distance.

Table 7. Analysis of Specimens Tested by Cai and Driver (2008) That Exhibited Mixed Failures						
			Test-to-Predicted Ratio			
Specimen	L_e (kips)	$R_{exp,u}$ (kips)	Using l_c (Eq. 4)[a]	Using l_c (Eq. 4)	Using l_{v1} (Eq. 9)	Using l_{v2} (Eq. 10)
C1E1a	1.00	243.27	0.850	0.981	0.955	0.968
C2E1b	1.00	249.94	0.866	1.005	0.978	0.992
C3E1c	1.00	250.17	0.868	1.007	0.981	0.993
C4E2a	1.25	279.80	0.930	1.044	1.035	1.047
C5E2b	1.26	267.61	0.890	0.993	0.984	0.996
C6E2c	1.26	259.05	0.861	0.965	0.955	0.968
C7E3a	1.50	272.40	0.906	0.946	0.950	0.962
C8E3b	1.50	259.74	0.864	0.903	0.908	0.917
C9E3c	1.51	273.21	0.908	0.947	0.952	0.962
C10E4a	1.76	273.14	0.908	0.908	0.908	0.912
C11E4b	1.75	280.81	0.934	0.934	0.934	0.937
C12E4c	1.75	265.90	0.884	0.884	0.884	0.887
C13E5a	2.00	290.70	0.966	0.966	0.966	0.966
C14E5b	2.00	267.03	0.888	0.888	0.888	0.888
C15E5c	2.01	287.71	0.957	0.957	0.957	0.957
C16E6	2.76	297.49	0.989	0.989	0.989	0.989
		Mean:	0.904	0.957	0.952	0.959

a The predicted strengths for these test-to-predicted ratios were computed without considering potential interaction between the limit states of bearing and tearout and the limit state of shear rupture of the bolt.

(i.e., Equation 4) as well as equations with the alternative tearout lengths (i.e., Equations 9 and 10). Also included in Table 7 are test-to-predicted ratios computed with the predicted strength taken as the lower of the strengths for the bolt group for (1) the limit states of bearing and tearout and (2) the limit state of bolt shear rupture.

The results of these specimens show that it is indeed unconservative to treat bearing and tearout separate from bolt shear rupture, given that doing so results in a 10% overprediction of strength on average. Using this method, specimens C1E1a, C2E1b, and C3E1c were controlled by bearing and tearout strength, and the rest were controlled by bolt shear rupture strength. More accurate but still somewhat unconservative results are obtained when considering the potential of mixed failures and summing the effective strengths of each individual bolt to obtain the strength of the bolt group. Little difference is seen between the use of the clear distance and either of the two alternative tearout lengths, all three result in a 4 to 5% overprediction of strength on average. The remaining error may be due to different bolts achieving their peak strength at different levels of deformation, which is not accounted for in the design equations. Further investigation on deformation compatibility in bolted connections which experience mixed failure is warranted, however, the observed error is small and can be accommodated in the margin of safety.

EXPERIMENTAL STUDY

The evaluation of published experiments showed that tearout equations using l_{v1} and l_{v2} had similarly improved results in comparison to the current equations. The database contains results from hundreds of experiments across a broad range of parameters. However, it only contains specimens with standard holes because the vast majority of concentrically loaded steel bolted connection tests failing in bearing, tearout, or splitting were performed with standard holes.

For connections with standard holes, l_{v1} is greater than l_{v2}. The difference between the two varies only slightly based on the diameter of the bolt, differing by a maximum of 7% for connections that satisfy minimum edge distance requirements and bolts as large as 1.5-in. diameter. The variation is greater, although still relatively small, over a range of hole types. To address this gap in data, a series of experimental tests was conducted to evaluate tearout strength for connections with different hole types.

Test Matrix

Tension tests of 22 single-bolt butt splice connections with different hole types and edge distances were completed. The specimens consisted of two outer pull plates and a single interior test plate as shown in Figure 6. Specimens were designed to fail in bearing, tearout, or splitting of the test plate. Specimens included those with standard holes and holes with minimal clearance, where the value of l_{v1} is greater than l_{v2}. Also included were specimens with oversize holes, holes with ⅛ in. more clearance than oversize holes, and short-slotted holes oriented perpendicular to the load, where the value of l_{v2} is greater than l_{v1}.

The test matrix is presented in Table 8. Two main variables are considered: the type of bolt hole and the edge distance. Four edge distances were investigated for each of the five bolt hole types. Nominal values of the edge distances were 1 in., 1.25 in., 1.5 in., and 2 in. The smallest edge distance (1 in.) is equal to the minimum edge distance permitted by the AISC *Specification* (AISC, 2016) for a ¾-in. bolt in a standard hole. Note that the 1-in. edge distance is not permitted for oversize holes but was used in these tests for consistency. For a ¾-in. bolt in a standard hole, the transition between tearout and bearing occurs at an edge distance of 1.91 in. per current equations. The largest edge distance (2.0 in.) was selected to be somewhat greater than this length and thus provide a comparison to a bearing-controlled failure. Two additional tests beyond the main set of 20 were also completed. Specimen NC2b was a duplicate of NC2a to investigate repeatability. Specimen STD1g

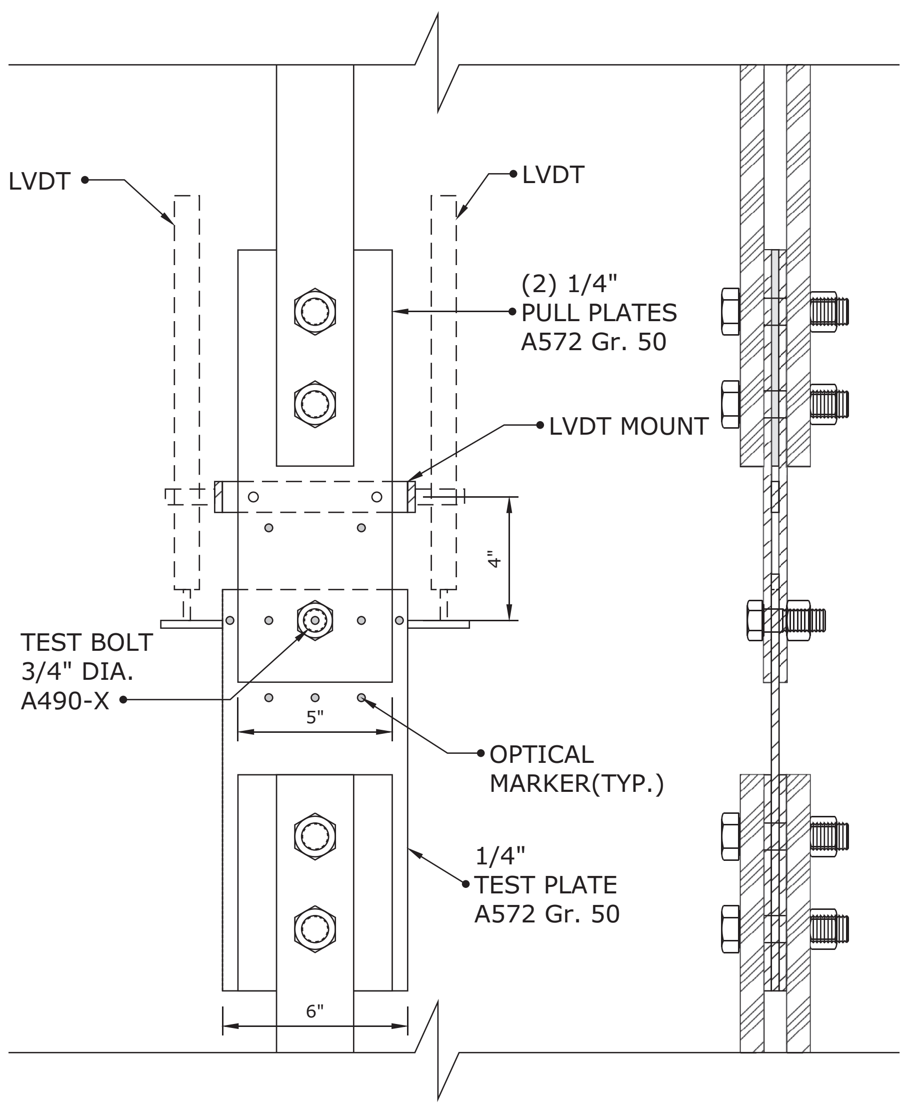

Fig. 6. Experimental test setup.

was a duplicate of STD1, but with the test bolt untightened (instead of in a snug-tight condition) and greased plates to investigate the effect of reduced friction.

Materials and Test Setup

The test plates were ¼-in.-thick ASTM A572 Gr. 50 steel and had a yield strength of 54.5 ksi and a tensile strength of 73.7 ksi, based on the mean of three tensile coupon tests conducted in accordance with ASTM E8 (2016). No special preparation was made to the plate surfaces before testing with the exception of specimen STD1g, where grease was applied to the faying surfaces. The test plates were installed in a universal testing machine and subjected to concentric tension load.

Two linear variable differential transformers (LVDTs) were installed on the test specimen to record movement of the pull plate relative to the test plate over a 4-in. gauge length. The LVDTs recorded the bolt hole deformation as well as elastic deformations of the plates over the gauge length; however, elastic deformations were minimal. An Optotrak optical tracking system was used for supplementary deformation measurements. The optical markers were installed on the test plate, pull plates, and the bolt. Measurements from the optical tracking system were used to verify the LVDT measurements as well as measure elastic elongation of the specimen and pull plate.

After applying a preload of 500 lb to bring the connection into bearing, the test bolt was finger tightened and then brought to a snug-tight condition with a few impacts of an impact wrench. The plies were ensured to be in firm contact. All other bolts were finger tightened. The preload was released prior to applying the main load.

Loading was applied in displacement control at a rate of 0.05 in/min. Most tests were stopped after a near complete loss of load-carrying capacity, typically after one or two loud sounds that likely indicated rupture. To investigate the progression of the failure mechanism, specimens labeled STD1, STD2, STD3, STD4, NC1, NC2b, and SSLT1 were stopped when a steep load drop was seen. Specimen NC2a was stopped even earlier at the first sign of any load drop. All specimens were allowed to achieve their maximum strength.

Results

Load-deformation curves for all specimens are presented in Figure 7. The load at ¼-in. deformation, $R_{exp,d}$, and the ultimate load, $R_{exp,u}$, are presented in Table 8 along with test-to-predicted ratios computed using the current and proposed equations. Measured values were used in calculating the predicted strengths. For specimens with short-slotted holes, l_{v1} was computed graphically with computer-aided drafting software by drawing the specimen using measured dimensions and measuring the length from the edge of the hole to the edge of the material along lines tangent to the bolt. The difficulty in determining l_{v1} in some cases is a drawback for its use in design equations; however, design tables could be developed to alleviate the problem.

Failure Mechanisms

Specimens were disassembled after testing to determine the failure mechanism. Upon disassembly, it was observed that most specimens had a splitting tear as well as shear rupture in the connected material along one or both sides of the bolt hole. For specimens with smaller edge distances (i.e., nominal edge distances of 1 in. and 1.25 in.), the splitting tear extended to the bolt hole, as shown in Figure 8(a). For specimens with larger edge distances, the split did not extend all the way to the bolt hole, as shown in Figure 8(b). Specimens STD4, NC4, STD1g, and NC2b did not exhibit any splitting.

For all specimens that exhibited splitting, it is likely that the initiation of splitting occurred prior to shear rupture in the connected material and coincided with the peak load. Testing of specimen NC2a was stopped shortly after the peak load was attained. Upon disassembly, the initiation of a splitting tear was observed, but no initiation of shear rupture in the connected material was observed. Interestingly, the duplicate specimen, NC2b, did not exhibit splitting failure and achieved a 6% lower strength. The initiation of splitting is seen in the load-deformation curves as a dip that occurs after peak load and flattens out prior to the steeper tearout shear rupture, as depicted in Figure 7.

Strength Evaluation

The means of the test-to-predicted ratios were calculated for each hole type to compare the accuracy of each tearout length, shown in Tables 9 and 10 for the ¼-in. deformation limit state and ultimate limit state, respectively.

The results of Tables 9 and 10 verify the trends identified in the analysis of the previously published experiments. The current tearout equation underestimates the load at ¼-in. deformation, which is much closer to the ultimate load than the equations imply. For load at ¼-in. deformation, differences between the equations using l_{v1} and l_{v2} are shown to be minimal for standard and oversize holes, and both were more accurate than the current equation. Across all hole types, the proposed equation with l_{v1} showed less variation but was unconservative for holes with minimal clearance. The strength of short-slotted holes was underpredicted by the equation using l_{v2}.

Frank and Yura (1981) tested four specimens with long-slotted holes oriented perpendicular to the load. They observed that the initial stiffness and load at ¼-in. deformation was reduced when compared to standard holes but that the ultimate strength, which was controlled by bearing for these specimens, was not reduced. As seen in Figure 7,

Table 8. Test Matrix

		Measured Properties						At ¼-in. Deformation				At Ultimate			
Name	Hole Type	L_e in.	l_c in.	l_{v1} in.	l_{v2} in.	l_{v1}/l_{v2}	d_h in.	$R_{exp,d}$ kips	TTP Using l_c (Eq. 4)	TTP Using l_{v1} (Eq. 9)	TTP Using l_{v2} (Eq. 10)	$R_{exp,u}$ kips	TTP Using l_c (Eq. 4)	TTP Using l_{v1} (Eq. 9)	TTP Using l_{v2} (Eq. 10)
STD1	Standard	1.02	0.615	0.861	0.818	1.052	0.812	19.9*	1.451	1.036	1.091	19.9	1.160	1.036	1.091
STD1g[1]	Standard	0.99	0.578	0.818	0.784	1.044	0.823	17.6	1.359	0.960	1.002	17.8	1.098	0.970	1.012
STD2	Standard	1.16	0.750	0.992	0.954	1.039	0.817	22.9*	1.378	1.042	1.083	22.9	1.103	1.042	1.083
STD3	Standard	1.56	1.157	1.403	1.361	1.031	0.815	31.4*	1.217	1.003	1.034	31.4	0.973	1.003	1.034
STD4	Standard	2.01	1.605	1.846	1.810	1.020	0.818	37.9	1.128	0.912	0.930	43.8	1.042	1.053	1.074
NC1	No clearance	1.03	0.650	0.983	0.838	1.173	0.753	20.7*	1.412	0.933	1.095	20.7	1.129	0.933	1.095
NC2a	No clearance	1.32	0.945	1.278	1.133	1.128	0.752	28.9	1.366	1.010	1.139	29.0	1.097	1.014	1.144
NC2b[2]	No clearance	1.27	0.901	1.240	1.087	1.140	0.744	26.4	1.291	0.939	1.070	27.4	1.070	0.972	1.108
NC3	No clearance	1.56	1.185	1.527	1.373	1.112	0.752	33.2	1.248	0.969	1.078	34.0	1.021	0.990	1.101
NC4	No clearance	2.03	1.661	2.015	1.848	1.091	0.747	41.0	1.218	0.974	0.983	42.4	1.009	1.009	1.019
OVS1	Oversize	1.05	0.584	0.769	0.819	0.940	0.938	20.0	1.537	1.167	1.097	20.3	1.246	1.182	1.111
OVS2	Oversize	1.28	0.813	1.000	1.045	0.957	0.928	24.0	1.298	1.055	1.010	24.4	1.053	1.070	1.024
OVS3	Oversize	1.54	1.079	1.266	1.311	0.965	0.929	29.8	1.223	1.042	1.006	31.0	1.018	1.084	1.047
OVS4	Oversize	2.05	1.590	1.781	1.821	0.978	0.923	36.7	1.088	0.914	0.894	42.0	0.995	1.045	1.022
XOVS1	Extra oversize	0.96	0.427	0.580	0.693	0.838	1.062	14.1*	1.487	1.094	0.917	14.1	1.189	1.094	0.917
XOVS2	Extra oversize	1.29	0.766	0.920	1.030	0.893	1.056	23.3	1.360	1.132	1.012	24.2	1.131	1.177	1.051
XOVS3	Extra oversize	1.51	0.983	1.138	1.247	0.913	1.054	26.2	1.198	1.035	0.945	27.1	0.992	1.071	0.977
XOVS4	Extra oversize	2.04	1.506	1.661	1.771	0.938	1.058	34.7	1.042	0.938	0.880	36.8	0.885	0.996	0.935
SSLT1	Short slot	1.02	0.616	0.730	0.819	0.891	0.812×0.994	18.1*	1.316	1.110	0.990	18.1	1.053	1.110	0.990
SSLT2	Short slot	1.31	0.900	1.015	1.104	0.919	0.816×0.997	21.4	1.096	0.974	0.893	21.8	0.894	0.992	0.911
SSLT3	Short slot	1.56	1.151	1.267	1.353	0.936	0.809×0.990	29.1	1.141	1.038	0.971	29.2	0.917	1.042	0.974
SSLT4	Short slot	2.10	1.700	1.814	1.901	0.954	0.803×0.992	35.0	1.041	0.858	0.833	40.7	0.971	1.000	0.971

* Ultimate load reached prior to 1/4-in. deformation.
1 Duplicate test but bolt was left untightened and plates were greased.
2 Duplicate test to verify repeatability.

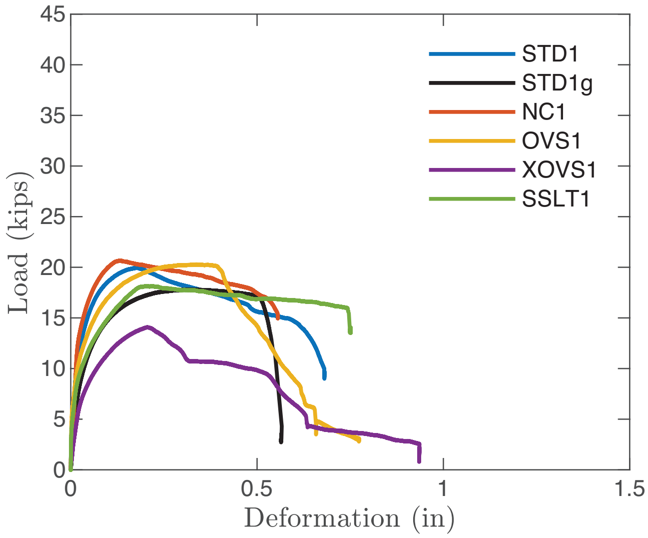

(a) Specimens with nominal edge distance of 1 in.

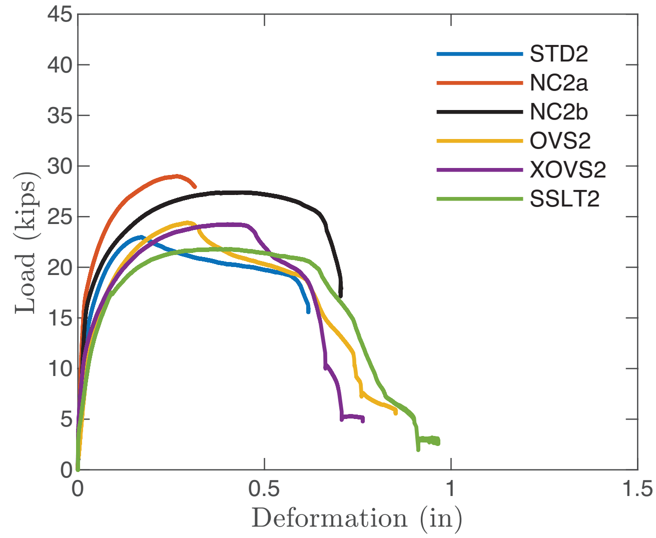

(b) Specimens with nominal edge distance of 1.25 in.

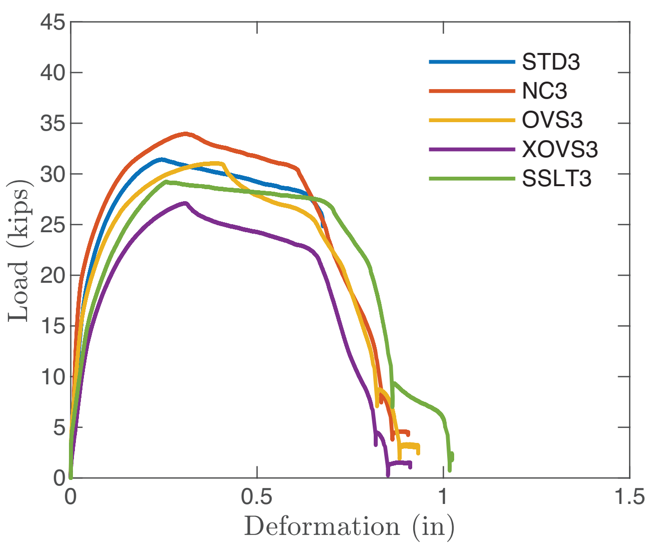

(c) Specimens with nominal edge distance of 1.5 in.

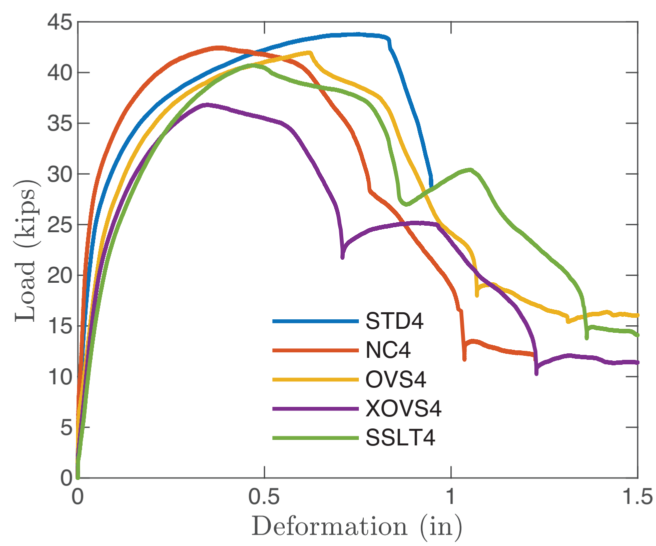

(d) Specimens with nominal edge distance of 2 in.

Fig. 7. Load-deformation curves for experimental tests.

Table 9. Mean Test-to-Predicted Ratio at the ¼-in. Deformation Limit State			
Hole Type	Using I_c (Eq. 3)	Using I_{v1} (Eq. 9)	Using I_{v2} (Eq. 10)
All	1.264	1.008	0.998
STD	1.293	0.998	1.035
NC	1.307	0.965	1.073
OVS	1.286	1.044	1.002
XOVS	1.272	1.050	0.938
SSLT	1.149	0.994	0.922

Table 10. Mean Test-to-Predicted Ratio at the Ultimate Limit State			
Hole Type	Using I_c (Eq. 3)	Using I_{v1} (Eq. 9)	Using I_{v2} (Eq. 10)
All	1.045	1.044	1.032
STD	1.070	1.034	1.071
NC	1.065	0.984	1.093
OVS	1.078	1.095	1.051
XOVS	1.049	1.085	0.970
SSLT	0.958	1.035	0.961

(a) Specimen OVS2 after testing *(b) Specimen OVS3 after testing*

Fig. 8. Photographs of specimens after testing.

the initial stiffness of the specimens with short-slotted holes was among the lowest of those tested in this work. However, both $R_{exp,d}$ and $R_{exp,u}$ were lower for the specimens with short-slotted holes than for the specimens with standard holes.

Although the mean test-to-predicted ratios for the ultimate limit state appear to be accurate for the current equation (Table 10), the results are not consistent across edge distances. This is seen by plotting the test-to-predicted ratios of all tested specimens using the current equation along with the proposed equation using l_{v1} (Figure 9). The linear best-fit lines depict the inconsistency at the ultimate limit state of the current equation across edge distances in comparison to the proposed equation, evident throughout different hole types.

Effect of Bolt Tightening

All but one specimen was tested with the bolt installed to a snug-tight condition. The exception was specimen STD1g, which was nominally identical to STD1 but with the bolt installed loose and grease applied to the faying surfaces so as to investigate the effect of friction. The load-deformation response of specimens STD1g and STD1 is presented in Figure 10.

Several observations can be made from this pair of specimens: (1) The greased specimen was less stiff than the snug-tightened specimens; (2) the load at ¼-in. deformation was 13% greater for the snug-tightened specimen than for the greased specimen; (3) the ultimate load was 12% greater for the snug-tightened specimen than for the greased specimen; and (4) splitting was observed for the snug-tightened specimen, but not the greased specimen.

While these observations were made for a single pair of specimens, the increase in $R_{exp,d}$ corresponds to the increase seen in previous testing data (Table 6). However, the increase in $R_{exp,u}$ was not seen in previous testing data. Also, it is not clear why different failure modes occurred for the two specimens.

RECOMMENDED STRENGTH EQUATIONS

Through the evaluation of existing and new experimental data presented in this work, it was determined that (1) the difference between ultimate load and load at ¼-in. deformation for specimens failing in tearout is less than implied by current equations, (2) current equations for tearout strength underpredict the load at ¼-in. deformation, and (3) current equations are not consistent across edge distances and tend to underpredict the strengths at smaller edge distances. Accordingly, increased accuracy in design can be achieved by replacing AISC *Specification* Equations J3-6c and J3-6d (AISC, 2016) with Equation 9, which utilizes l_{v1}. The equation with l_{v1} was selected since it provides somewhat better results over a wider range of types of bolt holes, particularly short-slotted holes. The same equation but with l_{v2} in lieu of l_{v1} (i.e., Equation 10) would provide similar benefits, and the relative simplicity of calculating l_{v2} may be preferable. A reliability analysis performed in other work confirmed both Equations 9 and 10 to provide a consistent and sufficient level of reliability (Franceschetti, 2020).

An example of the difference between the current and proposed equations is seen in Figure 11. The plotted case is for a single ¾-in.-diameter bolt in a standard hole. The minimum edge distance permitted by the AISC *Specification*

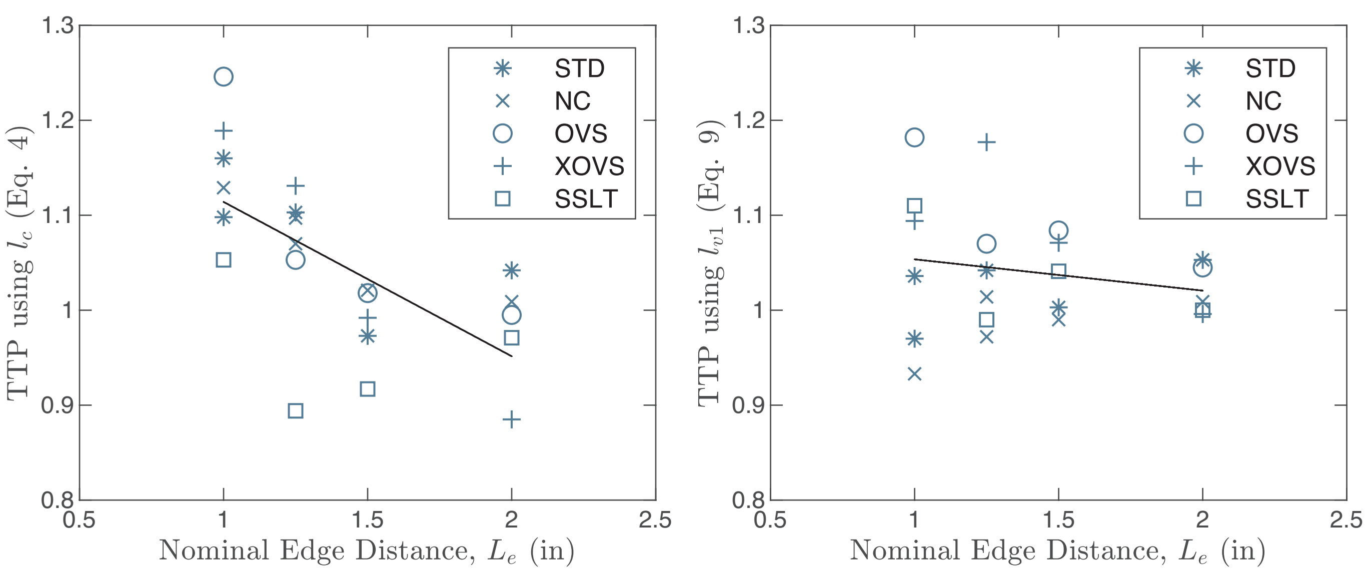

Fig. 9. Test-to-predicted ratios at ultimate limit state with best fit lines.

(1 in.) is shown with a dashed vertical line. Figure 11(a) demonstrates that the equations with the alternative tearout lengths (i.e., Equations 9 and 10) offer additional strength compared to the current equation when deformation at the bolt hole at service load is a design consideration. The difference in strength when deformation at the bolt hole at service load is not a design consideration is less.

While Equation 9 provides increased accuracy over current equations, the computation of the alternative tearout lengths is somewhat more complicated than the computation of the clear distance. This is especially true for eccentrically loaded bolt groups, which are not covered in this work but pose a challenge since the direction of force varies from bolt to bolt. Neither of the alternative tearout lengths have been validated for loads at an angle. The simplicity of the clear distance may continue to be desirable for these situations.

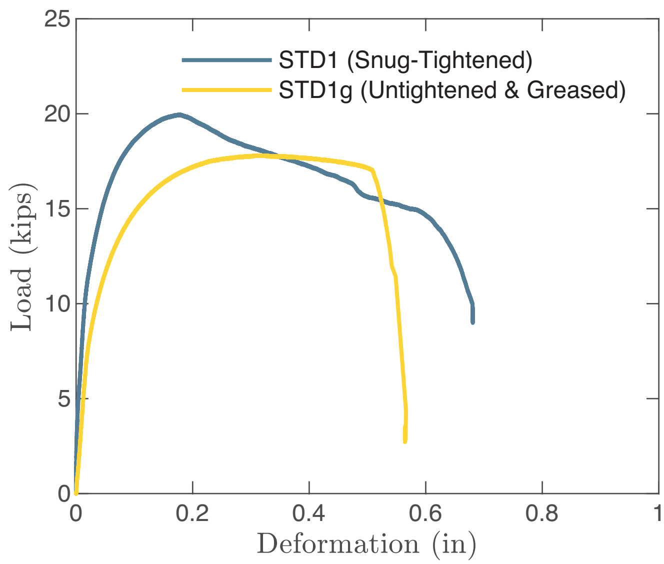

Fig. 10. Snug-tightened specimen versus untightened and greased specimen.

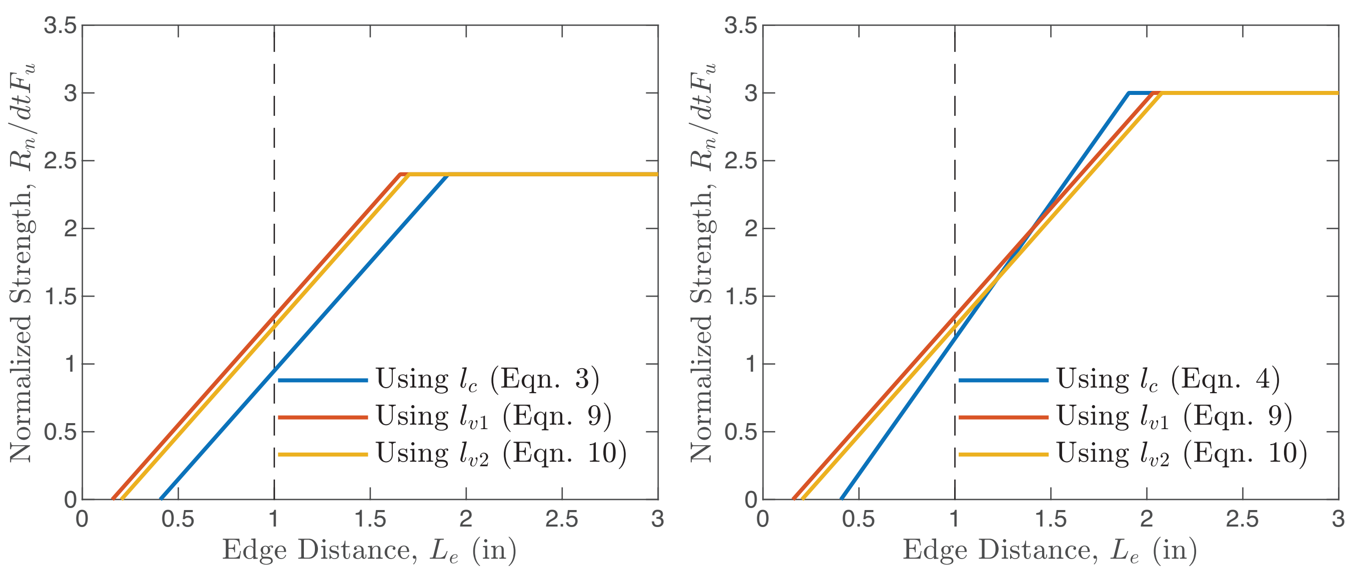

(a) When deformation at the bolt hole at service load is a design consideration

(b) When deformation at the bolt hole at service load is not a design consideration

Fig. 11. Comparison of bearing and tearout strength equations for a ¾-in.-diameter bolt in a standard hole.

CONCLUSIONS

A multifaceted investigation of the limit state of tearout and its impact on design of steel bolted connections has been conducted. Previously published experimental data was evaluated and supplemented with new experimental data to assess the accuracy of current provisions as well as potential alternative provisions. The following conclusions can be made from this work:

- Tearout affects the strength of bolt groups, even for cases of multiple bolts in a row.
- The current equation for tearout strength when deformation at the bolt hole at service load is a design consideration (i.e., load at ¼-in. deformation) is conservative, especially for shorter edge distances.
- The difference between load at ¼-in. deformation and ultimate load for the limit state of tearout is smaller than implied by current provisions.
- Bolt tightening increases the load at ¼-in. deformation. No clear effect of bolt tightening was found on the ultimate load.
- Two alternative tearout lengths, l_{v1} and l_{v2}, were investigated for their potential to improve the accuracy of design equations. Strength equations using these alternative tearout lengths were found to be more accurate than the current equations, which use the clear distance, l_c.
- Design equations with l_{v1} and l_{v2} are similarly accurate for connections with standard and oversize holes. The design equation using l_{v2} was found to be somewhat unconservative for short-slotted holes and holes with clearance greater than oversize. The design equation using l_{v1} was found to be accurate over the entire range of hole types investigated.
- Calculation of l_{v1} is more complicated than l_{v2}, especially for noncircular holes.
- Based on these observations, Equation 9 is recommended for the assessment of tearout strength in concentrically loaded connections. Additional development and validation is necessary for eccentrically loaded connections.

SYMBOLS

C_b Coefficient applied to the bearing strength

C_t Coefficient applied to the tearout strength

F_u Tensile strength of the connected material, ksi

L_e Edge distance measured from center of bolt hole, in.

$R_{exp,d}$ Experimentally determined load at ¼-in. deformation, kips

$R_{exp,u}$ Experimentally determined ultimate load, kips

R_n Nominal strength of connection, kips

d Bolt diameter, in.

d_h Bolt hole diameter, in.

l_c Clear distance from bolt hole edge, in.

l_{v1} Alternative tearout length proposed by Kamtekar (2012), in.

l_{v2} Alternative tearout length proposed by Clements and Teh (2013), in.

l_x General tearout length variable, in.

n Number of bolts

t Thickness of the connected material, in.

ACKNOWLEDGMENTS

Funding for this work was provided by the American Institute of Steel Construction (AISC). The opinions expressed in this work are those of the authors and do not necessarily reflect the views of AISC.

REFERENCES

AISC (1936), *Specification for the Design, Fabrication and Erection of Structural Steel for Buildings*, American Institute of Steel Construction, New York, N.Y.

AISC (1993), *Load and Resistance Factor Design Specification for Structural Steel Buildings*, American Institute of Steel Construction, Chicago, Ill.

AISC (1999), *Load and Resistance Factor Design Specification for Structural Steel Buildings*, American Institute of Steel Construction, Chicago, Ill.

AISC (2010), *Specification for Structural Steel Buildings*, ANSI/AISC 360-10, American Institute of Steel Construction, Chicago, Ill.

AISC (2016), *Specification for Structural Steel Buildings*, ANSI/AISC 360-16, American Institute of Steel Construction, Chicago, Ill.

ASME (2017), *Design of Below-the-Hook Lifting Devices*, American Society of Mechanical Engineers, New York, N.Y.

ASTM E8/E8M-16ae1 (2016), *Standard Test Methods for Tension Testing of Metallic Materials*, ASTM International, West Conshohocken, Pa.

Brown, J.D., Lubitz, D.J., Yavor, C.C., Frank, K.H., and Keating, P.B. (2007), *Evaluation of Influence of Hole Making upon the Performance of Structural Steel Plates and Connections*, Center for Transportation Research, The University of Texas, Austin, Texas.

Cai, Q. and Driver, R.G. (2008), *End Tear-Out Failures of Bolted Tension Members*, Structural Engineering Report No. 278, University of Alberta, Edmonton, Alberta.

Clements, D.D.A. and Teh, L.H. (2013), "Active Shear Planes of Bolted Connections Failing in Block Shear," *Journal of Structural Engineering*, Vol. 139, No. 3, pp. 320–327.

Draganić, H., Dokšanović, T., and Markulak, D. (2014), "Investigation of Bearing Failure in Steel Single Bolt Lap Connections," *Journal of Constructional Steel Research*, Vol. 98, pp. 59–72.

Duerr, D. (2006), "Pinned Connection Strength and Behavior," *Journal of Structural Engineering*, Vol. 132, No. 2, pp. 182–194.

Elliott, M.D., Teh, L.H., and Ahmed, A. (2019), "Behaviour and Strength of Bolted Connections Failing in Shear," *Journal of Constructional Steel Research*, Vol. 153, pp. 320–329.

Franceschetti, N. (2020), "Evaluation of Bolted Connections Susceptible to Tearout," MS Thesis, University of Tennessee, Knoxville, Knoxville, Tenn.

Frank, K.H., and Yura, J. (1981), *An Experimental Study of Bolted Shear Connections*, Report No. FHWA/RD-81/148, Department of Transportation, Washington, D.C.

Freitas, S.T.D. (2005), "Experimental Research Project on Bolted Connections in Bearing for High Strength Steel," Thesis, Delft University of Technology, Delft.

Gillett, P.E. (1978), "Ductility and Strength of Single Plate Connections," PhD Dissertation, The University of Arizona, Tucson, Ariz.

Kamtekar, A.G. (2012), "On the Bearing Strength of Bolts in Clearance Holes," *Journal of Constructional Steel Research*, Vol. 79, pp. 48–55.

Karsu, B. (1995), "The Load Deformation Response of Single Bolt Connections," MS Thesis, Virginia Polytechnic Institute and State University, Blacksburg, Va.

Kim, H.J., and Yura, J.A. (1999), "The Effect of Ultimate-to-Yield Ratio on the Bearing Strength of Bolted Connections," *Journal of Constructional Steel Research*, Vol. 49, No. 3, pp. 255–269.

Lewis, B.E., and Zwerneman, F.J. (1996), *Edge Distance, Spacing, and Bearing in Bolted Connections*, Oklahoma State University, Stillwater, Okla.

Može, P. and Beg, D. (2010), "High Strength Steel Tension Splices with One or Two Bolts," *Journal of Constructional Steel Research*, Vol. 66, No. 8-9, pp. 1,000–1,010.

Može, P. and Beg, D. (2011), "Investigation of High Strength Steel Connections with Several Bolts in Double Shear," *Journal of Constructional Steel Research*, Vol. 67, No. 3, pp. 333–347.

Može, P. and Beg, D. (2014), "A Complete Study of Bearing Stress in Single Bolt Connections," *Journal of Constructional Steel Research*, Vol. 95, pp. 126–140.

Puthli, R. and Fleischer, O. (2001), "Investigations on Bolted Connections for High Strength Steel Members," *Journal of Constructional Steel Research*, Vol. 57, No. 3, pp. 313–326.

Rex, C.O., and Easterling, W.S. (2003), "Behavior and Modeling of a Bolt Bearing on a Single Plate," *Journal of Structural Engineering*, Vol. 129, No. 6, pp. 792–800.

Salmon, C.G., Johnson, J.E., and Malhas, F.A. (2009), *Steel Structures: Design and Behavior*, 5th Edition, Pearson Prentice Hall, Upper Saddle River, N.J.

Sarkar, D. (1992), "Design of Single Plate Framing Connections," Thesis, University of Oklahoma, Norman, Okla.

Teh, L.H., and Uz, M.E. (2016), "Combined Bearing and Shear-Out Capacity of Structural Steel Bolted Connections," *Journal of Structural Engineering*, Vol. 142, No. 11.

Udagawa K. and Yamada T. (1998), "Failure Modes and Ultimate Tensile Strength of Steel Plates Jointed with High-Strength Bolts," *Journal of Structural and Construction Engineering (Transactions of AIJ)*, Vol. 63, No. 505, pp. 115–122.

Udagawa, K. and Yamada, T. (2004), "Ultimate Strength and Failure Modes of Tension Channels Jointed with High-Strength Bolts," *Proceedings of the 13th World Conference on Earthquake Engineering,* Vancouver, British Columbia.

Wang, Y.-B., Lyu, Y.-F., Li, G.-Q., and Liew, J.Y.R. (2017), "Behavior of Single Bolt Bearing on High Strength Steel Plate," *Journal of Constructional Steel Research*, Vol. 137, pp. 19–30.

Determination of Second-Order Effects and Design for Stability Using the Drift Limit

RAFAEL SABELLI, LARRY GRIFFIS, and LOUIS F. GESCHWINDNER

ABSTRACT

Buildings for which second-order effects are significant are often governed by drift limits. Amplifier-based approximate second-order analysis, as presented in AISC *Specification* Appendix 8 (2016), typically utilizes factors based on first-order drift, for which a preliminary design and an analysis are required. This paper derives equations for the amplifier used in approximate second-order analysis, B_2, based on the second-order drift. Upper-bound values of amplifiers based on the drift limit can thus be determined in advance of design, eliminating the need for iteration and simplifying the design process; these values are not excessively conservative for drift-governed designs.

Keywords: stability design, drift limit, second-order analysis, amplifier.

INTRODUCTION

This paper presents methods for utilizing information known in advance of member selection (loading, frame geometry, and drift limits) to determine upper-bound values of the B_2 amplifier used in approximate second-order analysis [defined in of the AISC *Specification* Appendix 8 (2016)]. The paper defines a second-order stability index that can be determined based on the drift limit and that can be used to calculate the B_2 amplifier. Two examples applying the second-order stability index are presented. The first is design example, consisting of member selection to meet both drift and strength criteria. The second is a hand calculation to confirm the validity of the results of a computer second-order analysis of a multi-story building.

SECOND-ORDER DRIFT

Many structures (especially moment frame structures) are drift controlled, meaning that the governing consideration in member selection is achieving sufficient system stiffness to meet a drift limit or limit deformations to prevent damage to key building components such as cladding or partitions. Such buildings are generally only as stiff as necessary to meet these requirements. Second-order effects tend to be significant for such flexible, drift-governed buildings, and many engineers use a limit such as 1.5 on second-order effects to ensure designs are not overly sensitive to loading and modeling assumptions. Because the second-order drift is the expected drift under a given set of load conditions, it is the appropriate quantity to limit in order to achieve acceptable performance.

Second-order effects reduce the stiffness of structures and thus increase the drift for a given applied lateral load. This reduction in system stiffness depends on the vertical load present, and at service levels, the effect is much smaller than under strength-level vertical loads. Nevertheless, there are many cases in which second-order effects are significant at service-load levels (LeMessurier, 1977; Griffis and White, 2013). Additionally, for seismic design (and for drift-sensitive safety conditions in wind design), drift under full design loads must be determined.

The ASCE/SEI-7 standard explicitly requires consideration of the second-order effect for seismic design (ASCE, 2016), and the ASCE *Prestandard for Performance-Based Wind Design* (ASCE, 2019) requires it for wind. The principles of mechanics require consideration of second-order effects, regardless of explicit treatment in building codes. It is recommended that second-order effects always be included in the calculation of drifts unless they can reliably be discounted.

Judgment-based drift limits for wind have historically been used in conjunction with first-order drift to achieve acceptable performance. This practice precedes the advent of reliable second-order analysis with finite-element analysis programs. Such an evaluation using first-order deformations may result in acceptable performance for buildings with a low to moderate second-order magnification, but for buildings with significantly higher second-order effects, it is effectively a much more permissive criterion and may

Rafael Sabelli, SE, Director of Seismic Design, Walter P Moore, San Francisco, Calif. Email: rsabelli@walterpmoore.com (corresponding)

Larry Griffis, PE, Senior Consultant, Walter P Moore, Austin, Texas. Email: lgriffis@walterpmoore.com

Louis F. Geschwindner, PhD, PE, Senior Engineer, Providence Engineering Corporation, and Professor Emeritus, Architectural Engineering, The Pennsylvania State University, State College, Pa. Email: lfg@psu.edu

Paper No. 2020-09

lead to unacceptable performance. Additionally, the first-order drift may not be sufficiently accurate for comparison to the quantified strain capacity of cladding systems, interior partitions, or other drift-sensitive building components. AISC Design Guide 3, *Serviceability Design Considerations for Steel Buildings,* (West et al., 2003) provides guidance on such drift-sensitive components.

In this study, second-order drifts are compared to drift limits, and therefore the phrase “drift limit” should be understood as such; the concept of a first-order drift limit is not adopted. Using second-order drifts and deformations for comparison to drift limits and deformation capacities of cladding and partitions will provide a more consistent criterion across the full range of second-order effects (Griffis, 1993; Aswegan et al., 2015).

Many engineers find the use of amplifiers for approximate second-order analysis expedient and appropriate for their structures. Methods of determining force and displacement amplifiers based on first-order drift may give very approximate results or require iteration. Determination of amplifiers in advance of design using the drift limit can eliminate the need for iteration, simplifying the design process. Such a process is illustrated in the design example in Appendix C of the paper by Sabelli (2020); the equations used in that example have been further refined in Sabelli and Griffis (2021).

While the equations and methods developed are applicable to structures with braced frames and mixed (dual) systems, the considerations addressed are most significant for moment-frame structures. Importantly, the amplifiers determined using the drift limit are reasonable, upper-bound estimates for drift-governed buildings (as is common for moment frames) but become unreasonably conservative for buildings much stiffer than required.

For buildings in which the deformation imposed on deformation-sensitive elements does not correlate to story drift, application of drift-based methods such as proposed here may be impractical.

AMPLIFIERS FOR APPROXIMATE SECOND-ORDER ANALYSIS AND DESIGN FOR STABILITY

Second-Order Effects and First-Order Displacements

Second-order effects can be expressed using a system “stability index,” which relates the geometric and mechanical stiffness. AISC Design Guide 28, *Stability Design of Steel Buildings,* (Griffis and White, 2013) defines the stability index, Q (shown here as Q_1, indicating that it uses first-order displacement):

$$Q_1 = \frac{P_{story}\Delta_1}{R_M HL} \tag{1}$$

where

H = first-order shear, kips

L = story height, in.

P_{story} = total gravity load, $P_{mf} + P_{lean}$, at LRFD level, kips

Q_1 = first-order stability index

R_M = stiffness-reduction coefficient to account for member P-δ influence on structure P-Δ

Δ_1 = first-order story drift corresponding to load H (Δ_H in the *Specification*), in.

and where

P_{lean} = gravity load on non-moment-frame columns, kips

P_{mf} = gravity load on moment-frame columns, kips

The AISC *Specification* ASD/LRFD adjustment factor α is omitted from the gravity-load definitions for brevity.

It should be noted that the stability index Q_1 defined here follows Griffis and White (2013) and includes the R_M coefficient; other literature has not consistently included this coefficient. AISC *Specification* Appendix 8, Equation A-8-8, for R_M is:

$$R_M = 1 - 0.15\frac{P_{mf}}{P_{story}} \tag{2}$$

See Sabelli and Griffis (2021) for a more accurate equation for R_M.

The force amplifier as presented in AISC *Specification* Appendix 8 utilizes the same quantities as does the stability index Q_1:

$$B_2 = \frac{1}{1 - \dfrac{P_{story}\Delta_1}{R_M HL}} \tag{3}$$

where

B_2 = amplifier for second-order effect

This amplifier can be expressed as a function of the stability index defined previously by combining Equations 1 and 3:

$$B_2 = \frac{1}{1 - Q_1} \tag{4}$$

Determination of amplification using Equation 4 requires a first-order drift, which typically is determined from a preliminary design and an analysis. AISC *Steel Construction Manual* Part 2 (2017) provides the “simplified method,” whereby the first-order drift is assumed to be equal to the drift limit, and thus an amplifier can be obtained prior to design (Carter and Geschwindner, 2008), although iteration may be required.

Second-Order Effects and Second-Order Displacements

While the simplified method of utilizing the drift limit as the first-order drift results in a reasonable, liberal estimate of the amplifier, a more accurate estimate can be obtained using methods based on second-order drift. Prior to design, the structure can be assumed to be exactly stiff enough to meet the drift limit, and the amplification can be determined by setting the target second-order drift equal to that drift limit. This method is elaborated below, following work done by Statler et al. (2011).

Sabelli and Griffis (2021) present the force amplifier B_2 as a function of the second-order drift based on the equilibrium in the deformed condition:

$$B_2 = 1 + \frac{P_{story}\Delta_2}{HL} \tag{5}$$

where

Δ_2 = second-order story drift

Additionally, Sabelli and Griffis show that Equations 3 and 5 and have as a corollary the following expression for drift amplification:

$$\frac{\Delta_2}{\Delta_1} = \frac{B_2}{R_M} \tag{6}$$

Sabelli and Griffis note, however, that Equation 6 requires use of a more accurate equation for R_M than Equation 2. For structures with low to moderate second-order effects, the value of R_M (determined per Sabelli and Griffis) is close to 1.0, and drift amplification can be approximated by:

$$\frac{\Delta_2}{\Delta_1} \approx B_2 \tag{7}$$

For convenience, a stability index Q_2 based on the second-order drift is defined here:

$$Q_2 = \frac{P_{story}\Delta_2}{HL} \tag{8}$$

where

Q_2 = second-order stability index

This index differs from Q_1 because Q_2 uses the second-order drift, Δ_2, in lieu of the first-order drift, Δ_1. Additionally, the coefficient R_M (which accounts for member P-δ influence on structure P-Δ) does not directly figure into Q_2, but contributes to the reduced stiffness that results in the displacement Δ_2 by means of inclusion of member P-δ effects in the analysis.

The force amplifier can be expressed thus by combining Equations 5 and 8:

$$B_2 = 1 + Q_2 \tag{9}$$

Equation 9 can thus be used to determine the force amplifier based on the second-order drift, which can be assumed to equal the drift limit for approximate analysis of drift-governed buildings.

Combining Equations 4 and 9, the two indices are related by the force amplifier:

$$Q_2 = B_2 Q_1 \tag{10}$$

Design for Stability Using Drift Limit

Incorporating the preceding methods, the "indirect analysis method" (IAM) (Sabelli, 2020) may be used to permit design for stability based on the drift limit. In this method, second-order analysis lateral-load effects are further amplified by a factor B_3 that addresses stiffness-reduction effects (including member imperfections and inelasticity as well as uncertainty in member stiffness, similar to the 0.8 stiffness-reduction factor in the direct analysis method). The IAM amplifier for stiffness reduction can be computed using the B_2 amplifier and the flexural stiffness reduction parameter τ_b (taking the smallest value for τ_b at each story):

$$B_3 = \frac{0.8\tau_b}{1-(1-0.8\tau_b)B_2} \tag{11}$$

where

τ_b = flexural stiffness reduction parameter based on column axial force from AISC *Specification* Section C2.3

The parameter τ_b is equal to 1.0 for braced-frame columns and for moment-frame columns with axial force not exceeding 50% of the yield force, and thus the parameter τ_b can be taken as 1.0 for the majority of real buildings. In such cases, Equation 11 simplifies to:

$$B_3 = \frac{4}{5 - B_2} \tag{12}$$

Thus, if B_2 can be determined based on the drift limit, so too can B_3. With these two amplifiers the upper-bound of the lateral-load effect can be determined in advance of design and analysis.

These amplifiers so determined can be utilized directly in the design process or may be used in a simple hand calculation to confirm the results of a computer second-order analysis (incorporating Equation 12 for a second-order analysis with direct-analysis stiffness).

RECOMMENDED DESIGN APPROACH FOR DRIFT-GOVERNED BUILDINGS

The design of most moment-frame buildings is governed by the need for sufficient stiffness to control drift and deformation demands, rather than the need for strength, regardless of whether wind or seismic loads govern the member selection. (This is also true of some braced-frame and dual-system buildings.) In such cases, the designer can streamline the design process by selecting member sizes to maintain a target story drift considering second-order effects directly and, subsequently verifying adequate strength, using the appropriate combination of vertical and lateral loads for each evaluation. The methods presented here utilize a drift limit to estimate these second-order effects and are thus applicable to conditions in which such a drift limit applies (whether by code or as a means to limit damage to deformation-sensitive elements) and for which the drift limit is a governing criterion.

Application of this approach to seismic design is complicated by the dependency of the loading on the building period (ASCE, 2016), which is a function of the system lateral stiffness. Incorporation of that dependency into the required stiffness is beyond the scope of this paper.

Example 1: Design Example

To illustrate application methods based on second-order drift, a design example is presented, based on Carter and Geschwindner (2008), as shown in Figure 1. The example shows member selection for column A to meet a drift limit and confirmation of adequate strength, including design for stability. The example has drift limits corresponding to both serviceability and strength evaluations.

Given:

Similar to many (if not most) building structures, the example structure has no sway under gravity loads, and thus the lateral restraint force, R_{nt}, is zero. This permits the application of amplifiers B_2 and B_3 to the lateral loads or to the lateral-load effects, rather than to the effect of lateral loads plus R_{nt}. (See AISC *Specification* Appendix 8 Commentary for additional information regarding the determination and use of R_{nt}.)

Different loads and drift limits are used in the example for LRFD and serviceability evaluations. Loads for the LRFD evaluation are taken from Carter and Geschwindner (2008). The drift limits and serviceability loads are assumed here. The drift limits have been selected such that design for drift requires the member sizes from Carter and Geschwindner. Members are selected based on the minimum moment of inertia that limits second-order drift to the drift limit. The drift is based on the second-order displacement, which is approximated here by applying the amplifier B_2 to the first-order cantilever displacement:

$$\Delta_2 \leq \frac{B_2 H L^3}{3EI} \tag{13}$$

where

E = modulus of elasticity, ksi

I = moment of inertia of cantilever column, in.^{4}

For simplicity, shear deformations are not included in the analysis.

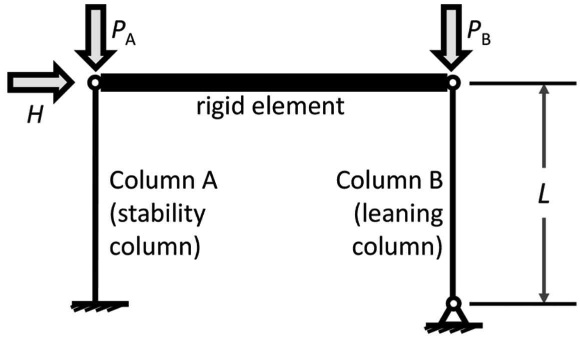

Fig. 1. Example frame.

Table 1. Loading and Design Information		
	Service	**Strength (LRFD)**
H (kips)	12	20
P_A (kips)	125	200
P_B (kips)	125	200
Drift limit	1.00 in. $= L/180$	1.80 in. $= L/100$

The required moment of inertia is:

$$I \geq \frac{B_2 H L^3}{3E\Delta_2} \tag{14}$$

Loads for the frame are shown in Table 1, along with the drift limits. The height L is 15 ft (180 in.).

Solution:

Determine Coefficient RM

From AISC *Specification* Appendix 8, Equation A-8-8, the R_M coefficient is determined using Equation 2:

$$\begin{aligned} R_M &= 1 - 0.15\frac{P_{mf}}{P_{story}} \qquad (2) \\ &= 1 - 0.15\frac{(200 \text{ kips})}{(400 \text{ kips})} \\ &= 0.925 \end{aligned}$$

Because the ratio of P_{mf} to P_{story} in this example does not change with the level of loading, this value of R_M applies to both serviceability and strength evaluations.

Service-Level Member Selection (Drift Only)

Using the service-level drift limit as the second-order drift, the upper bound of the amplifier B_2 is determined using Equation 5. This is used to determine the required moment of inertia of the cantilever column. Once member selection is made based on this service-level second-order drift limit, the first-order drift can be computed for recalculation of the force amplifier B_2 based on the actual system stiffness.

Equation 5 is used to determine the amplifier B_2 for the serviceability evaluation based on:

$$\begin{aligned} \frac{P_{story}}{H} &= \frac{(125 \text{ kips} + 125 \text{ kips})}{(12.0 \text{ kips})} \\ &= 20.8 \end{aligned}$$

$$\begin{aligned} \frac{\Delta_2}{L} &= \frac{(1.00 \text{ in.})}{(180 \text{ in.})} \\ &= 0.00556 \end{aligned}$$

The second-order stability index Q_2 is:

$$\begin{aligned} Q_2 &= \left(\frac{P_{story}}{H}\right)\left(\frac{\Delta_2}{L}\right) \qquad (8) \\ &= (20.8)(0.00556) \\ &= 0.116 \end{aligned}$$

The amplifier B_2 is:

$$B_2 = 1 + Q_2 \\ = 1 + 0.116 \\ = 1.12 \tag{9}$$

The error in neglecting the second-order effect is 12% unconservative in this serviceability evaluation. If the drift limit is used as a first-order drift (including the factor R_M of 0.925), the value of B_2 obtained using Equation 4 is 1.14. (The error associated with use of the drift limit as a first-order drift is tabulated at the end of this example.)

The required moment of inertia is:

$$I \geq \frac{B_2 H L^3}{3E\Delta_2} \\ \geq \frac{(1.12)(12.0 \text{ kips})(180 \text{ in.})^3}{3(29{,}000 \text{ ksi})(1.00 \text{ in.})} \\ = 901 \text{ in.}^4$$

A W14×90 (I = 999 in.^{4}) will be used. Note that neglecting the second-order effect would result in the selection of a smaller member (W14×82, I = 881 in.^{4}), which would in turn result in not meeting the drift limit. With the selected member the first-order drift is:

$$\Delta_1 = \frac{HL^3}{3EI} \\ = \frac{(12.0 \text{ kips})(180 \text{ in.})^3}{3(29{,}000 \text{ ksi})(999 \text{ in.}^4)} \\ = 0.805 \text{ in.}$$

$$\frac{\Delta_1}{L} = \frac{(0.805 \text{ in.})}{(180 \text{ in.})} \\ = 0.00447$$

The first-order stability index from Equation 1 is:

$$Q_1 = \left(\frac{1}{R_M}\right)\left(\frac{P_{story}}{H}\right)\left(\frac{\Delta_1}{L}\right) \\ = \left(\frac{1}{0.925}\right)(20.8)(0.00447) \\ = 0.101 \tag{1}$$

Using this value of Q_1 with Equation 4 gives:

$$B_2 = \frac{1}{1 - Q_1} \\ = \frac{1}{1 - 0.101} \\ = 1.11 \tag{4}$$

Thus, the value of B_2 determined from Equation 5 using the target second-order drift limit is effective in determining the required member size directly without the iteration that would be required using Equation 3.

LRFD-Level Evaluation (Drift and Strength)

Amplifiers Determined Prior to Analysis and Design

Next, the stability index for the strength evaluation is determined using the appropriate vertical load. Using the LRFD load level drift limit as the second-order drift, the stability index Q_2 is used to determine the amplifiers B_2 and B_2B_3 for stability design according to the IAM. The stability index Q_2 is based on:

$$\begin{aligned}\frac{P_{story}}{H} &= \frac{(200 \text{ kips} + 200 \text{ kips})}{(20.0 \text{ kips})} \\ &= 20.0\end{aligned}$$

$$\begin{aligned}\frac{\Delta_2}{L} &= \frac{(1.80 \text{ in.})}{(180 \text{ in.})} \\ &= 0.0100\end{aligned}$$

The second-order stability index is:

$$\begin{aligned}Q_2 &= \left(\frac{P_{story}}{H}\right)\left(\frac{\Delta_2}{L}\right) \\ &= (20.0)(0.0100) \\ &= 0.200\end{aligned} \tag{8}$$

The amplifier B_2 is:

$$\begin{aligned}B_2 &= 1 + Q_2 \\ &= 1 + 0.200 \\ &= 1.20\end{aligned} \tag{9}$$

If the drift limit is used as a first-order drift (Q_1 = 0.216 using Equation 1, including the factor R_M), the value of B_2 obtained from Equation 4 is 1.28.

The amplifier B_3 depends on the axial force in moment-frame columns. The axial force to yield force ratio for the cantilever column is below 0.5 (justifying use of Equation 12):

$$\begin{aligned}\frac{\alpha P_r}{P_s} &= \frac{\alpha P}{F_y A} \\ &= \frac{(1.0)(200 \text{ kips})}{(50 \text{ ksi})(26.5 \text{ in.}^2)} \\ &= 0.151 \le 0.50\end{aligned}$$

The amplifier B_3 is:

$$\begin{aligned}B_3 &= \frac{4}{5 - B_2} \\ &= \frac{4}{5 - 1.20} \\ &= 1.05\end{aligned} \tag{12}$$

The product B_2B_3 is:

$$\begin{aligned}B_2B_3 &= (1.20)(1.05) \\ &= 1.26\end{aligned}$$

The required moment of inertia is:

$$
\begin{aligned}
I &\geq \frac{B_2 H L^3}{3E\Delta_2} \\
&\geq \frac{(1.20)(20.0 \text{ kips})(180 \text{ in.})^3}{3(29{,}000 \text{ ksi})(1.80 \text{ in.})} \\
&= 894 \text{ in.}^4
\end{aligned}
$$

A W14×90 (I = 999 in.^{4}) satisfies the strength-level drift limit. At this point the member has been selected to meet the LRFD load level drift limit, and the strength evaluation can proceed using either the approximate values of B_2 and B_3 determined earlier, or more precise values determined based on the calculated drift from the selected member. While the former approach is more expedient, for purposes of comparison the latter approach will be used.

Amplifiers Determined Based on Analysis of Selected Member

The first-order drift for the selected member under LRFD loading is:

$$
\begin{aligned}
\Delta_1 &= \frac{HL^3}{3EI} \\
&= \frac{(20.0 \text{ kips})(180 \text{ in.})^3}{3(29{,}000 \text{ ksi})(999 \text{ in.}^4)} \\
&= 1.34 \text{ in.}
\end{aligned}
$$

$$
\begin{aligned}
\frac{\Delta_1}{L} &= \frac{(1.34 \text{ in.})}{(180 \text{ in.})} \\
&= 0.00744
\end{aligned}
$$

The first-order stability index, Q_1, for the LRFD strength evaluation is:

$$
\begin{aligned}
Q_1 &= \left(\frac{1}{R_M}\right)\left(\frac{P_{story}}{H}\right)\left(\frac{\Delta_1}{L}\right) \qquad (1) \\
&= \left(\frac{1}{0.925}\right)(20.0)(0.00744) \\
&= 0.161
\end{aligned}
$$

$$
\begin{aligned}
B_2 &= \frac{1}{1-Q_1} \qquad (4) \\
&= \frac{1}{1-0.161} \\
&= 1.19
\end{aligned}
$$

$$
\begin{aligned}
B_3 &= \frac{4}{5-B_2} \qquad (12) \\
&= \frac{4}{5-1.19} \\
&= 1.05
\end{aligned}
$$

$$
\begin{aligned}
B_2 B_3 &= (1.19)(1.05) \\
&= 1.25
\end{aligned}
$$

Note that this value of the product $B_2 B_3$ is 99% of the value obtained using the drift limit.

Table 2. Summary of B_2 Values				
Loading Level	**(1) Correct Value Using Calculated First-Order Drift (Equation 1)**	**(2) Approximation Using Drift Limit as First-Order Drift (Equation 1)**	**(3) Approximation Using Target Drift Limit as Second-Order Drift (Equation 8)**	**(4) Ignoring Second-Order Effects (Not Recommended)**
Service	1.11 (0%)	1.14 (+2.8%)	1.12 (+0.3%)	1.00 (–11.2%)
Strength	1.19 (0%)	1.28 (+7.0%)	1.20 (+0.1%)	1.00 (–19.2%)

From Carter and Geschwindner (2008), the design strengths are:

$$\phi P_c = 1{,}000 \text{ kips}$$

$$\phi M_n = 573 \text{ kip-ft}$$

The required flexural strength is determined using the B_2B_3 amplifier on the first-order load effect:

$$\begin{aligned} M_u &= B_2 B_3 HL \\ &= \frac{(1.25)(20.0 \text{ kips})(180 \text{ in.})}{12 \text{ in./ft}} \\ &= 375 \text{ kip-ft} \end{aligned}$$

The interaction check from AISC *Specification* Equation H1-1a using LRFD is:

$$\begin{aligned} \frac{P_r}{\phi P_c} + \left(\frac{8}{9}\right)\frac{M_u}{\phi M_n} &= \frac{(200 \text{ kips})}{(1{,}000 \text{ kips})} + \left(\frac{8}{9}\right)\frac{(375 \text{ kip-ft})}{(573 \text{ kip-ft})} \\ &= 0.782 \end{aligned}$$

Note that this is slightly lower than the value of 0.796 obtained by Carter and Geschwindner (2008) for the DM and by Sabelli (2020) for the IAM because the value of R_M was calculated in this example, as is permitted by the 2016 AISC *Specification* (AISC, 2016), rather than taken as 0.85 per the 2005 AISC *Specification* (AISC, 2005). Using $R_M = 0.85$, the first-order stability index would be $Q_1 = 0.175$; the corresponding demand-to-capacity ratio is 0.796, matching the previous studies.

Example Summary

Table 2 summarizes the values of B_2 obtained for both service-level and strength-level evaluations, including B_2: (1) determined using the calculated drift, (2) approximated using the drift limit as the first-order drift, and (3) approximated using the target drift limit as the second-order drift (as recommended in this paper). The latter two also show the percent error compared to the first. The last column (4) shows the error if second-order effects are not considered at all, which is not recommended.

Use of the target drift limit as the first-order drift is acceptable for purposes of damage control but is not recommended because of the conservative error shown in Table 2 (column 2), and the ease of utilizing the more accurate second-order methods presented herein (column 3). Ignoring second-order effects in drift determination (column 4) is not recommended due to the unconservative error, and the method's inaccuracy potentially leading to damage in cladding, partitions, and other building components.

Use of the drift limit as the second-order drift from Equations 5, 8, and 9 (as proposed in this paper) results in negligible overestimates for drift-governed designs as compared with using Equations 1, 3, and 4, which would normally require iteration. For cases utilizing the latter approach in which the selected members result in second-order drifts significantly below the drift limit, the use of the refined analysis with the selected member stiffness (using the first-order stability index and further iterations on member size) may permit refinement of the design but with more effort.

Table 3. Summary of Eight-Story Frame Loading, Criteria, and Analysis Results										
General		Drift Loading and Criteria			Drift Evaluation	Strength Loading		Strength Evaluation		
Level	L (in.)	P_{story} (kips)	$H_{service}$ (kips)	$\Delta_{allowable}$ (in.)	$\frac{\Delta_2}{\Delta_{all}}$	P_{story} (kips)	H (kips)	Δ_1 (in.)	Δ_2 (in.)	$\frac{\Delta_2}{\Delta_1}$
8	180	2,000	20.0	0.450	0.61	2,400	30	0.39	0.49	1.25
7	180	4,400	40.0	0.450	0.96	5,600	60	0.59	0.79	1.35
6	180	6,800	60.0	0.450	0.89	8,800	90	0.54	0.74	1.36
5	180	9,200	80.0	0.450	0.95	12,000	120	0.57	0.79	1.38
4	180	11,600	100.0	0.450	0.93	15,200	150	0.56	0.78	1.39
3	180	14,000	120.0	0.450	1.00	18,400	180	0.60	0.84	**1.41**
2	180	16,400	140.0	0.450	0.93	21,600	210	0.56	0.78	1.38
1	**180**	18,800	**160.0**	**0.450**	0.72	**24,800**	240	0.45	0.59	1.32

Example 2: Computer-Analysis Review Example

While Example 1 illustrates the application to a simple structure designed by hand, in current practice, computer analysis is utilized for the majority of structures of any significant complexity. Nevertheless, engineers should be equipped to critically evaluate the results of such analyses using simple methods in order to prevent errors.

In this section, the methods described earlier are utilized to evaluate the results of the Appendix C example from Sabelli (2020). That example presents the design and analysis (including second-order analysis) of an eight-story building with two-bay moment frames on the perimeter. For simplicity, an evaluation is made based on loads at the bottom story here, and a hand-calculated amplifier B_2 is compared to the drift amplification from a second-order analysis. The hand calculation does not rely on any analysis results, although it assumes the building drift is equal to the drift limit.

Given:

Selected design criteria, loading, and analysis results for the eight-story building are presented in Table 3; all information is taken from the Appendix C example from Sabelli (2020). Values used in the example are shown in bold. Readers are referred to Sabelli (2020) for more information.

Computation of Amplifier B_2

The required system effective stiffness based on the drift-design criteria is:

$$\begin{aligned}\frac{H}{\Delta_2} &= \frac{(160\text{ kips})}{(0.450\text{ in.})}\\ &= 356\text{ kips/in.}\end{aligned}$$

The second-order stability index, Q_2, for the strength evaluation (using the strength-level vertical loads) is:

$$\begin{aligned}Q_2 &= \left(\frac{P_{story}}{L}\right)\left(\frac{\Delta_2}{H}\right) \qquad (8)\\ &= \left(\frac{24{,}800\text{ kips}}{180\text{ in.}}\right)\frac{1}{356\text{ kips/in.}}\\ &= 0.388\end{aligned}$$

The corresponding amplifier B_2 is:

$$\begin{aligned} B_2 &= 1 + Q_2 \\ &= 1 + 0.388 \\ &= 1.39 \end{aligned} \tag{9}$$

Table 3 shows the ratio of second-order drift to first-order drift ranging from 1.25 to 1.41 for the strength evaluation, with the highest value corresponding to the floor with the drift exactly at the drift limit for the drift evaluation. [Note that the ratio of second-order drift to first-order drift only approximates the force amplification, per Equation 7, and as discussed in Sabelli and Griffis (2021).] The simple hand calculation above confirms the second-order analysis, giving the engineer higher confidence in the results. A similar hand calculation could be made incorporating Equation 12 to verify the direct analysis method results.

CONCLUSIONS

Equations for the force amplifier (B_2) are presented that utilize a second-order stability index, which can be based on a drift limit. Two examples are presented. A design example shows the application of the methods, determining the amplifiers prior to design based on the target drift limit. That example confirms that the methods result in very close approximations of the amplifiers determined after member selection for the simple, drift-governed design presented. A second example illustrates the use of the second-order stability index to estimate the magnitude of the second-order effect prior to member selection and building analysis. The amplification value so determined is compared to the second-order effect from a computer analysis, providing confirmation of that analysis.

SYMBOLS

B_2 Amplifier for second-order effect (AISC *Specification* Appendix 8)

B_3 IAM amplifier to account for stiffness reduction due to inelasticity (Sabelli, 2020)

E Modulus of elasticity, ksi (AISC *Specification*)

H First-order shear at the load level under consideration, kips

I Moment of inertia, in.^{4}

L Story height, in.

P_{lean} Load on leaning columns, kips

P_{mf} Load on moment-frame columns, kips

P_{story} Story gravity load, kips

Q_1 First-order stability index (Q in Design Guide 28)

Q_2 Second-order stability index

R_M Coefficient to account for member P-δ influence on structure P-Δ

R_{nt} Lateral reaction of frame restrained from translation used in approximate second-order analysis, kips (AISC *Specification* commentary)

Δ_1 First-order story drift, in. (Δ_H in the AISC *Specification*)

Δ_2 Second-order story drift, in. (Design Guide 28)

τ_b Flexural stiffness reduction parameter (AISC *Specification* Section C2.3)

REFERENCES

AISC (2005), *Specification for Structural Steel Buildings*, ANSI/AISC 360–05, American Institute of Steel Construction, Chicago, Ill.

AISC (2016), *Specification for Structural Steel Buildings*, ANSI/AISC 360–16, American Institute of Steel Construction, Chicago, Ill.

AISC (2017), *Steel Construction Manual*, 15th Ed., American Institute of Steel Construction, Chicago, Ill.

ASCE (2016), *Minimum Design Loads and Associated Criteria for Buildings and Other Structures*, ASCE/SEI 7–16, American Society of Civil Engineers, Reston, Va.

ASCE (2019), *Prestandard for Performance-Based Wind Design*, American Society of Civil Engineers, Reston, Va.

Aswegan, K., Charney, F., and Jarrett, J. (2015), "Recommended Procedures for Damage-Based Serviceability Design of Steel Buildings under Wind Loads," *Engineering Journal,* AISC, Vol. 52, No. 1, pp. 1–26.

Carter, C.J. and Geschwindner, L.F. (2008), "A Comparison of Frame Stability Analysis Methods in ANSI AISC 360–05," *Engineering Journal*, AISC, Vol. 45, No. 3, pp. 159–170.

Griffis, L.G. (1993), "Serviceability Limit States Under Wind Loads," *Engineering Journal*, AISC, Vol. 30, No. 1, pp 1–16.

Griffis, L.G. and White, D.W. (2013), *Stability Design of Steel Buildings,* Design Guide 28, AISC, Chicago, Ill.

LeMessurier, W.J. (1977), “A Practical Method of Second Order Analysis Part 2; Rigid Frames,” *Engineering Journal*, AISC, Vol. 14, No. 2, pp. 49–67.

Sabelli, R. (2020), “The Indirect Analysis Method of Design for Stability: An Amplifier to Address Member Inelasticity, Member Imperfections, and Uncertainty in Member Stiffness,” *Engineering Journal*, AISC, Vol. 57, No. 2, pp. 109–133.

Sabelli, R. and Griffis, L.G. (2021), “Mechanical, Effective, and Geometric Stiffness: A Refined Approach to the R_M Coefficient to Account for the Influence of P-δ on P-Δ,” *Engineering Journal*, AISC, Vol. 58, No. 2.

Statler, D.E., Ziemian, R.D., and Robertson, L.E. (2011), “The Natural Period as an Indicator of Second-Order Effects,” *Proceedings of the Annual Stability Conference Structural Stability Research Council*, Pittsburgh, Pa.

West, M., Fisher, J., and Griffis, L.A. (2003), *Serviceability Design Considerations for Steel Buildings,* Design Guide 3, AISC, Chicago, Ill.

Simplified Equations for Shear Strength of Composite Concrete-Filled Steel Tubes

HADI KENARANGI, MICHEL BRUNEAU, AMIT H. VARMA, and
MUBASHSHIR AHMAD

ABSTRACT

Shear strength of filled composite members, namely, circular or rectangular concrete-filled steel tubes (CFST), have been investigated in past research. Results established the relative contributions of the steel tube and concrete infill to the total shear strength and showed that the concrete contribution depends on the development of a compression strut in the concrete infill when shear-span values are low. While experimental results and numerical models are available in the literature, simple equations that empirically encompass this behavior are preferable for design purposes. This paper provides an overview of the technical approach that has been followed to propose such equations for consideration and possible implementation in future editions of design specifications. The shear strength obtained using the proposed equation is compared with the shear test database from the existing literature and found to be safe; it accurately captures the contribution of the steel tube to the total shear strength and conservatively approximates that of the concrete.

Keywords: concrete-filled steel tubes, shear strength, composite behavior, mechanics-based equation, resistance factor, calibration, design.

INTRODUCTION AND BACKGROUND

Concrete-filled steel tubes (CFST) have a demonstrated ability to provide strength and ductility, which has made them desirable for both seismic and non-seismic applications (Bruneau and Marson, 2004; Hajjar, 2000; Hajjar et al., 2013; Han and Yang, 2005; Lai et al., 2017). Much research has demonstrated that these members can develop their plastic flexural strength (e.g., Bruneau and Marson, 2004; Lai et al., 2014; Leon et al., 2007; Roeder et al., 2010; Varma et al., 2002) and equations in design specifications typically account for full development of the plastic flexural strength of such members under combined bending and axial load.

Considerably less knowledge exists on the shear strength of such members. This may be attributable to challenges in experimentally developing the full shear strength of large concrete-filled tubes, and to the fact that shear is rarely a governing limit state for CFST members. For example, in the 2016 AISC *Specification for Structural Steel Buildings* (AISC, 2016b), hereafter referred to as the AISC *Specification*, the shear strength of composite concrete-filled tubes is specified to be either that of the steel section alone or that of the concrete section alone, presumably on the assumption that there exist few instances where a shear strength greater than this is necessary.

However, in some instances, more accurate prediction of this shear strength is desirable or needed. For example, this would be the case at the panel-zone locations of CFST columns in a composite moment frame (Fischer and Varma, 2014), or in CFST drilled shafts spanning across a thin, liquefiable soil layer located between two stiff layers during lateral spreading. In both of these cases, the CFST is subjected to double curvature bending over short lengths and subject to high resulting shear forces. In these cases, the shear strength of the CFST can become a significant consideration in its design.

It is important for design purposes to understand the physical behavior of composite CFST subjected to shear and to develop design equations that capture the respective contribution of the steel tube and concrete infill of the CFST to its total shear strength (contribution of internal reinforcement is not considered here for reasons described later). Design equations that are anchored in the mechanics of structural behavior provide more confidence in the design. For example, overestimating the strength of one component could result in an unexpected failure should that component become dominant in providing the total shear strength of that member.

Hadi Kenarangi, Structural and Earthquake Engineer, Modjeski and Masters, Inc., Mechanicsburg, Pa. Email: hkenarangi@modjeski.com (corresponding)

Michel Bruneau, SUNY Distinguished Professor, Department of Civil, Structural, and Environmental Engineering, University at Buffalo, Buffalo, N.Y. Email: bruneau@buffalo.edu

Amit H. Varma, Karl H. Kettelhut Professor, Lyles School of Civil Engineering, Purdue University, Ind. Email: ahvarma@purdue.edu

Mubashshir Ahmad, Graduate Student, Lyles School of Civil Engineering, Purdue University, Ind. Email: ahmad54@purdue.edu

Paper No. 2020-10

CIRCULAR CONCRETE-FILLED STEEL TUBES

The work presented in this section (1) summarizes recent research on the shear strength of circular concrete-filled members that illustrate the relative contributions of steel and concrete to the total shear strength and the contribution of a diagonal compression concrete strut to that strength (Kenarangi and Bruneau, 2020a, 2020b), (2) presents proposed (and calibrated) simplified design equations to simplify the more complex mechanics-based shear strength equation previously developed for composite CFST members (Kenarangi and Bruneau, 2020b), and (3) compares experimental results against the strength predicted by the proposed simplified equations.

2016 AISC *Specification* Shear Strength of Circular CFST

The shear strength of circular filled composite members given by the 2016 AISC *Specification* Section I4, is based on (1) the shear strength of the steel tube alone, (2) the available shear strength of the reinforced concrete portion alone, or (3) the shear strength of the steel tube plus the shear strength of the reinforcing steel.

Using this approach, for case 1, the shear strength of the circular steel tube alone using AISC *Specification* Equation G5-1 is:

$$V_{n(AISC)} = 0.5 F_{cr} A_g \tag{1}$$

where $V_{n(AISC)}$ is the nominal shear strength of a circular steel tube and F_{cr} is the critical shear buckling stress taken as the larger of AISC *Specification* Equations G5-2a or G5-2b:

$$F_{cr} = \frac{1.6E_s}{\sqrt{\frac{L_v}{D}}\left(\frac{D}{t}\right)^{\frac{5}{4}}} \le 0.6F_y \tag{2}$$

$$F_{cr} = \frac{0.78E_s}{\left(\frac{D}{t}\right)^{\frac{3}{2}}} \le 0.6F_y \tag{3}$$

where

A_g = gross area of the steel tube cross section, in.^{2}

D = outside diameter of the steel tube, in.

E_s = modulus of elasticity of the steel, ksi

F_y = specified minimum yield stress of the steel tube, ksi

L_v = distance between points of maximum and zero shear, in.

t = design wall thickness, in.

Although not explicitly specified in AISC *Specification* Section I4, in concrete-filled steel tubes, the concrete fill provides support against buckling of the steel tube, and therefore, F_{cr} is taken as $0.6F_y$ for these sections. This would result in:

$$\begin{aligned} V_{n(AISC)} &= 0.5(0.6F_y)F_{cr}A_g \\ &= 0.3F_y \pi Dt \\ &= 0.94DtF_y \end{aligned}$$

Incidentally, this result corresponds to the first occurrence of yield at one point on the entire cross section (at its center in this case), as derived using classical equations to calculate elastic shear stresses (i.e., $\frac{V_y Q}{Ib}$, from any mechanics of materials textbook, with V_y calculated when the shear stress is τ_y).

For case 2, the shear strength of the concrete alone would be:

$$V_{c(ACI)} = 0.0632 A_c \sqrt{f_c'} \tag{4}$$

where

A_c = area of the concrete section, in.^{2}

f_c' = uniaxial compressive strength of the concrete, ksi

Case 3 provides a marginal increase in shear strength over case 1, proportionally to how much the area of shear reinforcement adds to the area of the steel tube.

All the current AISC *Specification* Section I4 options are conservative and result in inefficient material use and increase in costs when shear governs the design.

Complex Shear Strength Equation

In order to investigate the behavior of circular CFST members under shear deformation, a series of finite element analyses were performed using element types and material models validated against experimental results, as described in more detail in Kenarangi and Bruneau (2020b). Analyses showed that a significant diagonal compression strut with a 45° angle developed in the concrete for some shear span-to-diameter (a/D) ratios. This is illustrated in Figure 1, which shows iso-surfaces for two different a/D ratios. To more clearly illustrate the development of the compression strut, principal stresses lower than 2.5 ksi are not shown in these figures. As a/D increases or decreases beyond the optimum case of a/D = 0.5 [which is the geometry shown in Figure 1(a)], the strength of the compression strut rapidly becomes less significant, as shown in Figure 1(b).

Based on observations from finite element analysis results, equations for the contribution of the infill concrete to the total shear strength of the CFST were developed. In these equations, the critical concrete strut cross section, A_{strut}, was located at the mid-length of the strut and was calculated from geometry to be:

$$A_{strut} = \frac{\sqrt{2}}{2}\left[4R_c^2 \arcsin\left(\frac{b}{2R_c}\right) + b\sqrt{4R_c{}^2 - b^2}\right] \tag{5}$$

where

$R_c = D_c/2$

$$b = \frac{D_c - H}{2} \qquad 0 \le b \le \frac{H}{2} \tag{6}$$

and

D_c = concrete core diameter, in.

H = height of the specimen in double curvature shear setup, which is equal to $2a$, in.

The resulting strut force, F_{strut}, calculated by multiplying A_{strut} by a uniformly distributed stress conservatively assumed to be equal to f_c', was then converted into horizontal (shear) and vertical (axial) force components, respectively, corresponding to the contribution to shear strength provided by the strut, V_{strut}, and a vertical force component of the strut, P_{strut}, transferred to the steel tube. Therefore,

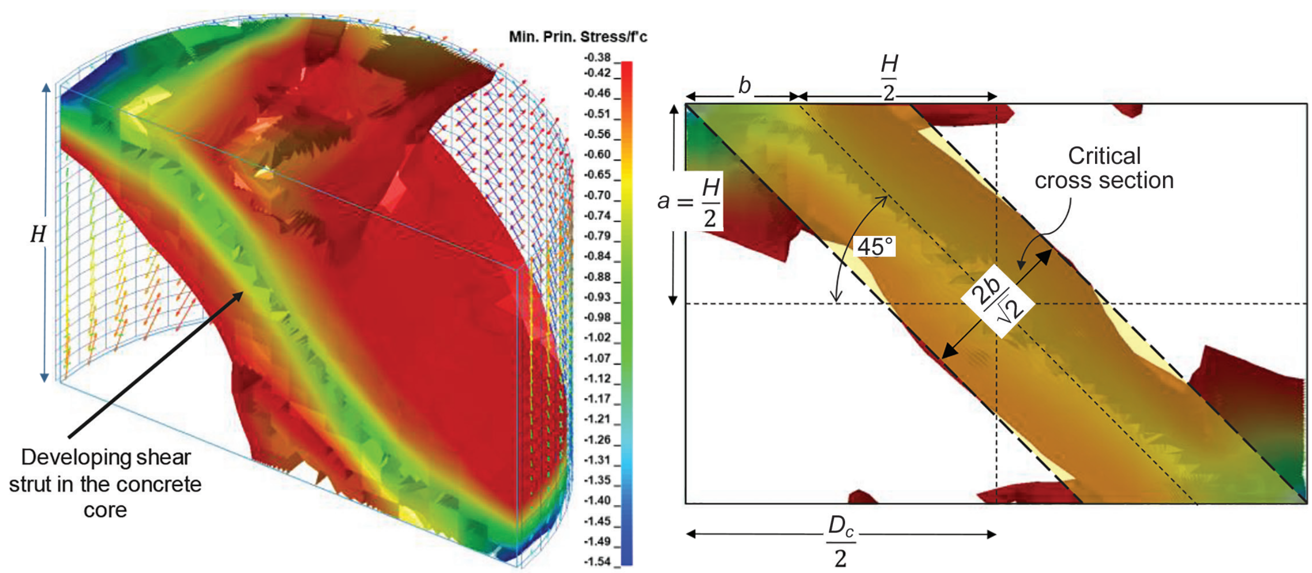

(a) $0.25 \le a/D \le 0.5$

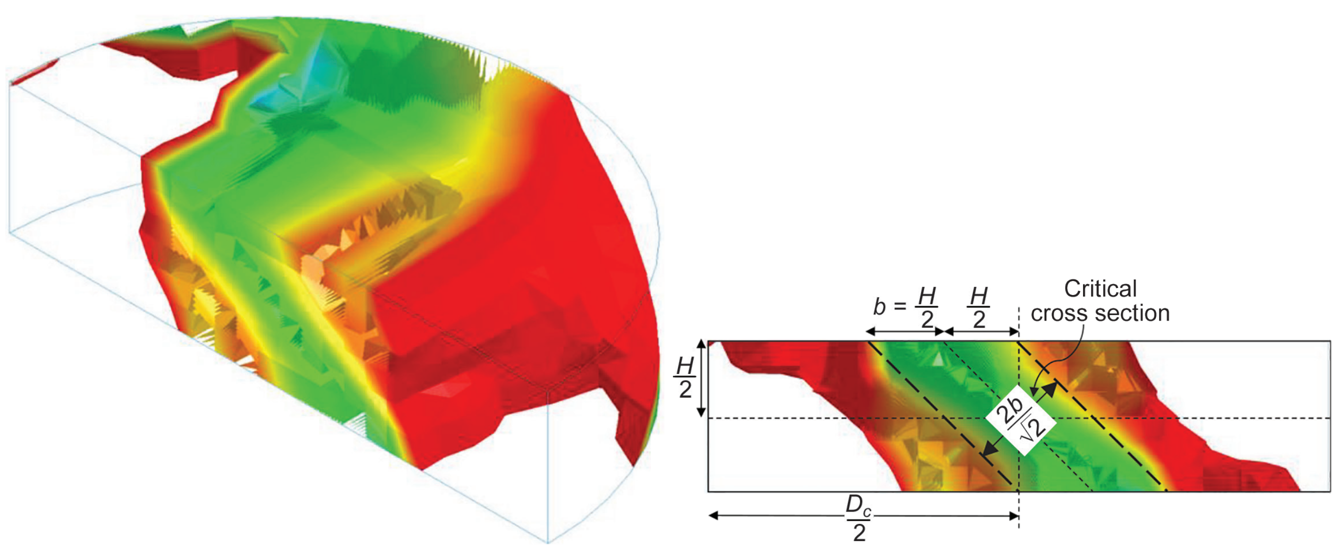

(b) $a/D < 0.25$

Fig. 1. Definition of diagonal compression strut in CFST.

$$V_{strut} = \frac{\sqrt{2}}{2} A_{strut} f_c' \quad (7a)$$

$$P_{strut} = \frac{\sqrt{2}}{2} A_{strut} f_c' \quad (7b)$$

At large shear span ratios, no strut develops, and the shear strength of the concrete defaults to the existing shear strength equations for concrete. Therefore, a lower limit of concrete shear strength, V_c, was defined here for V_{conc}, as shown in Equations 8 and 9. In Equation 9, the term outside the parenthesis is the nominal shear resistance of the concrete in accordance with ACI. The term inside the parenthesis was added to include the axial load effect on the shear resistance of the concrete. This term was adapted from ACI 318 (2011, 2014) Section 22.5.6 (which was the edition of ACI 318 in effect at the time this research was conducted).

$$V_{conc} = \max\left(V_{strut}, V_c\right) \quad (8)$$

where

$$V_c = 0.0632 A_c \sqrt{f_c'} \left(1 + \frac{P_{strut}}{2A_c}\right) \quad (9)$$

To calculate the nominal shear resistance of the steel tube, it was assumed that the tube cross section was fully yielded under combined tension and shear, and the effect of bending moment was neglected. In this case, the total shear resistance of the steel tube, V_s, can be calculated by integrating the maximum shear stress (which is tangent to the surface) over the steel tube cross section as shown in Figure 2 and calculated in Equation 10.

$$V_s = 2\int_{-\pi/2}^{\pi/2} \tau_{s,max} Rt \cos(\phi)\, d\phi \quad (10)$$

where R is the average radius of the steel tube and $\tau_{s,max}$ is the maximum shear stress on the steel tube cross section, calculated as:

$$\tau_{s,max} = \frac{1}{\sqrt{3}} \sqrt{F_y^2 - T^2} \quad (11)$$

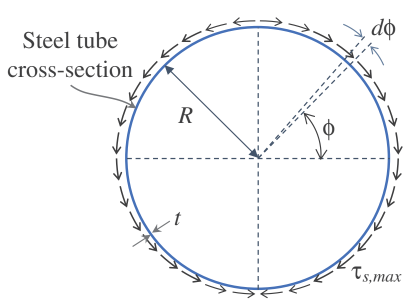

Fig. 2. Shear distribution on the steel tube cross section.

where F_y is the yield stress of the steel tube and $T = P_{strut}/A_s$ is the resultant tensile stress on the steel tube cross section due to the interaction of the concrete strut with the steel tube.

The resulting V_s obtained from Equation 10 is shown in Equation 12. The term under the square root shows that the shear strength of the steel tube reduces as the strut force increases, and P_{strut} should be less than A_sF_y. (Note: For a diagonal strut at 45°, $P_{strut} = V_{strut}$.)

$$V_s = \frac{2Dt}{\sqrt{3}} \sqrt{F_y^2 - \left(\frac{P_{strut}}{A_s}\right)^2} \quad (12)$$

Note that for all sections considered, the presence of P_{strut} was found to only have a marginal effect on the value of tube V_s. Also, in calculation of the shear contribution of the steel tube, the effect of the moment was neglected. This effect can be considered in the steel tube shear strength by including the stresses from bending moment using a similar but more complex equation (Kenarangi and Bruneau, 2020b).

Finally, the nominal shear strength of the composite CFST shaft was taken as equal to the summation of the shear strength of the concrete core and the steel tube, as shown in Equation 13.

$$V_{CFST} = V_s + V_{conc} \quad (13)$$

As mentioned before, the potential contribution of the reinforcing cage to the total shear strength is not included in this equation as it has a minimal contribution.

The proposed shear strength in Equation 13 was compared to finite element results with different shear span to diameter ratios. Figures 3(a) and 3(b) show the cases in which the bending moment is neglected or is included in calculation of the shear strength, respectively. In these figures the strengths were normalized to the summation of the strengths calculated by Equations 1 and 4. In these figures, M_p is the theoretical plastic flexural capacity of the section. The difference in the steel tube shear strength between these two cases is less than 8% for $a/D < 0.5$. This difference increases with the a/D ratio. Equations modified to account for the effect of axial load simultaneously acting on the cross section were also developed by Kenarangi and Bruneau (2020b), but these more complex equations are not presented here because the strength predicted by the equation used here was found to be adequately conservative in that case.

The proposed nominal shear strength obtained per these equations was compared with available test results by Kenarangi and Bruneau (2020a), Qian et al. (2007), Xu et al. (2009), Xiao et al. (2012), Nakahara and Tsumura (2014), Ye et al. (2016), and Roeder et al. (2016). Experimental values were found to be, on average, 55% higher than the shear strength calculated by the proposed formula. To explain this result, Figure 4 shows cyclic hysteretic behavior obtained by finite element analysis for one of the specimens tested by Kenarangi and Bruneau (2020a) that failed under a shear dominant mode (note that none of the existing test data were tested under a pure shear condition because there is always a combination of flexure and shear at failure). In this figure, the shear forces carried by the steel tube and the infill concrete, as obtained from the finite element analysis, are compared with values at the maximum experimental strength point. This shows that at the displacement when the maximum experimentally obtained strength was reached, Equation 13 gives a good estimate of the shear strength resisted by the steel tube but underestimates the shear strength resisted by the concrete. This was done deliberately at the time as it was believed that this level of conservatism would be acceptable.

Simplified Shear Strength Equation for Circular CFST

Equations 5 through 13, while formulated to capture fundamental mechanisms that develop in CFST in shear, were deemed to be informative but too complex for practical use. Furthermore, while capturing well the contribution of steel to the total strength (and in a manner consistent with theoretical results from plastic analysis), they remained conservative when accounting for the contribution of the infill concrete to the total shear strength. The following alternative equation is therefore proposed, in a format that keeps the rational value derived for the contribution of steel to the total strength, and empirically increases the contribution of the concrete infill to match experimental results.

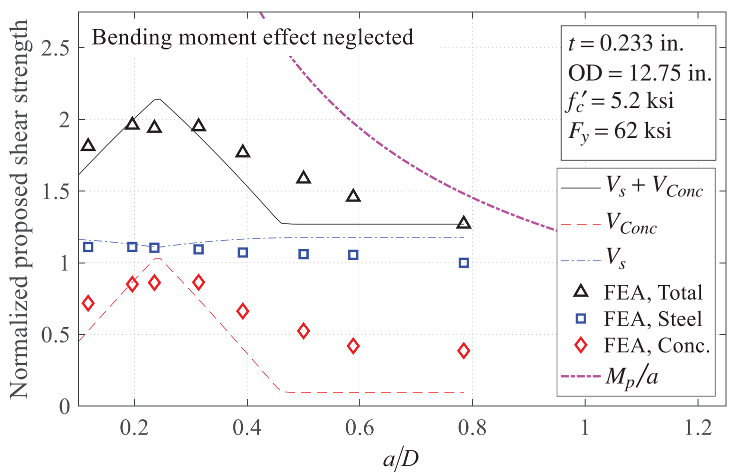

(a) Bending moment effects are neglected

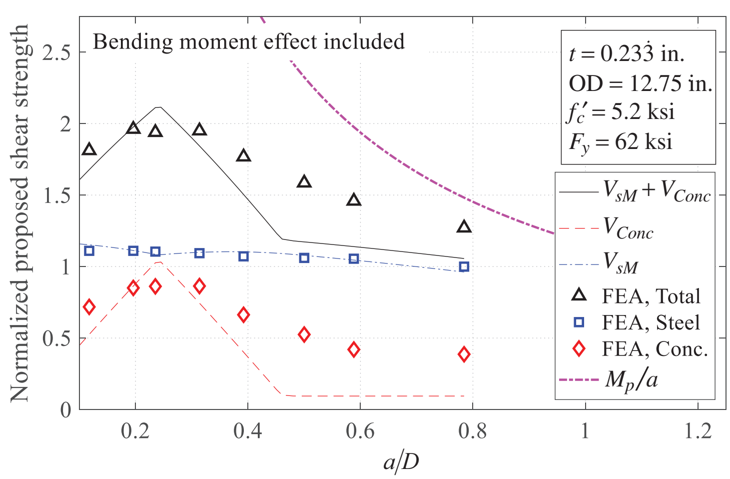

(b) Bending moment effects are included

Fig. 3. Normalized proposed shear strength vs. shear span to diameter ratios.

In this equation

$$V_n = V_s + V_c \tag{14}$$

where

$$V_s = \frac{2Dt}{\sqrt{3}} F_y = 1.15 D t F_y \tag{15}$$

and

$$V_c = 0.0316 \beta A_c \sqrt{f_c'} \tag{16}$$

in which the value of β is calibrated to be 18 and 20 for circular and rectangular CFST, respectively, for reasons explained in a subsequent section. Incidentally, this equation for V_s is the same one used in the Eurocode (CEN, 2005) as the upper strength limit for compact hollow circular tubes.

Note that while the proposed alternative shear strength equation does not explicitly consider the contribution of the developed compressive diagonal strut in the concrete, it empirically does so through the large β values used. Also note that the potential contribution of the reinforcing cage to the total shear strength is not included in the equations because the effect of the reinforcing cage was shown to have no significant impact on shear strength in experiments (Kenarangi and Bruneau, 2020a).

Experimental Database

For reasons mentioned earlier, there are a limited number of experimental tests developing the shear strength of circular CFST. The majority of these tests have been conducted using three- or four-point bending setups with simple end supports and under monotonic loadings (Roeder et al., 2016; Xiao et al., 2012; Xu et al., 2009). These test setups generate single curvature deflection along the member and, depending on the distance of the supports from each other, can produce flexure, flexure-shear, and shear dominant failures for long to short support distances, respectively. More representative of the loading likely to be experienced in panel zones, only some tests have considered specimens subjected to double-curvature deflection rather than single curvature, and even fewer have considered cyclic loading conditions. Monotonic double-curvature shear tests on small diameter CFST (4.7-in. diameter) have been performed by Ye et al. (2016) using a three-point bending setup and fixed support conditions at both ends. Cyclic double-curvature tests have been performed by Nakahara and Tsumura (2014) on 6.5-in.-diameter CFST and by Bruneau et al. (2018) on 12.75-in.- and 16-in.-diameter CFSTs with and without internal reinforcing cages, using a pantograph device to apply cyclic loading to specimens subjected to double-curvature deformations.

Summary of Experimental Results

The experimental tests considered here are listed in Table 1. In this table, D is the diameter of the steel tube; a is the clear span between the supports for single-curvature test setups and half of this value for the double-curvature test setups; P is the applied axial compressive load; and P_0 is the summation of yield strength of the steel tube and crushing capacity of the concrete, ignoring buckling (i.e., $P_0 = A_c f_c' + A_s F_y$). Note that only two sets of results were obtained

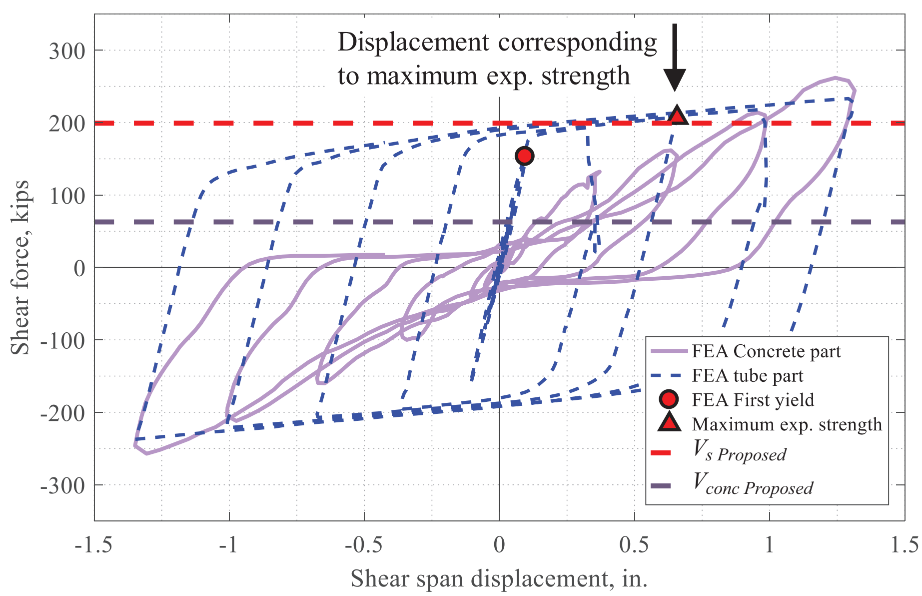

Fig. 4. Comparison of component shear forces of a 12.75-in.-diameter CFST tested by Kenarangi and Bruneau (2020a) with the proposed formula.

Table 1. Summary of the Existing Test Data on Shear Strength of Circular CFST Members

Research	Test Setup	Loading Type	Diameter Range, in.	$\frac{a}{D}$ Range	$\frac{P}{P_0}$ Range
Bruneau et al. (2018)	Double curvature	Cyclic pantograph	12, 16	0.4	0
Roeder et al. (2016)	Single curvature	Monotonic four-point bending	20	0.25–1.0	0 and 0.085
Ye et al. (2016)	Double curvature	Monotonic three-point bending	4.7	0.15–0.75	0–0.73
Nakahara and Tsumura (2014)	Double curvature	Cyclic pantograph	6.5	0.5	0–0.4
Xiao et al. (2012)	Single curvature	Monotonic three-point bending	6.5	0.14–1.0	0–0.62
Xu et al. (2009)	Single curvature	Monotonic three-point bending	5.5	0.1–0.5	0

from cyclic loading, which was not deemed sufficient here to differentiate between results obtained from cyclic and monotonic loading.

Database for Shear Strength

For the Roeder et al. (2016) tests, the specimens that reportedly had a dominant flexural failure were excluded in the evaluation of the proposed shear formula. For the Ye et al. (2016) tests, the specimens with shear span-to-diameter ratio of less than 0.1 were also excluded. The Qian et al. (2007) tests on specimens with a low-shear span-to-diameter ratio (typically 0.1) were not considered here due to suspiciously high strength compared to all other researchers' results (with $V_{exp}/V_{simplified}$ values as high as 3.48). For all the existing test results, any test with $M_{exp}/M_p > 1.15$ was considered as a flexural dominant failure and was excluded from evaluations. The plastic moment, M_p, is the composite section plastic moment calculated using the plastic stress distribution method (PSDM). A few cases for which $1.0 < M_{exp}/M_p < 1.15$ were included when they were reported by the original researchers as failing in shear.

Also, it should be noted that not all the tested specimens may have exhibited a shear failure mode. The test result observations provided by Xiao et al. (2012) and Ye et al. (2016) for specimens having a/D values as low as 0.1 and 0.15 suggest that some of those specimens may have had a mixed failure mode of shear combined with other local-crushing phenomena.

Comparison of Experimental Results with Shear Strength Equations

To compare with experimental results, the ratios of the shear strength obtained experimentally and obtained using the proposed equation have been calculated for the available test data (Bruneau et al., 2018; Nakahara and Tsumura, 2014; Roeder et al., 2016; Xiao et al., 2012; Xu et al., 2009; Ye et al., 2016). Results are presented in Tables 2 and 3 for tests with and without axial load, respectively.

Values of the ratio of the strengths of the existing shear tests, V_{exp}, to their corresponding shear strengths calculated by the proposed simplified equation, V_{CFST}, are plotted in Figure 5 for specimens for which no axial load was applied. Note that values of the experimentally applied moments to the plastic moment, M_{exp}/M_p, included in Tables 2 and 3 show that the values plotted here correspond to specimens that exhibited shear-dominant failures (i.e., not flexure-dominant failures). Maximum calculated ratio of M_{exp}/M_p for the tests plotted in Figure 5 is 1.05. The horizontal axis in this figure represents the shear span-to-diameter ratio, a/D. The mean and standard deviation values of the results are included in the figure. As shown, on average, the experimental values are about 11% more than the values predicted by the proposed simplified formula.

The experimental-to-proposed simplified shear strength ratios for all the available test data, also including specimens for which axial load was applied, are shown in Figure 6. Figure 6(a) shows the ratio of experimental to calculated shear strengths versus the applied external axial load, and Figure 6(b) shows this ratio versus the shear span-to-diameter ratio. As shown, on average, the experimental values are about 35% more than the values predicted by the proposed formula. According to Figure 6(a), the proposed formula gives particularly more conservative values for the cases with more than $0.5P/P_0$ applied axial load. Also, Figure 6(b) shows that the predicted values using the proposed formula is more conservative for a/D ratios of less than 0.2. Maximum calculated ratio of M_{exp}/M_p for all the considered specimens, including the axial load, is 1.12.

While the results obtained with the proposed simplified

Table 2. Existing Experiments—Properties, Results, and Comparison with the Proposed Equation for Tests without Axial Load

Specimen	D (in.)	a (in.)	$\frac{a}{D}$	t (in.)	$\frac{D}{t}$	f_c' (ksi)	E_c (ksi)	F_y (ksi)	$\frac{P}{P_0}$	P (kips)	V_{exp} (kips)	V_{CFST} (kips)	$\frac{V_{exp}}{V_{CFST}}$	M_{exp} (kip-in.)	M_p (kip-in.)	$\frac{M_{exp}}{M_p}$
Bruneau et al. (2018)																
KB1	16.0	6.5	0.41	0.232	68.8	2.9	2757	51	0	0	437	401	1.09	2841	3428	0.83
KB3	12.8	5.0	0.39	0.232	54.8	4.5	3434	58	0	0	396	342	1.16	1980	2489	0.80
KB4	12.8	5.0	0.39	0.232	54.8	4.5	3434	58	0	0	397	342	1.16	1985	2489	0.80
KB5	12.8	5.0	0.39	0.232	54.8	4.5	3434	58	0	0	414	342	1.21	2070	2489	0.83
KB6	12.8	5.0	0.39	0.232	54.8	4.5	3434	58	0	0	407	342	1.19	2035	2489	0.82
KB7	12.8	5.0	0.39	0.232	54.8	4.5	3434	58	0	0	404	342	1.18	2020	2489	0.81
Roeder et al. (2016)																
R12	20	10	0.5	0.233	86	6.2	4031	54	0	0	651	714	0.91	6510	6211	1.05
R19	20	10	0.5	0.349	57	9.1	4891	57	0	0	952	964	0.99	9520	9684	0.98
R7	20	7.5	0.38	0.233	86	6.5	4111	50	0	0	705	702	1.00	5288	5826	0.91
R8	20	7.5	0.38	0.233	86	6.5	4121	54	0	0	802	723	1.11	6015	6233	0.96
R10	20	7.5	0.38	0.233	86	6.2	4014	54	0	0	665	712	0.93	4988	6207	0.80
R11	20	7.5	0.38	0.233	86	6.6	4162	57	0	0	600	743	0.81	4500	6551	0.69
R16	20	7.5	0.38	0.233	86	8.6	4750	57	0	0	765	805	0.95	5738	6691	0.86
R21	20	7.5	0.38	0.233	86	0.0	0	57	0	0	449	305	1.47	3368	5160	0.65
R14	20	5.0	0.25	0.233	86	8.6	4747	55	0	0	826	797	1.04	4130	6538	0.63
R15	20	5.0	0.25	0.233	86	8.8	4802	55	0	0	796	803	0.99	3980	6550	0.61
R20	20	5.0	0.25	0.233	86	2.8	2704	57	0	0	712	590	1.21	3560	6089	0.58
Ye et al. (2016)																
Ye1	4.7	0.7	0.15	0.079	60	4.6	3481	49	0	0	54	41	1.31	38	101	0.38
Ye2	4.7	0.7	0.15	0.079	60	4.6	3481	49	0	0	54	41	1.32	39	101	0.38
Nakahara and Tsumura (2014)																
N1	6.5	3.3	0.5	0.193	33.9	9.3	5336	79	0	0	150	166	0.90	491	713	0.69
Xiao et al. (2012)																
X1	6.3	2.5	0.40	0.217	29	3.8	3137	55	0	0	141	116	1.21	354	485	0.73
X2	6.3	2.5	0.40	0.217	29	4.7	3509	55	0	0	152	119	1.27	382	492	0.78
X3	6.3	2.5	0.40	0.217	29	4.3	3348	55	0	0	146	118	1.24	368	489	0.75
X4	6.5	2.6	0.40	0.173	38	3.8	3137	50	0	0	116	99	1.17	301	399	0.75
X5	6.5	2.6	0.40	0.173	38	4.7	3509	50	0	0	128	102	1.24	332	406	0.82
X6	6.5	2.6	0.40	0.173	38	4.3	3348	50	0	0	118	101	1.17	307	403	0.76
X7	6.5	2.6	0.40	0.118	55	3.8	3137	59	0	0	84	86	0.98	219	329	0.66
X8	6.5	2.6	0.40	0.118	55	4.7	3509	59	0	0	93	90	1.03	242	336	0.72
X9	6.5	2.6	0.40	0.118	55	4.3	3348	59	0	0	87	89	0.98	225	333	0.68
X25	6.3	0.9	0.14	0.217	29	3.8	3137	55	0	0	112	116	0.97	97	485	0.20
X26	6.3	0.9	0.14	0.217	29	4.7	3509	55	0	0	118	119	0.99	102	492	0.21
X27	6.3	0.9	0.14	0.217	29	4.3	3348	55	0	0	124	118	1.05	107	489	0.22
X28	6.3	0.9	0.14	0.217	29	4.3	3348	55	0	0	157	118	1.33	136	489	0.28
X29	6.5	0.9	0.14	0.173	38	4.3	3348	50	0	0	146	101	1.45	132	403	0.33
X30	6.5	0.9	0.14	0.118	55	4.3	3348	59	0	0	101	89	1.14	92	333	0.28
X31	6.5	0.9	0.14	0.173	38	3.8	3137	50	0	0	118	99	1.20	107	399	0.27
X32	6.5	0.9	0.14	0.173	38	4.7	3509	50	0	0	129	102	1.26	117	406	0.29
X33	6.5	0.9	0.14	0.173	38	4.3	3348	50	0	0	126	101	1.25	115	403	0.28
X34	6.5	0.9	0.14	0.118	55	3.8	3137	59	0	0	90	86	1.04	81	329	0.25

Table continues on the next page

Specimen	D (in.)	a (in.)	$\frac{a}{D}$	t (in.)	$\frac{D}{t}$	f'_c (ksi)	E_c (ksi)	F_y (ksi)	$\frac{P}{P_0}$	P (kips)	V_{exp} (kips)	V_{CFST} (kips)	$\frac{V_{exp}}{V_{CFST}}$	M_{exp} (kip-in.)	M_p (kip-in.)	$\frac{M_{exp}}{M_p}$
Xiao et al. (2012) (continued)																
X35	6.5	0.9	0.14	0.118	55	4.7	3509	59	0	0	96	90	1.06	87	336	0.26
X36	6.5	0.9	0.14	0.118	55	4.3	3348	59	0	0	92	89	1.04	83	333	0.25
X55	6.3	3.2	0.50	0.256	25	2.9	2764	65	0	0	169	147	1.15	538	652	0.82
X57	6.5	3.3	0.50	0.161	40	2.9	2764	59	0	0	99	101	0.99	324	425	0.76
Xu et al. (2009)																
Xu16	5.5	0.6	0.1	0.145	38	4.9	3576	53	0	0	93	76	1.23	51	255	0.20
Xu17	5.5	1.1	0.2	0.145	38	4.9	3576	53	0	0	83	76	1.10	91	255	0.36
Xu18	5.5	1.7	0.3	0.145	38	4.9	3576	53	0	0	80	76	1.06	132	255	0.52
Xu19	5.5	2.8	0.5	0.145	38	4.9	3576	53	0	0	68	76	0.90	188	255	0.74
Xu26	5.5	0.6	0.1	0.145	38	4.9	3576	53	0	0	88	76	1.16	188	255	0.74
Xu27	5.5	1.1	0.2	0.145	38	4.9	3576	53	0	0	79	76	1.04	48	255	0.19
Xu28	5.5	1.7	0.3	0.145	38	4.9	3576	53	0	0	75	76	0.99	87	255	0.34

Table 2. Existing Experiments—Properties, Results, and Comparison with the Proposed Equation for Tests without Axial Load (continued)

Table 3. Existing Experiments—Properties, Results, and Comparison with the Proposed Equation for Tests with Axial Load

Specimen	D (in.)	a (in.)	$\frac{a}{D}$	t (in.)	$\frac{D}{t}$	f'_c (ksi)	E_c (ksi)	F_y (ksi)	$\frac{P}{P_0}$	P (kips)	V_{exp} (kips)	V_{CFST} (kips)	$\frac{V_{exp}}{V_{CFST}}$	M_{exp} (kip-in.)	M_p (kip-in.)	$\frac{M_{exp}}{M_p}$
Roeder et al. (2016)																
R13	20	7.5	0.38	0.233	86	5.3	3737	54	0.09	202	710	683	1.04	5325	6134	0.87
Ye et al. (2016)																
Ye3	4.7	0.7	0.15	0.079	60	4.6	3481	49	0.24	32	60	41	1.47	43	101	0.42
Ye4	4.7	0.7	0.15	0.079	60	4.6	3481	49	0.24	32	57	41	1.38	40	101	0.40
Ye5	4.7	0.7	0.15	0.079	60	4.6	3481	49	0.59	78	71	41	1.73	51	101	0.50
Ye6	4.7	0.7	0.15	0.079	60	4.6	3481	49	0.59	78	72	41	1.74	51	101	0.50
Ye7	4.7	0.7	0.15	0.079	60	4.6	3481	49	0.73	97	75	41	1.82	53	101	0.53
Ye8	4.7	0.7	0.15	0.079	60	4.6	3481	49	0.73	97	71	41	1.73	51	101	0.50
Ye11	4.7	0.7	0.15	0.079	60	4.6	3481	49	0.49	65	65	41	1.58	46	101	0.46
Ye12	4.7	0.7	0.15	0.079	60	4.6	3481	49	0.49	65	64	41	1.56	45	101	0.45
Ye13	4.7	2.4	0.5	0.079	60	4.6	3481	49	0.49	65	39	41	0.96	93	101	0.92
Ye14	4.7	2.4	0.5	0.079	60	4.6	3481	49	0.49	65	44	41	1.06	103	101	1.02
Ye17	4.7	0.7	0.15	0.079	60	8.3	4670	49	0.34	65	79	48	1.65	56	106	0.53
Ye18	4.7	0.7	0.15	0.079	60	8.3	4670	49	0.34	65	76	48	1.58	54	106	0.51
Ye19	4.7	0.7	0.15	0.118	40	4.6	3481	60	0.37	65	88	58	1.51	62	173	0.36
Ye20	4.7	0.7	0.15	0.118	40	4.6	3481	60	0.37	65	88	58	1.51	62	173	0.36
Nakahara and Tsumura (2014)																
N2	6.3	3.1	0.5	0.089	70	9.6	5655	73	0.1	41	109	99	1.10	343	316	1.08
N3	6.5	3.3	0.5	0.193	33	9.3	5336	79	0.3	174	162	166	0.98	530	713	0.74
N4	6.3	3.1	0.5	0.089	70	9.6	5655	73	0.3	123	96	99	0.97	303	316	0.96
N5	6.5	3.3	0.5	0.197	33	7.0	4887	79	0.1	51	153	160	0.96	501	700	0.72
N6	6.5	3.3	0.5	0.197	33	7.0	4887	79	0.2	102	156	160	0.98	508	700	0.73
N7	6.5	3.3	0.5	0.197	33	7.0	4887	79	0.4	205	148	160	0.93	484	700	0.69
N8	6.3	3.1	0.5	0.089	70	9.6	5655	73	0.15	61	102	99	1.03	321	316	1.02
N9	6.3	3.1	0.5	0.089	70	9.6	5655	73	0.2	82	112	99	1.13	354	316	1.12

Table continues on the next page

Table 3. Existing Experiments—Properties, Results, and Comparison with the Proposed Equation for Tests with Axial Load (continued)																
Specimen	D (in.)	a (in.)	$\frac{a}{D}$	t (in.)	$\frac{D}{t}$	f'_c (ksi)	E_c (ksi)	F_y (ksi)	$\frac{P}{P_0}$	P (kips)	V_{exp} (kips)	V_{CFST} (kips)	$\frac{V_{exp}}{V_{CFST}}$	M_{exp} (kip-in.)	M_p (kip-in.)	$\frac{M_{exp}}{M_p}$
Xiao et al. (2012)																
X10	6.3	2.5	0.40	0.217	29	3.8	3137	55	0.32	105	164	116	1.41	412	485	0.85
X11	6.3	2.5	0.40	0.217	29	4.7	3509	55	0.31	109	169	119	1.41	425	492	0.86
X12	6.3	2.5	0.40	0.217	29	4.3	3348	55	0.31	106	175	118	1.49	442	489	0.90
X13	6.5	2.6	0.40	0.173	38	3.8	3137	50	0.31	89	142	99	1.44	368	399	0.92
X14	6.5	2.6	0.40	0.173	38	4.7	3509	50	0.30	94	147	102	1.43	381	406	0.94
X15	6.5	2.6	0.40	0.173	38	4.3	3348	50	0.30	90	152	101	1.51	394	403	0.98
X16	6.5	2.6	0.40	0.118	55	3.8	3137	59	0.30	77	108	86	1.25	280	329	0.85
X17	6.5	2.6	0.40	0.118	55	4.7	3509	59	0.28	80	109	90	1.21	283	336	0.84
X18	6.5	2.6	0.40	0.118	55	4.3	3348	59	0.28	77	111	89	1.26	289	333	0.87
X19	6.3	2.5	0.40	0.217	29	3.8	3137	55	0.64	210	158	116	1.36	398	485	0.82
X20	6.3	2.5	0.40	0.217	29	4.7	3509	55	0.62	219	182	119	1.52	459	492	0.93
X21	6.5	2.6	0.40	0.173	38	3.8	3137	50	0.62	179	146	99	1.48	380	399	0.95
X22	6.5	2.6	0.40	0.173	38	4.7	3509	50	0.60	188	157	102	1.54	409	406	1.01
X23	6.5	2.6	0.40	0.118	55	3.8	3137	59	0.60	154	123	86	1.42	318	329	0.97
X24	6.5	2.6	0.40	0.118	55	4.7	3509	59	0.56	160	130	90	1.44	339	336	1.01
X37	6.3	0.9	0.14	0.217	29	3.8	3137	55	0.32	105	202	116	1.75	175	485	0.36
X38	6.3	0.9	0.14	0.217	29	4.7	3509	55	0.31	109	225	119	1.88	195	492	0.40
X39	6.3	0.9	0.14	0.217	29	4.3	3348	55	0.31	106	214	118	1.81	185	489	0.38
X40	6.5	0.9	0.14	0.173	38	3.8	3137	50	0.31	89	185	99	1.88	168	399	0.42
X41	6.5	0.9	0.14	0.173	38	4.7	3509	50	0.30	94	202	102	1.97	183	406	0.45
X42	6.5	0.9	0.14	0.173	38	4.3	3348	50	0.30	90	191	101	1.90	173	403	0.43
X43	6.5	0.9	0.14	0.118	55	3.8	3137	59	0.30	77	152	86	1.76	137	329	0.42
X44	6.5	0.9	0.14	0.118	55	4.7	3509	59	0.28	80	169	90	1.87	153	336	0.45
X45	6.5	0.9	0.14	0.118	55	4.3	3348	59	0.28	77	157	89	1.78	143	333	0.43
X46	6.3	0.9	0.14	0.217	29	3.8	3137	55	0.64	210	211	116	1.82	183	485	0.38
X47	6.3	0.9	0.14	0.217	29	4.7	3509	55	0.62	219	236	119	1.98	204	492	0.42
X48	6.3	0.9	0.14	0.217	29	4.3	3348	55	0.62	211	270	118	2.29	234	489	0.48
X49	6.5	0.9	0.14	0.173	38	3.8	3137	50	0.62	179	230	99	2.34	209	399	0.52
X50	6.5	0.9	0.14	0.173	38	4.7	3509	50	0.60	188	236	102	2.30	214	406	0.53
X51	6.5	0.9	0.14	0.173	38	4.3	3348	50	0.60	180	202	101	2.01	183	403	0.45
X52	6.5	0.9	0.14	0.118	55	3.8	3137	59	0.60	154	172	86	1.99	156	329	0.47
X53	6.5	0.9	0.14	0.118	55	4.7	3509	59	0.56	160	185	90	2.05	168	336	0.50
X54	6.5	0.9	0.14	0.118	55	4.3	3348	59	0.57	155	193	89	2.18	175	333	0.53

equation are safe even when including the results from Xiao et al. (2012) and Ye et al. (2016) with a/D ratios less than or equal to 0.15 (as shown in Figure 6), by excluding the test results of $a/D \leq 0.15$, the mean value of experimental-to-proposed shear strengths would improve to 1.15 with a lower standard deviation of 0.19.

The shear strengths from the steel tube and concrete infill of a circular CFST calculated by the proposed simplified equation for different shear span ratios are shown in Figure 7. Results from monotonic finite element analyses are also shown in this figure for comparison. This figure shows how the simplified equation compares to the finite element analyses results for different shear span to depth ratios.

RECTANGULAR CONCRETE-FILLED STEEL TUBES

This section presents for rolled and built-up rectangular (and square) CFST: the experimental database, proposed simplified shear strength equation, and comparison of calculated to experimental shear strengths.

Experimental Database

Compared to circular CFST, fewer shear tests on rectangular CFST are found in the literature. The shear tests available in the literature can be categorized based on the type of loading and test setup used. For example, tests have been conducted using (1) a pantograph type test setup, (2) a three- or four-point beam bending type test setup, and (3) a beam-to-column subassembly type test setup for panel-zone shear. The experimental database, described in the following subsections, includes tests with shear span-to-depth (a/D) ratios ranging from 0.075 to 1.5; axial load ratios (P/P_0) ratios ranging from 0.0 to 0.65; plate slenderness ratios (D/t) ranging from 21 to 67; concrete compressive strength, f_c', ranging from 2.4 to 17 ksi; and steel yield stress, F_y, ranging from 42 to 117 ksi. In the following discussion and database, a is the shear span defined by the loading during the test; D is the total depth of the specimen in the direction of shear loading; P is the applied compressive axial force; P_0 is the section axial capacity of the rectangular CFST calculated as the sum of the steel yield strength, A_sF_y, and the concrete compressive strength, A_cf_c'; b is the width of the CFST member; t is the thickness of the steel tube; f_c' is the uniaxial compressive strength of concrete; F_y is the yield strength of steel; A_s is the cross-sectional area of steel tube; and A_c is the cross-sectional area of the concrete infill. Tests with an a/D ratio greater than 1.5 exhibit flexure-dominant behavior and, therefore, have been excluded in this study.

Tomii and Sakino (1979) were one of the earliest researchers to investigate the fundamental flexure and shear behavior of rectangular CFST members. Forty small-scale specimens were tested and categorized into five series of tests, depending on the parameter values. Sakino and Ishibashi (1985) continued the work and conducted tests on 21 small-scale specimens that could be categorized into six series based on the parameters. Both research studies were conducted using the same pantograph type test setup that subjected the specimens to double-curvature bending under constant axial load and monotonic or cyclic shearing force.

Koester (2000) conducted experimental investigations to evaluate the fundamental shear behavior of rectangular CFST members and the panel-zone behavior of rectangular CFST-to-steel beam connections. The connection panel-zone region was idealized as shown in Figure 8, and a schematic view of the test setup is shown in Figure 9. This paper only includes the specimens exhibiting shear failure and having regular steel tube geometry (no cutouts, etc.).

Koester (2000) also conducted six full-scale tests on subassemblies consisting of square CFST column-to-steel beam moment connections, where the moment connections were split-tee. through-bolted moment connections. The tests were conducted by subjecting the subassembly specimens to cyclic lateral loading using the schematic shown in Figure 10. Ricles et al. (2004) supplemented the research

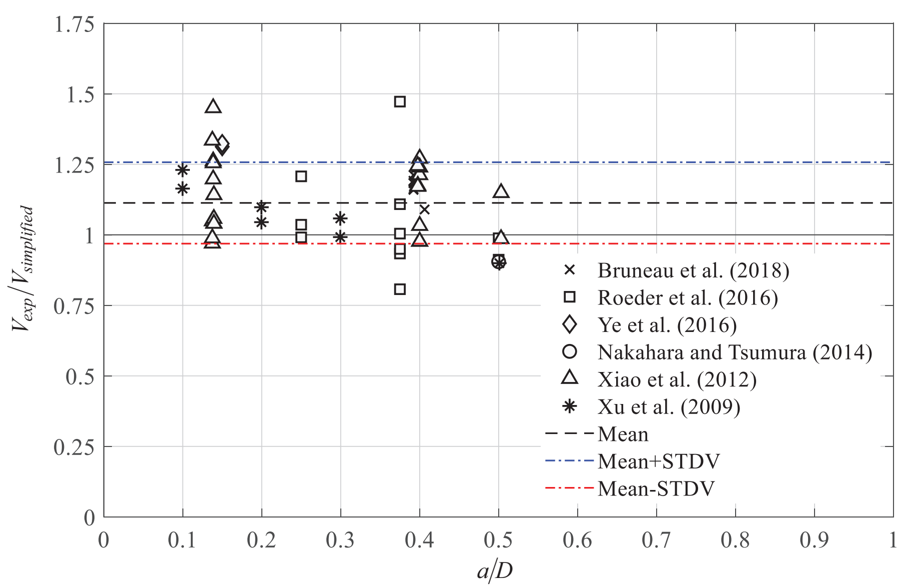

Fig. 5. Ratio of strength from existing test results with no axial load to proposed simplified shear strength formula as a function of shear span, a/D.

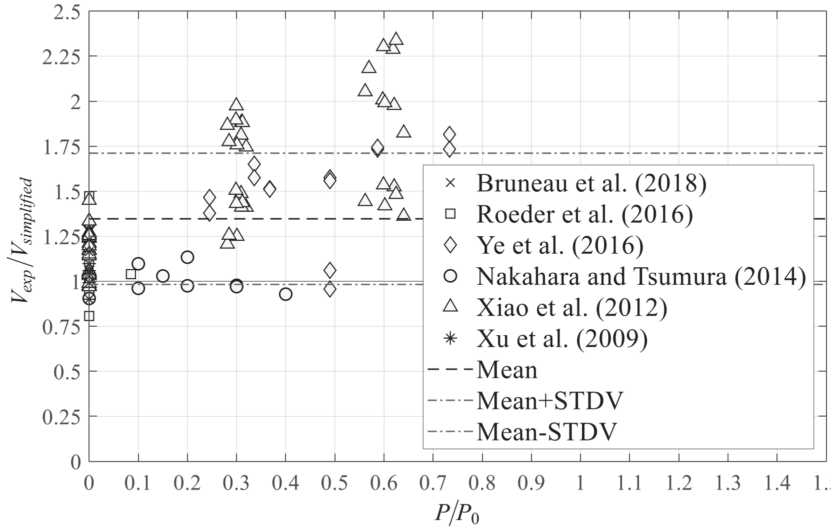

(a) Normalized applied axial load, P/P_0

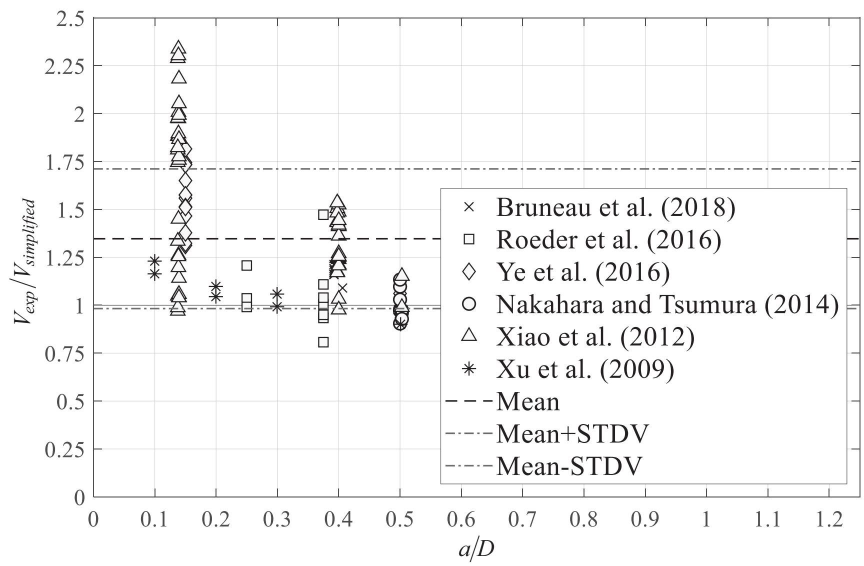

(b) Shear span, a/D

Fig. 6. Ratio of strength from existing test results to proposed simplified shear strength formula.

conducted by Koester (2000) and evaluated the seismic behavior of two interior joint type subassemblies consisting of square CFST columns—steel beam moment connections with weak panel zones. The panel zones had interior steel plate diaphragms that were complete joint penetration welded on only three or four sides.

Nishiyama et al. (2004) studied the effect of high-strength concrete and steel material on the shear strength of the panel zone of CFST column-to-steel beam joint subassemblies. Five specimens consisting of subassemblies made from square CFST columns and steel beams were tested. Both interior and exterior joint types with through and outer diaphragms were studied. The specimens were designed to fail under panel-zone shear by reducing the thickness of the CSFT steel tube in the panel zone. The axial load on columns was held constant as a reversed cyclic lateral load was applied at the beam ends, as shown in Figure 11. Fukumoto and Morita (2005) continued the work and presented three more tests on interior joint type steel beam-square CFST column subassemblies with interior diaphragms.

Wu et al. (2005) studied the seismic behavior of square CFST column-to-steel beam joints by testing three interior joint type subassemblies using a setup similar to Figure 11. Shawkat et al. (2008) tested four rectangular CFST under three-point bending in a displacement-controlled mode. Ye et al. (2016) tested 18 small-scale specimens under various combinations of axial compression and shear. The specimens were fixed at the ends, subjected to constant axial

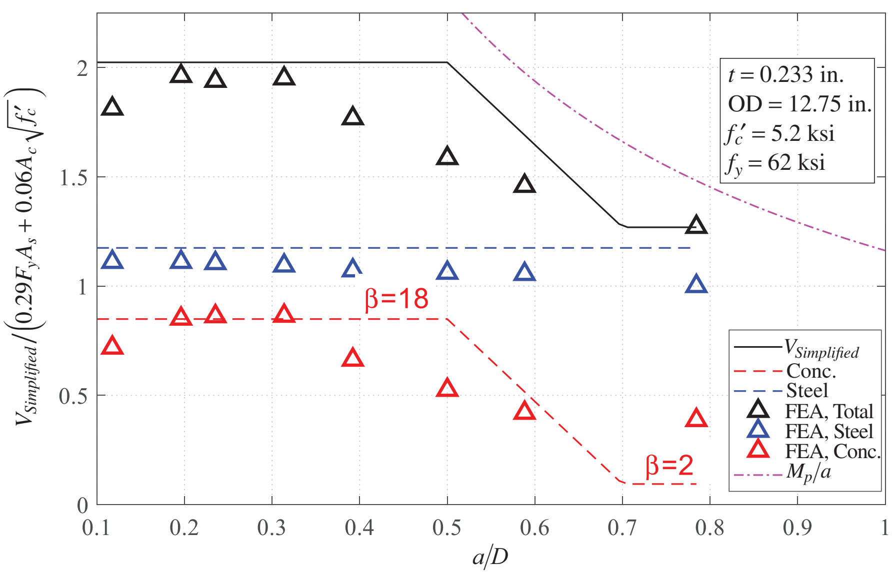

Fig. 7. Normalized proposed simplified shear strength vs. shear span-to-diameter ratios.

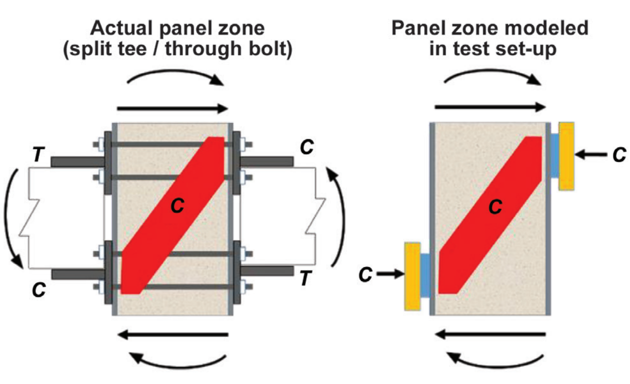

Fig. 8. Panel-zone region in connections and idealization for testing (adapted from Koester, 2000).

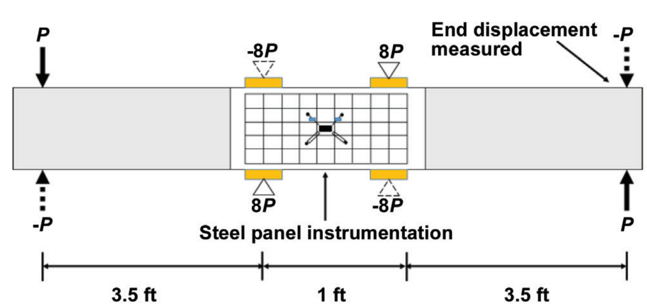

Fig. 9. Schematic view of test setup for idealized small-scale specimens (adapted from Koester, 2000).

loading, and tested under monotonic three-point bending to produce double curvature using the test setup with schematic shown in Figure 12.

Summary of Results

The compiled experimental database is summarized in Table 4 along with the relevant parameters, including test setup; loading type; cross-section dimensions; shear span-to-depth ratio, a/D; and axial load ratio, P/P_0. The general conclusions and results from the research database are as follows:

1. Rectangular CFST are typically flexure critical and very difficult to fail in shear due to their high shear strength, which includes contributions from the webs of the steel tube and the concrete infill (Tomii and Sakino, 1979; Koester, 2000).
2. Changing the failure mode from flexure critical to shear critical depends primarily on the shear span-to-depth ratio, a/D. The a/D ratio has to be made extremely small (<1.0) to force shear failure. Specimens with $1.0 \leq a/D < 3.0$ generally fail in combined shear and flexure, and specimens with $a/D \geq 3.0$ generally fail in flexure (Sakino and Ishibashi, 1985).

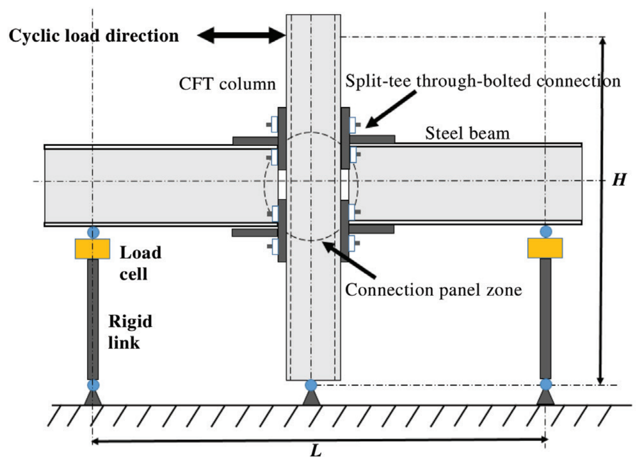

Fig. 10. Schematic view of test setup with cyclic lateral loading applied at column top (adapted from Koester, 2000).

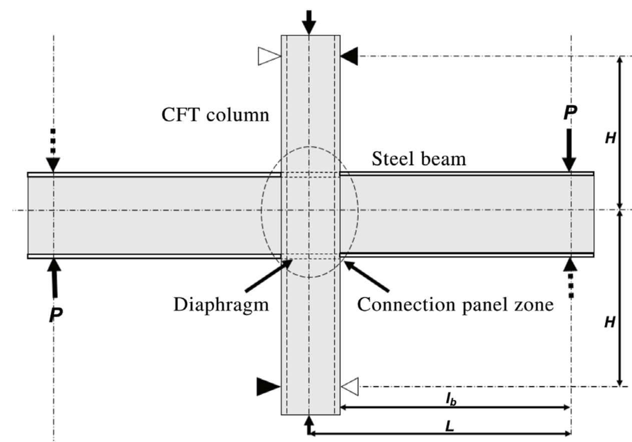

Fig. 11. Schematic view of test setup with cyclic loading applied at beam ends (adapted from Nishiyama et al., 2004).

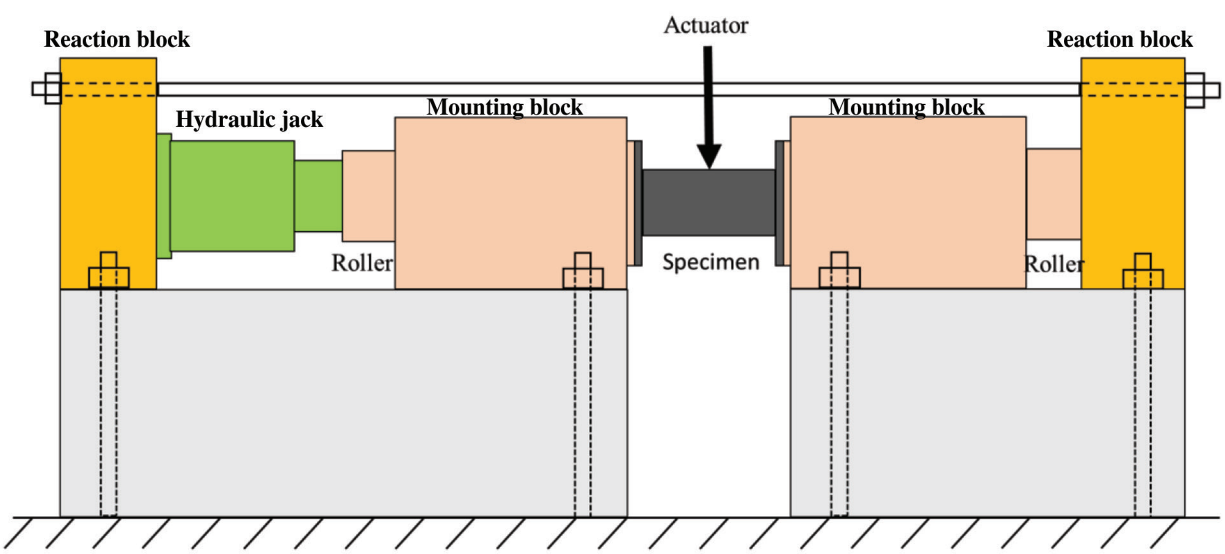

Fig. 12. Schematic view of the test setup (adapted from Ye et al., 2016).

Table 4. Summary of the Existing Test Data on Shear Strength of RCFST Members					
Research	**Test Setup**	**Loading Type**	**Section, in. × in.**	**a/D Range**	**P/P_0 Range**
Tomii and Sakino (1979)	Pantograph	Double-curvature bending	3.9 × 3.9	0.83–1	0–0.5
Sakino and Ishibashi (1985)	Pantograph	Double-curvature bending	3.9 × 3.9	1–1.5	0–0.5
Koester (2000)	Four-point bending	Cyclic bending	8 × 8, 12 × 12, 16 × 16	0.75	0
Ricles et al. (2004)	Beam-to-column Subassembly	Cyclic lateral loading	16 × 16	0.75	0.12
Nishiyama et al. (2004)	Beam-to-column Subassembly	Cyclic lateral loading	9.8 × 9.8, 6.4 × 6.4	0.5	0.2–0.65
Fukumoto and Morita (2005)	Beam-to-column Subassembly	Monotonic lateral loading	7.9 × 7.9	0.75	0
Wu et al. (2005)	Beam-to-column Subassembly	Cyclic lateral loading	15.7 × 15.7	0.6	0.16–0.19
Shawkat et al. (2008)	Three-point bending	Monotonic bending	4.0 × 5.9	1.0	0
Ye et al. (2016)	Three-point bending	Monotonic bending	4.7 × 4.7	0.075–0.75	0–0.65

3. Applying axial compression (P/P_0) further increases the shear strength of specimens (Ye et al., 2016). This increase is due to the reduction in concrete cracking and increase in concrete contribution to the shear strength.

4. Increasing the steel yield strength or increasing the steel plate thickness of specimens generally increases their shear strength due to the increase in the steel contribution to the shear strength (Nishiyama et al., 2004, Fukumoto and Morita, 2005).

5. Specimens failing in shear, particularly panel-zone shear specimens, exhibit reasonable ductility and deformation capability (Wu et al., 2005, Nishiyama et al., 2004).

6. The load bearing width does not affect the shear strength or the load-displacement behavior of subassembly panel-zone specimens (Koester, 2000).

7. The effects of reducing the D/t ratio were inconclusive. For small-scale specimens, with all other parameters held constant, lower D/t ratios resulted in increased concrete contribution to the shear strength, owing to better confinement. However, this beneficial effect was not observed in full-scale specimen tests with lower D/t ratios (Koester .2000).

Database for Shear Strength

The compiled experimental database was reviewed carefully to identify and include specimens that failed in shear and were shear critical. The following provides additional discussion and rationale for including or excluding specific specimens in the final database for shear strength of rectangular CFST.

- Tomii and Sakino (1979) and Sakino and Ishibashi (1985) reported that their specimens did not have clear shear failures. The specimens developed diagonal shear cracks in the concrete, but both the flanges yielded (due to flexure) at the ultimate state. These specimens were eventually considered flexure critical (with high shear demands), but not shear critical. They were not included in the final database of tests considered for evaluating the shear strength of rectangular CFST.
- Koester (2000) included some specimens that were tested for examining mechanics-based models for shear strength. These specimens had cutouts in the steel webs or different filling material than concrete. These exploratory specimens were not included in the final database.
- For the subassembly specimens tested by Koester (2000), Ricles et al. (2004), Nishiyama et al. (2004), Fukumoto and Morita (2005), and Wu et al. (2005),

the specimens that failed due to weld fracture in the connection, or due to the formation of plastic hinges in the steel beams before shear failure in the panel zones, were not included in the final database. All the specimens that failed in panel-zone shear yielding and failure were included in the final database.

- The specimens tested by Shawkat et al. (2008) could not be included because they were found to be flexure critical. Some of the specimens tested by Ye et al. (2016) could not be included because they had premature weld fracture failure before reaching shear strength.

Simplified Shear Strength Equation for Rectangular CFST

A simplified Equation 17 is proposed to calculate the nominal shear strength, V_n, of rectangular CFST, while accounting for contributions of the steel and concrete. The steel contribution, V_s, is calculated using Equation 18 as the shear strength of the webs of the rectangular cross section, $0.6A_wF_y$. In this equation, A_w is the area of the webs calculated as the total depth, D, minus 2 times half the flange thickness, t_f, multiplied by their thickness, t_w. The concrete contribution, V_c, is calculated using Equation 19 as $0.0316\beta A_c\sqrt{f_c'}$, where f_c' is in ksi and A_c is the area of the concrete infill calculated as the product of the internal dimensions of the cross section, $A_c = bd$. The factor β accounts for the effects of the diagonal compression strut that forms between the load points as shown in Figure 8 when the shear span-to-depth ratio is small. β is calculated using Equation 20a and the shear span-to-depth ratio, a/D. When $a/D \le 0.75$, β is equal to 20. When $a/D > 0.75$, β is equal to 2, which is the typical value for concrete contribution in members.

$$V_n = V_s + V_c \tag{17}$$

where

$$V_c = 0.0316\beta A_c\sqrt{f_c'} \tag{18}$$

$$V_s = 0.6A_wF_y \tag{19}$$

$$\beta = 20 \text{ for } a/D \le 0.75 \tag{20a}$$

$$\beta = 2 \text{ for } a/D > 0.75 \tag{20b}$$

It is important to note that this simplified shear strength equation does not explicitly account for the effect of axial force, P/P_0. It considers the fact that axial compression increases shear strength, and therefore the shear strength calculated for P/P_0 equal to zero (using Equations 17 to 20) will be conservative for situations with higher axial compression. The proposed method accounts for the effects of concrete strut formation through an empirical factor β. It does not account directly or explicitly for the mechanics of compression strut formation in the concrete.

Comparison of Experimental Results with Shear Strength Equations

Because the simplified shear strength equation does not account for the effects of axial force, the final experimental database was parsed into specimens subjected to low levels of axial force ($P/P_0 \le 0.25$), shown in Table 5, and higher levels of axial force ($P/P_0 > 0.25$), shown in Table 6. These tables include the reference source of the specimens and various material and geometric parameters, including the shear span-to-depth ratio, a/D, tube slenderness, D/t, and ratio and axial load, P/P_0. The tables also include the experimental values of shear strength, V_{exp}, and the corresponding flexural moment strength, M_{exp}, in the specimens. The shear strength, V_n, calculated using Equations 17 to 20, and the plastic moment capacity, M_p, calculated according to AISC *Specification* Section I1.2a (2016b), using the plastic stress distribution method while accounting for the effects of axial force, P, are included in the tables. The comparisons of the experimental values of shear strength and corresponding flexural moment with the calculated capacities—that is, V_{exp}/V_n and M_{exp}/M_p—are also included in the tables, and lead to the following statistics. The comparisons of V_{exp}/V_n in Table 5 have a mean value of $\mu = 1.19$, a standard deviation of $\sigma = 0.15$, and a coefficient of variation (CoV) of 0.13. The comparisons of V_{exp}/V_n in Table 6 have $\mu = 1.61$, $\sigma = 0.11$, and a CoV of 0.07. When considered all together, irrespective of the axial load level, the comparisons of V_{exp}/V_n have a $\mu = 1.3$, $\sigma = 0.24$, and a CoV of 0.18. Thus, the proposed simplified shear strength equation is reasonably accurate for specimens with axial load level P/P_0 less than 25%. As expected, the proposed equation is more conservative for specimens with an axial load level P/P_0 greater than 25%. For specimens with $P/P_0 < 0.25$, Figure 13(a) shows the variation of V_{exp}/V_n with respect to the a/D ratio, and Figure 13(b) shows the variation of V_{exp}/V_n with respect to the D/t ratio. For the range of parameters considered, there is no correlation with respect to the a/D ratio or the D/t ratio for these specimens. For the complete database from Tables 5 and 6, including all ratios P/P_0, Figure 14(a) shows the variation of V_{exp}/V_n with respect to the a/D ratio, and Figure 14(b) shows the variation of V_{exp}/V_n with respect to the axial load level P/P_0. As seen in these figures, even for the complete database, there is no correlation with respect to the a/D ratio of the specimens, but increasing the axial load level P/P_0 increases the V_{exp}/V_n ratio and the conservatism of the simplified shear strength equation.

RELIABILITY ANALYSIS

Reliability analyses were conducted to establish an appropriate β factor that should be used in the empirically magnified concrete strength equation to make it possible to use

Table 5. Existing Experiments—Properties, Results, and Comparison with the Proposed Equation for Tests with $P/P_0 < 25\%$

Specimen	b (in.)	D (in.)	a (in.)	$\frac{a}{D}$	t (in.)	$\frac{D}{t}$	f'_c (ksi)	F_y (ksi)	$\frac{P}{P_0}$	P (kips)	V_{exp} (kips)	V_n (kips)	$\frac{V_{exp}}{V_n}$	M_{exp} (kip-ft.)	M_p (kip-ft.)	$\frac{M_{exp}}{M_p}$
Koester (2000)																
8.4A	8	8	6	0.75	0.25	32	6.2	54.1	0	0	233	214	1.09	116	115	1.01
8.6A	8	8	6	0.75	0.25	32	6.2	54.1	0	0	241	214	1.12	120	115	1.05
8.8A	8	8	6	0.75	0.25	32	6.2	54.1	0	0	237	214	1.11	118	115	1.03
8.4B	8	8	6	0.75	0.375	21	6.0	52.6	0	0	313	262	1.20	156	157	1.00
8.6B	8	8	6	0.75	0.375	21	6.1	52.6	0	0	313	263	1.19	156	157	1.00
8.8B	8	8	6	0.75	0.375	21	5.9	52.6	0	0	316	261	1.21	158	157	1.01
8.B-C	8	8	6	0.75	0.25	32	5.9	61.5	0	0	232	229	1.01	116	129	0.90
8.P-C	8	8	6	0.75	0.25	32	3.9	61.5	0	0	203	213	0.95	101	126	0.81
8.P2-C	8	8	6	0.75	0.25	32	5.9	61.5	0	0	227	229	0.99	113	126	0.90
CFT.2	12	12	9	0.75	0.45	27	7.2	53.1	0	0	571	540	1.06	428	450	0.95
CFT.3	12	12	9	0.75	0.45	27	7.3	53.1	0	0	598	542	1.10	448	450	1.00
CFT.4	12	12	9	0.75	0.45	27	7.4	53.1	0	0	610	543	1.12	457	450	1.02
Nishiyama et al. (2004)																
R1	9.8	9.8	4.9	0.5	0.18	54	16.0	71.3	0.20	383	566	371.3	1.52	228	255	0.90
R2	9.8	9.8	4.9	0.5	0.18	55	7.9	71.3	0.20	240	438	308.9	1.42	177	208	0.85
R3	9.9	9.9	4.9	0.5	0.19	53	14.9	109.6	0.20	425	632	458.1	1.38	255	350	0.73
R4	9.3	9.3	4.9	0.5	0.18	52	14.9	64.1	0.20	328	476	323.6	1.47	192	209	0.92
Fukumoto and Morita (2005)																
SP1	7.9	7.9	5.9	0.75	0.24	33	9.3	74.1	0	0	337	252.7	1.34	179	184	0.97
SP2	7.9	7.9	5.9	0.75	0.35	22	9.3	74.8	0	0	428	316.1	1.35	227	243	0.94
SP3	7.9	7.9	5.9	0.75	0.31	25	17.0	117.2	0	0	554	437.5	1.27	294	373	0.79
Wu et al. (2005)																
FSB-6	15.7	15.7	9.8	0.6	0.24	67	3.7	62.5	0.19	336	602	557.3	1.08	549	562	0.98
FSB-8	15.7	15.7	9.8	0.6	0.31	50	4.2	55.4	0.16	336	659	620.9	1.06	602	636	0.95
FSB-10	15.7	15.7	9.8	0.6	0.39	40	3.9	51.7	0.16	336	669	656.1	1.02	610	707	0.86
Ye et al. (2016)																
S1-1a	4.7	4.7	0.7	0.15	0.08	60	4.6	49.1	0	0	55	49.9	1.10	4.6	12	0.38
S1-1b	4.7	4.7	0.7	0.15	0.08	60	4.6	49.1	0	0	57	49.9	1.14	4.8	12	0.40
S1-2a	4.7	4.7	0.7	0.15	0.08	60	4.6	49.1	0.22	36	65	49.9	1.31	5.5	14	0.39
S1-2b	4.7	4.7	0.7	0.15	0.08	60	4.6	49.1	0.22	36	61	49.9	1.23	5.1	14	0.37

Specimen	b (in.)	D (in.)	a (in.)	$\frac{a}{D}$	t (in.)	$\frac{D}{t}$	f'_c (ksi)	F_y (ksi)	$\frac{P}{P_0}$	P (kips)	V_{exp} (kips)	V_n (kips)	$\frac{V_{exp}}{V_n}$	M_{exp} (kip-ft.)	M_p (kip-ft.)	$\frac{M_{exp}}{M_p}$
Ye et al. (2016)																
S1-3a	4.7	4.7	0.7	0.15	0.08	60	4.6	49.1	0.52	87	82	50	1.64	6.8	10.8	0.63
S1-3b	4.7	4.7	0.7	0.15	0.08	60	4.6	49.1	0.52	87	77	50	1.54	6.4	10.8	0.59
S1-4a	4.7	4.7	0.7	0.15	0.08	60	4.6	49.1	0.65	109	85	50	1.71	7.1	7.1	1.01
S1-4b	4.7	4.7	0.7	0.15	0.08	60	4.6	49.1	0.65	109	85	50	1.71	7.1	7.1	1.00
S2-2a	4.7	4.7	0.7	0.15	0.08	60	4.6	49.1	0.43	73	71	50	1.42	5.9	12.4	0.48
S2-2b	4.7	4.7	0.7	0.15	0.08	60	4.6	49.1	0.43	73	73	50	1.45	6.1	12.4	0.49
S3-1a	4.7	4.7	0.7	0.15	0.08	60	8.3	49.1	0.3	73	100	60	1.68	8.4	17.3	0.48
S3-1b	4.7	4.7	0.7	0.15	0.08	60	8.3	49.1	0.3	73	103	60	1.72	8.6	17.3	0.50
S4-1a	4.7	4.7	0.7	0.15	0.12	40	4.6	60.3	0.32	73	111	67	1.66	9.3	21	0.44

Table 6. Existing Experiments—Properties, Results, and Comparison with the Proposed Equation for Tests with $P/P_0 > 25\%$

the common-strength reduction factor, ϕ, of 0.9 typically used in the 2016 AISC *Specification*. Reliability analysis is usually conducted to calculate ϕ for values obtained using a proposed strength equation, but calibrating the strength instead is acceptable here given the empirical nature of the magnification for the concrete strength contribution to the total strength. These reliability analyses were conducted using ASCE/SEI 7, Equation C2.3 2 (2016), namely:

$$\phi = \left(\frac{\mu_R}{R_n}\right) e^{-\alpha_R \beta V_R} = PMFe^{-\alpha_R \beta V_R} \tag{21}$$

where β is the reliability index in this case (and not the empirical magnification factor expressed by the same Greek letter). As experiments have shown the shear failure mode of CFST to be ductile, a reliability index of 3.0 was selected. As recommended by ASCE/SEI 7 (2016), the linearization approximation constant, α, was set equal to 0.70 to separate the resistance and demand uncertainties.

In Equation 21, $\left(\frac{\mu_R}{R_n}\right)$ is the mean ratio of the experimental-to-nominal strength calculated using the associated design equation, equal to the product PMF, where P is the bias (mean ratio) of experimental strength to the strength calculated using measured material properties (i.e., steel coupon and concrete cylinder strengths), M is the bias in the material properties calculated as the mean ratio of the measured-to-nominal material strength, and F is the bias due to fabrication issues calculated as the mean ratio of the measured-to-nominal cross-sectional properties.

In Equation 21, V_r is calculated as:

$$V_R = \sqrt{V_P^2 + V_M^2 + V_F^2} \tag{22}$$

where

V_F = the coefficient of variation due to fabrication effects

V_M = the coefficient of variation due to material effects

V_P = the coefficient of variation reflecting uncertainties in the design

Circular Concrete-Filled Steel Tubes

For circular CFST, P is the mean ratio of the shear strengths V_{exp}/V_n, equal to 1.11 as reported in Figure 5 when using an empirical magnification factor of 18, and with corresponding standard deviation of 0.14 and coefficient of variation, V_p, of 0.13. M was assumed to be 1.1 and 1.3 in two contemplated scenarios to bracket the possible expected strength by using R_y values typically reported for steel and concrete individually in the AISC *Seismic Provisions* (2016a). F was conservatively taken as 1.0, as recommended by Ellingwood et al. (1980). V_F was taken as 0.05 based on Ravindra and Galambos (1978). For the case where values for steel were used, V_M was taken as 0.07 based on the material property study conducted by Liu (2003). For the case where values for concrete were used, V_M was taken as 0.18 based on MacGregor (1976).

The resulting V_R values obtained considering steel and concrete variability as two independent cases are 0.16 and 0.23, respectively. These resulted in strength reduction factors, ϕ, of 0.88 and 0.90, respectively. These are approximately equal to the strength reduction factor of 0.90 used throughout most of the 2016 AISC *Specification*. Note that the same calibration exercise using an empirical magnification factor of 20 resulted in a strength reduction factor closer to 0.85 and thus, deemed too low to justify using in light of the desirable target of 0.90.

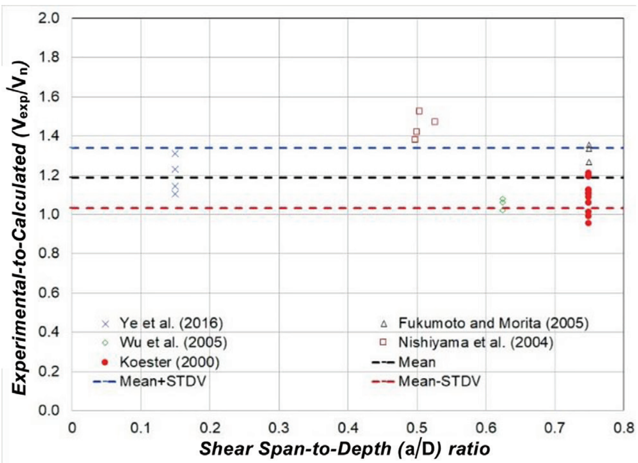

(a) *Shear span-to-depth* a/D *ratio*

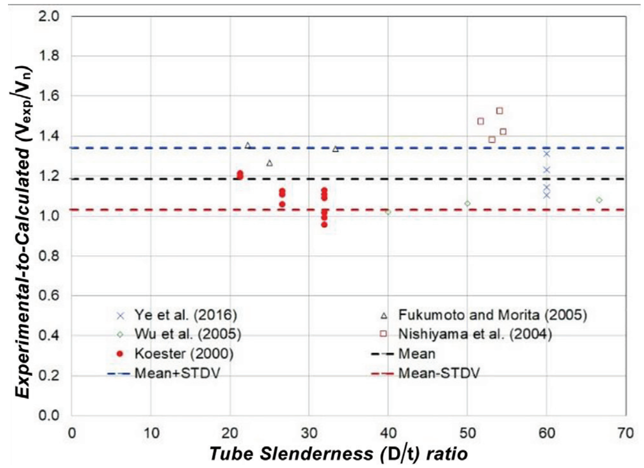

(b) *Tube slenderness* D/t *ratio*

Fig. 13. Variation of V_{exp}/V_n *for specimens with* $P/P_0 < 25\%$ *from Table 5.*

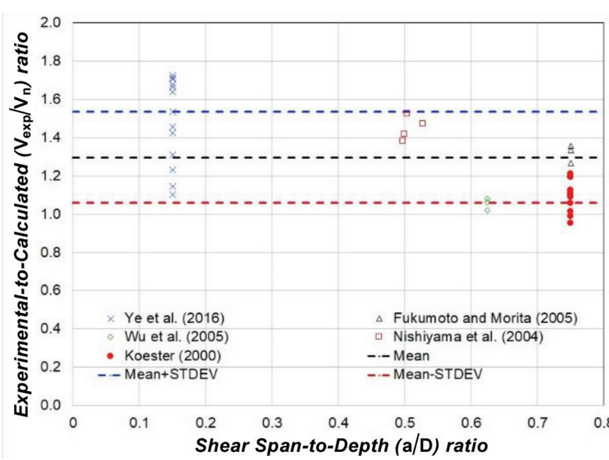

(a) *Shear span-to-depth* a/D *ratio*

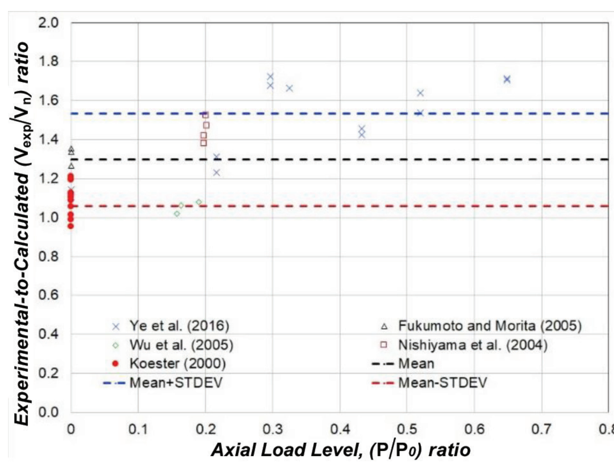

(b) *Axial* P/P_0 *levels*

Fig. 14. Variation of V_{exp}/V_n *for all specimens included in Tables 5 and 6.*

Rectangular Concrete-Filled Steel Tubes

For rectangular CFST, the reliability analysis was limited to the specimens listed in Table 5 with a low axial load level ($P/P_0 \leq 0.25$). As mentioned earlier, the mean value, μ, of V_{exp}/V_n is 1.19; the standard deviation, σ, is 0.15; and the coefficient of variation, V_P, is 0.13. Similar to circular CFST, M = 1.3, V_M = 0.18, F = 1.0, and V_F = 0.05 were considered. The resulting value of ϕ calculated using Equation 21 was equal to 0.96. If the values of M and V_M are changed to 1.1 and 0.07 to be conservative, then the resulting value of ϕ calculated using Equation 21 is equal to 0.94.

PROPOSED INTEGRATED DESIGN EQUATION

On the basis of the results obtained, it is possible to formulate the following integrated requirements for the shear strength of both circular and rectangular CFST, in a format that can directly be introduced into design specifications:

The design shear strength, $\phi_v V_n$, is determined using $\phi_v = 0.90$ and Equation 24 to calculate the nominal shear strength, V_n, as follows:

$$V_n = 0.6A_v F_y + 0.03\beta A_c \sqrt{f_c'} \tag{23}$$

where

A_c = area of concrete in the filled composite member, in.^{2}

A_s = cross-sectional area of steel section, in.^{2}

A_v = shear area of steel, in.^{2}; the shear area for a circular section is equal to $\dfrac{2A_s}{\pi}$ and, for a rectangular section, is equal to the sum of the area of webs in the direction of in-plane shear

f_c' = concrete strength, ksi

β = 2 for members with $M_u/V_u d \geq 0.7$, where M_u and V_u are equal to the maximum moment and shear demands, respectively, along the member length, and d is equal to the member depth in the direction of bending

β = 20 for members with rectangular cross sections and $M_u/V_u d \leq 0.5$

β = 18 for members with circular cross sections and $M_u/V_u d \leq 0.5$

Linear interpolation between the limiting β values should be used for members with $M_u/V_u d$ between 0.5 and 0.7.

The proposed variation in the value of β reflects the fact that there is a lack of data on the shear strength of circular members for span ratios greater than 0.5. A transition from the β values of 18 and 20 down to the value of 2 is expected, but the exact point at which this happens is unknown, other than the fact that it should occur at a shear span greater than 0.5. Although the experimental data for rectangular members presented in this paper suggests a β value of 20 is acceptable for shear span-to-depth ratios up to 0.75, at this time, a relatively rapid transition to a value of 2 at a shear span of 0.7 is proposed, as illustrated in Figure 15, in superposition to "back-calculated" values corresponding to each of the experimental data considered. More abrupt transitions can be problematic when implemented in design software. A smoother transition is possible and will be considered when more data become available.

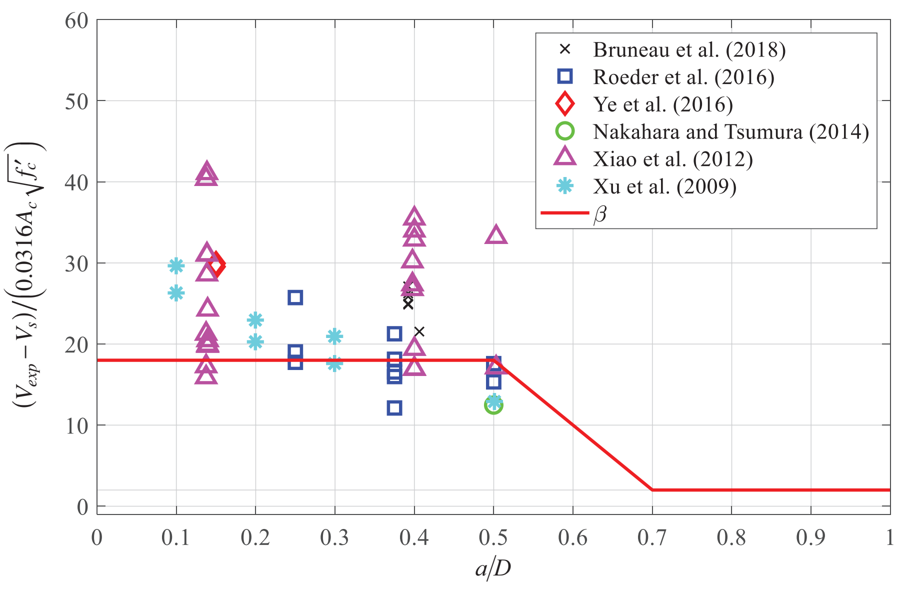

Fig. 15. Recommended transition for β in proposed equations for shear strength of circular CFST.

CONCLUSION

Simplified equations for the shear strength of composite concrete-filled tubes were proposed and calibrated. The format of the proposed equation is consistent for rectangular and circular cross sections, only differing in values used for the shear area and for the β factor resulting from calibration of the ϕ factors. Finite element analysis was performed to compare the expected strength of such composite members with that calculated by the simplified equation. The proposed equation is shown to accurately represent the contribution of the steel tube to the total strength and empirically approximates the contribution of the concrete in composite CFST. Consistent with the philosophy adopted throughout the AISC *Specification* (2016b) and the AISC *Seismic Provisions* (2016a) for various structural members, the contribution of the steel tube is established based on the derived equation for plastic cross-section strength, and this contribution to the total strength of the composite section was confirmed to be accurate by finite element analysis. The contribution of the concrete fill was derived to achieve simple modifications to existing equations, recognizing that a diagonal concrete compression strut provides a significant contribution to that shear strength, but without encumbering the design equations with the complex mathematical expressions that would be required to represent that phenomenon with physical models. The proposed shear strength formula is valid up to a specified shear span-to-diameter ratio.

The effectiveness of the proposed equation was compared with shear test data from the existing literature and was found to be safe. When used with a resistance factor of 0.90, the average ratio of experimental values to calculated values was 1.23 for circular concrete-filled members (1.5 including the experiments with axial loads), with a standard deviation of 0.16 (0.4 including cases with axial load). For rectangular members, the average ratio of experimental values to calculated values was 1.19 for the specimens with axial load level less than 25% (1.61 for the experiments with axial load level greater than 25%) with standard deviations of 0.15 (0.11 for the experiments with axial load level greater than 25%).

Compared to current provisions, the proposed equations utilize the plastic strength of the steel tube and do not cap the strength to the steel tube buckling limit. Also, the proposed equations also reflect that the total strength of the composite section is obtained by summation of steel and concrete strengths and recognize that the concrete strength can be significantly increased by the development of a diagonal compression strut in the concrete, which has been neglected in the current equations.

Future experimental and analytical research is desirable to better understand and quantify the shear strength contribution of the concrete infill for shear spans ratios greater than 0.5, to possibly extend the range of high shear strength to a broader range of applications. Furthermore, given that only a limited number of specimens in past experiments were subjected to a cyclic loading regime, it would be desirable in future research to conduct more inelastic cyclic tests over a more extensive range of parameters to further assess the limits of applicability of the proposed model.

ACKNOWLEDGMENTS

The contributions of the members of the AISC Committee on Specifications Task Committee 5: Composite Members, through discussion and guidance of various ballot proposals, is acknowledged.

REFERENCES

ACI (2011), *Building Code Requirements for Structural Concrete*, ACI 318-11 and commentary, American Concrete Institute, Farmington Hills, Mich.

ACI (2014), *Building Code Requirements for Structural Concrete,* ACI 318-14 and commentary, American Concrete Institute, Farmington Hills, Mich.

AISC (2016a), *Seismic Provisions for Structural Steel Buildings*, ANSI/AISC 341-16, American Institute of Steel Construction, Chicago, Ill.

AISC (2016b), *Specification for Structural Steel Buildings*, ANSI/AISC 360-16, American Institute of Steel Construction, Chicago, Ill.

AIJ (1987), "AIJ Standard for Structural Calculation of Steel Reinforced Concrete Structures," *AIJ 5-26-20*, Shiba, Minato, Tokyo, Japan.

ASCE (2016), *Minimum Design Loads and Associated Criteria for Buildings and Other Structures*, ASCE/SEI 7-16, American Society of Civil Engineers, Reston, Va.

Bruneau, M., Kenarangi, H., and Murphy, T.P. (2018), *NCHRP Research Report 872 Contribution of Steel Casing to Single Shaft Foundation Structural Resistance*, Transportation Research Board, Washington, D.C.

Bruneau, M. and Marson, J. (2004), "Seismic Design of Concrete-Filled Circular Steel Bridge Piers," *Journal of Bridge Engineering*, Vol. 9, No. 1, pp. 24–34.

Ellingwood, B. (1980), *Development of a Probability Based Load Criterion for American National Standard A58: Building Code Requirements for Minimum Design Loads in Buildings and Other Structures*, U.S. Department of Commerce, National Bureau of Standards.

CEN (2005), *Eurocode 3: Design of Steel Structures*, European Committee for Standardization, Brussels, Belgium.

Fischer, E. and Varma, A.H. (2014), "Design of Split-Tee Connections for Special Composite Moment Resisting Frames," *Engineering Journal*, AISC, Vol. 52, No. 3, pp. 185–201.

Fukumoto, T. and Morita, K. (2005), "Elastoplastic Behavior of Panel Zone in Steel Beam-to-Concrete Filled Steel Tube Column Moment Connections," *Journal of Structural Engineering*, Vol. 131, No. 12, pp. 1,841–1,853.

Hajjar, J.F. (2000), "Concrete-Filled Steel Tube Columns under Earthquake Loads," *Progress in Structural Engineering and Materials*, Vol. 2, No. 1, pp. 72–81.

Hajjar, J.F., Gourley, B.C., Tort, C., Denavit, M.D., and Schiller, P.H. (2013), "Steel-Concrete Composite Structural Systems," Department of Civil and Environmental Engineering, Northeastern University, Boston, Mass. http://www.northeastern.edu/compositesystems.

Han, L.H. and Yang, Y.F. (2005), "Cyclic Performance of Concrete-Filled Steel CHS Columns under Flexural Loading," *Journal of Constructional Steel Research*, Vol. 61, No. 4, pp. 423–452.

Kenarangi, H. and Bruneau, M. (2020a), "Investigation of Cyclic Shear Behavior of Circular Reinforced Concrete Filled Steel Tubes," *Journal of Structural Engineering*, 146, No. 5.

Kenarangi, H. and Bruneau, M. (2020b), "Shear Strength of Composite Circular Reinforced Concrete-Filled Steel Tubes," *Journal of Structural Engineering*, Vol. 146, No. 1.

Koester, B. (2000), "Panel Zone Behavior of Moment Connections between Rectangular Concrete-Filled Steel Tubes and Wide Flange Beams," PhD dissertation, Department of Civil and Environmental Engeering, University of Texas-Austin, Austin, Texas.

Lai, Z., Huang, Z., and Varma, A.H. (2017), "Seismic Analysis and Performance of High Strength Composite Special Moment Frames (C-SMFs)," *Structures*, Vol. 9, pp. 165–178.

Lai, Z., Varma, A.H., and Zhang, K. (2014), "Noncompact and Slender Rectangular CFT Members: Experimental Database, Analysis, and Design," *Journal of Constructional Steel Research*, Vol. 101, pp. 455–468.

Leon, R.T., Kim, D.K., and Hajjar, J.F. (2007), "Limit State Response of Composite Columns and Beam-Columns Part I: Formulation of Design Provisions for the 2005 AISC Specification," *Engineering Journal*, AISC, Vol. 44, No. 1, pp. 341–358.

Liu, J. (2003), "Examination of Expected Yield and Tensile Strength Ratios, Report + Addendum Report to AISC," Purdue University, West Lafayette, Ind.

MacGregor, J.G. (1976), "Safety and Limit States Design for Reinforced Concrete," *Canadian Journal of Civil Engineering*, Vol. 3, No. 4, pp. 484–513.

Nakahara, H. and Tsumura, R. (2014), "Experimental Study on Shearing Behavior of Circular CFT Short Column," *Journal of Structural and Construction Engineering (Transactions of AIJ)*, Vol. 79, No. 703, pp. 1,385–1,393.

Nishiyama, I., Fujimoto, T., Fukumoto, T., and Yoshioka, K. (2004), "Inelastic Force-Deformation Response of Joint Shear Panels in Beam-Column Moment Connections to Concrete-Filled Tubes," *Journal of Structural Engineering*, Vol. 130, No. 2, pp. 244–252.

Qian, J., Cui, Y., and Fang, X. (2007), "Shear Strength Tests of Concrete Filled Steel Tube Columns," *Tumu Gongcheng Xuebao (China Civil Engineering Journal)*, Vol. 40, No. 5, pp. 1–9.

Ravindra, M.K. and Galambos, T.V. (1978), "Load and Resistance Factor Design for Steel," *Journal of the Structural Division*, Vol. 104, No. 9, pp. 1,337–1,353.

Ricles, J.M., Peng, S.W., and Lu, L.W. (2004), "Seismic Behavior of Composite Concrete Filled Steel Tube Column-Wide Flange Beam Moment Connections," *Journal of Structural Engineering*, Vol. 130, No. 2, pp. 223–232.

Roeder, C., Lehman, D., and Bishop, E. (2010), "Strength and Stiffness of Circular Concrete-Filled Tubes," *Journal of Structural Engineering*, Vol. 136, No. 12, pp. 1,545–1,553.

Roeder, C., Lehman, D., and Maki, A. (2016), "Shear Design Expessions for Concrete Filled Steel Tube and Reinforced Concrete Filled Tube Components," Washington State Department of Transportation (WSDOT).

Sakino, K. and Ishibashi, H. (1985), "Experimental Studies on Concrete Filled Square Steel Tubular Short Columns Subjected to Cyclic Shearing Force and Constant Axial Force," *Journal of Structural and Construction Engineering (Transactions of AIJ)*, Vol. 353, pp. 81–91.

Shawkat, W., Fahmy, W., and Fam, A. (2008), "Cracking Patterns and Strength of CFT Beams under Different Moment Gradients," *Composite Structures*, Vol. 84, No. 2, pp. 159–166.

Tomii, M. and Sakino, K. (1979), "Experimental Studies on Concrete Filled Square Steel Tubular Beam-Columns Subjected to Monotonic Shearing Force and Constant Axial Force," *Transactions of the Architectural Institute of Japan*, Vol. 281, pp. 81–92.

Varma, A.H., Ricles, J.M., Sause, R., and Lu, L.W. (2002), "Experimental Behavior of High Strength Square Concrete Filled Steel Tube (CFT) Columns," *Journal of Structural Engineering*, Vol. 128, No. 3, pp. 309–318.

Wu, L.Y., Chung, L.L., Tsai, S.F., Shen, T.J., and Huang, G.L. (2005), "Seismic Behavior of Bolted Beam-to-Column Connections for Concrete Filled Steel Tube," *Journal of Constructional Steel Research*, Vol. 61, No. 10, pp. 1,387–1,410.

Xiao, C., Cai, S., Chen, T., and Xu, C. (2012), "Experimental Study on Shear Capacity of Circular Concrete Filled Steel Tubes," *Steel and Composite Structures*, Vol. 13, No. 5, pp. 437–449.

Xu, C., Haixiao, L., and Chengkui, H. (2009), "Experimental Study on Shear Resistance of Self-Stressing Concrete Filled Circular Steel Tubes," *Journal of Constructional Steel Research*, Vol. 65, No. 4, pp. 801–807.

Ye, Y., Han, L.H., Tao, Z., and Guo, S.L. (2016), "Experimental Behaviour of Concrete-Filled Steel Tubular Members under Lateral Shear Loads," *Journal of Constructional Steel Research*, Vol. 122, pp. 226–237.

APPENDIX

Other Shear Strength Equations for Rectangular CFST

Other researchers have also developed and proposed equations for calculating the shear strength of rectangular CFST. These include Koester (2000), AIJ (1987), and Fukumoto and Morita (2005). The equations proposed by Koester were quite similar to the proposed simplified equations, with a few deviations. According to Koester, and as shown in Equation 24, the nominal shear strength, V_{nK}, is the sum of the steel and concrete contributions. The steel contribution is calculated as the shear yield strength of the flat portions of the hollows structural section (HSS) steel tubes used for the specimen. In Equation 25, d_{fl} is the depth of the flat portion of steel tube. The concrete contribution is calculated as $0.0316\beta_K A_c\sqrt{f_c'}$, where β_K is equal to 28 and is slightly larger than the value in Equation 19.

$$V_{nK} = V_{sK} + V_{cK} \tag{24}$$

$$V_{sK} = 0.6F_y(2d_{fl}t_w) \tag{25}$$

$$V_{cK} = 0.0316\beta_K A_c\sqrt{f_c'} \tag{26}$$

$$V_{nF} = V_{sF} + V_{cF} \tag{27}$$

$$V_{sF} = A_w\sqrt{\frac{F_y^2 - f_P^2}{3}} \tag{28}$$

$$V_{cF} = \left(\frac{D_c}{2}\tan\theta + 4\sqrt{\frac{M_{pf}}{D_c f_c'}}\sin\theta\right)D_c f_c' \tag{29}$$

Fukumoto and Morita (2005) proposed Equations 27 to 29 to calculate the panel-zone shear strength of rectangular CFST, particularly those made from higher-strength materials. In Equation 27, V_{nF} is the nominal shear strength, which is the sum of the shear yield strength of the steel tube, V_{sF}, and the shear strength contribution of the concrete infill, V_{cF}. As shown in Equation 28, V_{sF} accounts for the effects of axial compression on the shear yield strength of the steel, where f_P is the axial stress in the steel tube due to the applied compression. As shown in Equation 29, V_{cF} includes the contribution of the main concrete compressive strut and the confining struts resulting from the formation of plastic hinges in the flange plates of the steel tube. In Equation 29, D_c is the depth of the concrete panel, θ is the angle of the concrete strut with respect to the vertical and depends on the a/D ratio, and M_{pf} is the plastic moment capacity of the steel tube flange plate. It is important to note that V_{cF} does not account for the effects of axial compression.

AIJ (1987) provides Equation 31 to calculate the panel-zone shear strength, V_{nJ}, of rectangular CFST:

$$V_{nJ} = \frac{1.2(2f_{sc}\gamma\nu_c + f_{ss}\nu_s)}{d} \tag{31}$$

where

f_{sc} = short-term shear strength of concrete, MPa
 = min $(0.05f_c', 0.74 + 0.015f_c')$
γ = $2.5 \times D/d \le 4.0$ for a square section
d = center-to-center distance between beam flanges, mm
v_c = volume of concrete in the panel, mm^3
f_{ss} = short-term shear strength of steel, MPa
 = $F_y/\sqrt{3}$
v_s = volume of steel web of the shear panel, mm^3

It is important to note that V_{nJ} does not account for the effects of axial compression.

These equations were used to calculate the shear strengths of the specimens included in the final database. Table 7 shows the ratios of the experimental-to-calculated shear strength for all the specimens included in Table 5, which had a low axial load level ($P/P_0 \le 0.25$). As shown by the ratios and the statistical evaluation (μ, σ, and CoV) at the bottom of the table, the Fukumoto and Morita (2005) approach seems to be the most accurate (on average) and with the least CoV. However, it calculates shear strength ratios in the range of 0.80–0.89 for a few specimens tested by Ye et al. (2016). The AIJ (1987) method is the most conservative and has just a couple of ratios less than 1.0. The Koester (2000) approach is also quite accurate (on average), but it does have a few values in the 0.90–0.95 range for specimens tested by Wu et al. (2005) and Ye et al. (2016). The proposed simplified approach is reasonably accurate and has just a couple of ratios less than 1.0.

Table 8 shows the ratios of the experimental-to-calculated shear strength for all the specimens included in Table 6, which had a higher axial load level ($P/P_0 \ge 0.25$).

Table 7. V_{exp}/V_n Ratios for Specimens with $P/P_0 < 0.25$ from Table 5						
Specimen	V_{exp} **(kips)**	V_n **(kips)**	$\frac{V_{exp}}{V_n}$	$\frac{V_{exp}}{V_{nK}}$	$\frac{V_{exp}}{V_{nJ}}$	$\frac{V_{exp}}{V_{nF}}$
Koester (2000)						
8.4A	233	214	1.09	1.02	1.22	1.12
8.6A	241	214	1.12	1.05	1.27	1.15
8.8A	237	214	1.11	1.03	1.25	1.13
8.4B	313	262	1.20	1.25	1.25	1.16
8.6B	313	263	1.19	1.25	1.25	1.16
8.8B	316	261	1.21	1.27	1.27	1.18
8.B-C	232	229	1.01	0.96	1.11	1.03
8.P-C	203	213	0.95	0.93	1.00	1.01
8.P2-C	227	229	0.99	0.94	1.09	1.01
CFT.2	571	540	1.06	1.02	1.16	1.01
CFT.3	598	542	1.10	1.07	1.22	1.06
CFT.4	610	543	1.12	1.08	1.24	1.07
Nishiyama et al. (2004)						
R1	566	371	1.52	1.27	1.56	1.08
R2	438	309	1.42	1.22	1.46	1.23
R3	632	458	1.38	1.21	1.36	1.01
R4	476	324	1.47	1.22	1.56	1.08
Fukumoto and Morita (2005)						
SP1	337	253	1.34	1.19	1.41	1.15
SP2	428	316	1.35	1.33	1.31	1.14
SP3	554	438	1.27	1.21	1.20	0.96
Wu et al. (2005)						
FSB-6	602	557	1.08	0.93	1.19	1.24
FSB-8	659	621	1.06	0.93	1.16	1.14
FSB-10	669	656	1.02	0.93	1.08	1.07
Ye et al. (2016)						
S1-1a	55	50	1.10	0.90	0.91	0.80
S1-1b	57	50	1.14	0.94	0.95	0.83
S1-2a	65	50	1.31	1.07	1.09	0.95
S1-2b	61	50	1.23	1.01	1.02	0.89
		Average	1.19	1.09	1.21	1.06
		Standard deviation	0.15	0.14	0.17	0.11
		CoV	0.13	0.13	0.14	0.11

Table 8. V_{exp}/V_n Ratios for Specimens with $P/P_0 > 0.25$ from Table 6						
Specimen	V_{exp} (kips)	V_n (kips)	$\frac{V_{exp}}{V_n}$	$\frac{V_{exp}}{V_{nK}}$	$\frac{V_{exp}}{V_{nJ}}$	$\frac{V_{exp}}{V_{nF}}$
Ye et al. (2016)						
S1-3a	82	50	1.64	1.34	1.36	1.22
S1-3b	77	50	1.54	1.26	1.27	1.14
S1-4a	85	50	1.71	1.40	1.42	1.29
S1-4b	85	50	1.71	1.40	1.41	1.29
S2-2a	71	50	1.42	1.17	1.18	1.05
S2-2b	73	50	1.45	1.19	1.21	1.07
S3-1a	100	60	1.68	1.34	1.40	0.99
S3-1b	103	60	1.72	1.38	1.44	1.02
S4-1a	111	67	1.66	1.45	1.39	1.21
		Average	1.62	1.33	1.34	1.14
		Standard deviation	0.11	0.10	0.10	0.12
		CoV	0.07	0.07	0.07	0.10

As shown by the ratios and the statistical evaluation (μ, σ, and CoV) at the bottom of the table, the Fukumoto and Morita (2005) approach seems to be the most accurate (on average), but this is incidental because the approach did not actually account for the effects of axial compression on concrete shear strength contribution. This can be explained further as follows. For the Ye et al. (2016) specimens, the shear span-to-depth ratio is extremely small (0.075), which leads to very high concrete contributions (V_{cF}). This causes overestimation of shear strengths for low axial load cases in (shear strength ratios in the 0.80–0.95 range) and seemingly appropriate prediction for high axial load cases in Table 8 (shear strength ratios in the 0.99–1.29 range). Both the AIJ (1987) and the Koester (2000) approaches are also conservative with respect to the test results. The proposed simplified approach is the most conservative for higher axial load levels.

Guide for Authors

Scope *Engineering Journal* is dedicated to the improvement and advancement of steel construction. Its pages are open to all who wish to report on new developments or techniques in steel design, research, the design and/or construction of new projects, steel fabrication methods, or new products of significance to the uses of steel in construction. Only original papers should be submitted.

General Papers intended for publication should be submitted by email Margaret Matthew, editor, at **matthew@aisc.org**.

The articles published in the *Engineering Journal* undergo peer review before publication for (1) originality of contribution; (2) technical value to the steel construction community; (3) proper credit to others working in the same area; (4) prior publication of the material; and (5) justification of the conclusion based on the report.

All papers within the scope outlined above will be reviewed by engineers selected from among AISC, industry, design firms, and universities. The standard review process includes outside review by an average of three reviewers, who are experts in their respective technical area, and volunteers in the program. Papers not accepted will not be returned to the author. Published papers become the property of the American Institute of Steel Construction and are protected by appropriate copyrights. No proofs will be sent to authors. Each author receives three copies of the issue in which his contribution appears.

Manuscripts Manuscripts must be provided in Microsoft Word format. Include a PDF with your submittal so we may verify fonts, equations and figures. View our complete author guidelines at **aisc.org/ej**.

Smarter. Stronger. Steel.

American Institute of Steel Construction
130 E Randolph St, Ste 2000, Chicago, IL 60601
312.670.2400 | aisc.org/ej